Periodic Forced Vibrations, Normal Modes and Damping, with Measurements on a 'Cello

John Coffey, Cheshire, UK.

January 2016

Key words: vibration, oscillation, resonance, mass-and-spring, forced, acoustics, normal mode, damping, matrix, finite element analysis, FEA, Lagrange equations, elastic pendulum, 'cello, experimental measurement, frequency spectrum, decay time constant, Mecway, Rayleigh damping,

1 Introduction

This is another article in a series describing my personal investigations into the acoustics of the violin family of musical instruments. Starting from the general theory of small amplitude oscillations of a linear system, it considers numerical methods which in principle could be used for calculating the vibration of the top plate of a violin, viola or 'cello (violoncello, to give it its full name) under the periodic forcing action of the two feet of the bridge as a string is bowed steadily. I give particular attention to damped resonances and include original experimental measurements of the time constant which characterise the decay in sound from a 'cello and hence its timbre at different musical pitches. The examples are original, but the subject is well documented[1].

The article begins with the relatively simple case of a structure made from particle masses connected together by springs, with negligible friction as they move. It is well documented in books on dynamics[2] that such a system with N degrees of freedom, if disturbed from equilibrium by a *small* amount, will oscillate in one or more of N characteristic patterns, each called a normal mode. Each normal mode is a pattern of collective motion involving the whole system in which all particles vibrate at the same frequency and either in phase or exactly 180° out of phase. Each normal mode has its own distinctive frequency. Normal modes can be identified only when the system is 'linear'. The meaning of a 'linear system' is illustrated in Appendix 1 by an example of a non-linear system and its linear approximation. A consequence of linearity is that the principle of superposition applies. This means that the free motion of the system, after it has been given some small but arbitrary initial disturbance, can be represented as a superposition of normal modes whose amplitudes are determined by the initial disturbance. These modes are independent so no energy is transferred from one to the other. We therefore have two equivalent ways of representing free motion: either as the time variation of each separate particle or as a superposition of normal modes.

If the system is driven by an external periodic force the behaviour is different. Once the transients of starting have died away under the resistive damping which in practice is always present,

[1] A comprehensive book which application to finite element methods is 'The Finite Element Method in Engineering' by Singiresu S Rao, Elsevier Science Books, 4th edition 2004.

[2] See for example 'Classical Mechanics' by R Douglas Gregory, Cambridge Univ Press, 2006

the system will attempt to follow the driving forces. The simplest case is where only one sinusoidal force is applied and damping is very light. It is well known that all the particles of the system will then move in a sinusoidal matter at the same frequency as the applied force and essentially all in phase with it. A dramatic phenomenon occurs when the driving force is close to one of the natural frequencies of free motion. This is resonance, when the structure continues to absorb energy from the driving source, the stored energy being limited only by what is lost through friction, sound radiation or other modes of dissipation. The system's energy appears as high velocities of the masses and large extensions of the springs.

The analysis in this article applies to structures with several degrees of freedom subject to more than one force and/or at more than one frequency. Under continuous periodic but not necessarily sinusoidal driving forces applied at various positions, the system will attempt to follow the driving forces, but its motion will be modulated by the inherent tendency to move in the shapes of its normal modes and by the tendency to resonate. The resulting motion is determined in part by the positions where the forces are applied, by their strength, and in part by how close the driving frequency is to the natural frequencies. The mathematical machinery using matrices developed for describing free oscillations can be extended to the calculation of forced oscillations. It leads to forced oscillation being understood as a superposition of 'driven modes' which share many properties with the free modes. We therefore again have two equivalent ways of representing the motion: either as the time variation of each separate particle or as a superposition of modes. The reasoning and formulation can in principle be adapted to finite element schemes for determining the response of a continuous structure approximated by a mesh of elastic elements. The topic is known as 'modal analysis'.

The analysis opens in §2 by retelling the general theory of small oscillations and illustrating it with a one-dimensional 3-mass-3-spring system. A key concept is free normal modes. Section §3 extends this to harmonic forced oscillations without damping. It introduces what I am calling 'driven modes' – counterparts of the normal modes of free oscillation. §4 extends this to periodic but non-harmonic driving forces with several Fourier components, which includes square, triangular and saw-tooth wave forms. The frequency spectrum of response to a driving force is a central goal of this analysis because in a violin-family instrument it describes how the force from the strings is modulated by the resonant characteristics of the wooden belly. §5 extends the mathematical tools to deal with light damping. §6 considers how the method is adapted in some finite element programs to model transient and teh dynamic response to varying forces. The method, described in the well-known textbook by S S Rao, involves integration of the time-dependent differential equations over a sequence of time steps. I demonstrate two modified versions which are more accurate. The final section, §7, makes the transition from discrete mass-and-spring systems to continuous elastic structures by considering the simple case of a one-element plate under forced oscillation. The finite element software used in this example is Mecway v4 *mecway.com*. I am grateful to Victor Kemp, Mecway's developer, for explaining aspects of the program's functioning. The section closes by linking modal analysis to the computer program I wrote[3] to calculate sound radiation from a vibrating structure, such as a violin, viola or 'cello.

There are two Appendices. The first, §8, carries out the dynamical calculation of the motion of the elastic pendulum – a mass on a spring or elastic chord which swings in a plane and can bounce up and down as it swings. This is used as an example of linear approximation to a non-linear system. The second and quite long Appendix 2 in §9 describes my original experimental efforts to determine

[3] 'Physics of sound radiation from vibrating surfaces' 2015, on *www.mathstudio.co.uk*.

the decay time constants τ, due to damping, at a series of resonances in a 'cello and, more limited, in a viola. These are direct measurements of the modal resistance factor. The mathematical foundation of the experiments is explained using the solution of the second order damped differential equation of motion for a system with only one resonance.

2 Free vibrations of a simple mass-spring system

This section illustrates how complicated systems with many dynamic elements can be recast in terms of 'normal modes' of oscillation in which the system moves so that the displacement of its particles can be described in terms of a single 'normal co-ordinate' for each mode. Each normal co-ordinate is a linear combination of the displacements from equilibrium of each particle. The theory is developed first for the case where there are no external forces driving the system – the particles merely vibrate under out-of-balance forces in the springs after some initial disturbance.

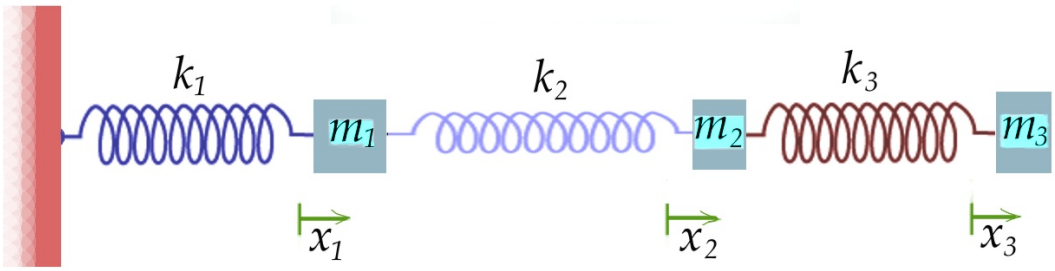

Figure 1: 3 masses on a smooth table connected by springs and fixed to a support to the left, with the masses free to oscillate only in the x direction.

Consider the system in Figure 1. The springs have stiffnesses k_1, k_2, k_3. At instant t mass m_1 is displaced distance x_1 from its equilibrium position, and similarly for the other two. The extensions of the springs are therefore x_1, $x_2 - x_1$ and $x_3 - x_2$ respectively. Assuming no damping, by Newton's second law the equations of motion for each mass are

$$\begin{aligned} -k_1 x_1 + k_2(x_2 - x_1) &= m_1 \ddot{x}_1 \\ -k_2(x_2 - x_1) + k_3(x_3 - x_2) &= m_2 \ddot{x}_2 \\ -k_3(x_3 - x_2) &= m_3 \ddot{x}_3 \end{aligned}$$

where the double dot $\ddot{}$ denotes double differentiation with respect to time. We look for simple harmonic solutions of the form $x = A \sin \omega t$, in which case $\ddot{x} = -\omega^2 x$. Moving to matrix notation, introduce the displacement vector $\mathbf{x}$, mass matrix $\mathbf{M}$ and stiffness matrix[4] $\mathbf{K}$ by:

$$\mathbf{x} = \begin{pmatrix} x_1 \\ x_2 \\ x_3 \end{pmatrix}, \qquad \mathbf{M} = \begin{pmatrix} m_1 & 0 & 0 \\ 0 & m_2 & 0 \\ 0 & 0 & m_3 \end{pmatrix}, \qquad \mathbf{K} = \begin{pmatrix} k_1 + k_2 & -k_2 & 0 \\ -k_2 & k_2 + k_3 & -k_3 \\ 0 & -k_3 & k_3 \end{pmatrix}.$$

The equations of motion in matrix form are

$$\mathbf{K}.\mathbf{x} = -\mathbf{M}.\ddot{\mathbf{x}} = \omega^2 \mathbf{M}.\mathbf{x} \qquad (1a)$$

[4] The change in signs of the spring constants k is common and is done to avoid carrying a minus sign forwards throughout the analysis.

or, in full,

$$\begin{pmatrix} k_1+k_2 & -k_2 & 0 \\ -k_2 & k_2+k_3 & -k_3 \\ 0 & -k_3 & k_3 \end{pmatrix} \begin{pmatrix} x_1 \\ x_2 \\ x_3 \end{pmatrix} = \omega^2 \begin{pmatrix} m_1 & 0 & 0 \\ 0 & m_2 & 0 \\ 0 & 0 & m_3 \end{pmatrix} \begin{pmatrix} x_1 \\ x_2 \\ x_3 \end{pmatrix}. \qquad (1b)$$

In passing, note that the total kinetic energy T in this system is $\frac{1}{2}(m_1\dot{x_1}^2+m_2\dot{x_2}^2+m_3\dot{x_3}^2) = \frac{1}{2}\,\dot{\mathbf{x}}^T\mathbf{M}.\dot{\mathbf{x}}$ where ^{T} denotes matrix transpose. Similarly the elastic potential energy V stored in the springs is $\frac{1}{2}(k_1x_1^2 + k_2(x_2-x_1)^2 + k_3(x_3-x_2)^2) = \frac{1}{2}\,\mathbf{x}^T\mathbf{K}.\mathbf{x}$. Appendix 1 gives an example of equations of motion being derived using Lagrange's equations and presents them in a more general matrix form involving T and V. Eq A6 in Appendix 1 reminds the reader that $\mathbf{M}$ and $\mathbf{K}$ derive respectively from the kinetic and potential energies and their generalisations are $\mathbf{T}$ and $\mathbf{V}$, often obtained from Lagrange's equations. In these terms the general equation of motion for a system of connected masses is $\mathbf{T}\,\ddot{\mathbf{x}} + \mathbf{V}\,\mathbf{x} = 0$ which for oscillations becomes $(\omega^2\mathbf{T} - \mathbf{V})\mathbf{x} = 0$.

Eq 1 is readily written in the standard form for eigenvalue evaluation, $\mathbf{M}^{-1}.\mathbf{K}.\mathbf{x} = \omega^2\mathbf{x}$. Write

$$\mathbf{E} = \mathbf{M}^{-1}.\mathbf{K} = \begin{pmatrix} \frac{k_1+k_2}{m_1} & -\frac{k_2}{m_1} & 0 \\ -\frac{k_2}{m_2} & \frac{k_2+k_3}{m_2} & -\frac{k_3}{m_2} \\ 0 & -\frac{k_3}{m_3} & \frac{k_3}{m_3} \end{pmatrix}. \qquad (2)$$

Let $\mathbf{I}$ be the 3-by-3 identity matrix. The eigenvalues and hence eigenvectors are found by setting the determinant of $(\mathbf{E} - \omega^2\,\mathbf{I})$ to zero, since this is the condition for a non-trivial solution of the simultaneous equations (not all ω zero):

$$\begin{vmatrix} \frac{k_1+k_2}{m_1} - \omega^2 & -\frac{k_2}{m_1} & 0 \\ -\frac{k_2}{m_2} & \frac{k_2+k_3}{m_2} - \omega^2 & -\frac{k_3}{m_2} \\ 0 & -\frac{k_3}{m_3} & \frac{k_3}{m_3} - \omega^2 \end{vmatrix} = 0\,. \qquad (3)$$

The expanded version of this is the characteristic or secular equation and its roots are the three eigenvalues ω^2.

I have chosen this 3-mass-3-spring example because it contains the essential features of these vibration problems without being either too trivial or too computationally opaque. From here on it is best if we assign numerical values and I have chosen

$$m_1 = 4, \quad m_2 = 1, \quad m_3 = 1, \quad k_1 = 2, \quad k_2 = 2, \quad k_3 = 1 \text{ units.}$$

The above determinant evaluates to

$$\begin{vmatrix} 1-\omega^2 & -\frac{1}{2} & 0 \\ -2 & 3-\omega^2 & -1 \\ 0 & -1 & 1-\omega^2 \end{vmatrix} = -(\omega^4 - 4\omega^2 + 1)(\omega^2 - 1) = 0 \qquad (4)$$

so the eigenvalues are

$$\omega_1^2 = 2 - \sqrt{3}, \qquad \omega_2^2 = 1, \qquad \omega_3^2 = 2 + \sqrt{3}$$

and the resonant frequencies are $\omega_1 = 0\cdot518$, $\omega_2 = 1$, $\omega_3 = 1\cdot932$ rad/sec. Each is the frequency of one of the three modes and the respective eigenvalues give the relative displacements of the three masses in that mode. In this case the three frequencies are distinct; there are no degenerate pairs of modes.

Some comments relating to linear algebra may be helpful. The following graphical representation of a 3-by-3 positive definite matrix $\mathbf{E}$ gives insight into the meaning of its eigenvalues and eigenvectors. Think of $\mathbf{E}$ as an operator acting on the position vector $\mathbf{x}$ to map points $\mathbf{x}$ into points $\mathbf{x}'$. Now if $\mathbf{x}$ are points on the unit sphere, centre O, then $\mathbf{x}' = \mathbf{E}.\mathbf{x}$ is an ellipsoid centred on O. Consider the lines formed by joining each point on the sphere to its transformed point. In general these lines will not pass through O, but three will; these are in the directions of the eigenvectors. On these three lines the length from O to the ellipsoid is the respective eigenvalue. The eigenvalues are therefore factors by which the unit sphere is stretched in the only three directions which undergo no rotation under the mapping. Figure 2 is a 2-D illustration of this for the matrix $\mathbf{H} = (4 \quad 2 \mid -1 \quad 1)$. This has eigenvectors in the directions of the two lines $x + y = 0$ and $x + 2y = 0$. The length OA is 2 units, OB is 3, these being the respective eigenvalues. To find the equation of the ellipse note that $\mathbf{H}^{-1} = \frac{1}{6}(1 \quad -2 \mid 1 \quad 4)$ so $x^2 + y^2 = 1 \;\rightarrow\; (x' - 2y')^2 + (x' + 4y)^2 = 36$, which is $x'^2 + 2x'y' + 10y^2 = 18$.

The three eigenvectors of $\mathbf{E}$ will be called $\mathbf{p_1}$, $\mathbf{p_2}$, $\mathbf{p_3}$. They are linearly independent and so form a basis spanning the 3D vector space on which $\mathbf{E}$ operates. This means that all possible free vibrations of the system can be represented as a weighted sum of them. (I will consider in the next sub-section the extent to which motions under external forces can also be so represented.) The eigenvectors are found by substituting each eigenvalue in turn into Eq 4. For example, for mode 2 with $\omega^2 = 1$ we have

$$\begin{pmatrix} 0 & -\frac{1}{2} & 0 \\ -2 & 2 & -1 \\ 0 & -1 & 0 \end{pmatrix} \begin{pmatrix} x_1 \\ x_2 \\ x_3 \end{pmatrix} = 0\,.$$

The solution to this set of indeterminate simultaneous linear equations is

$$\begin{pmatrix} x_1 \\ x_2 \\ x_3 \end{pmatrix} = c \begin{pmatrix} 1 \\ 0 \\ -2 \end{pmatrix} = \begin{pmatrix} p_{12} \\ p_{22} \\ p_{32} \end{pmatrix} = \mathbf{p}_2\,,$$

where c is any constant. In terms of amplitudes of motion, each eigenvector gives the relative displacement of the three masses in the respective mode. The constant c serves to scale the amplitude of all motion in that mode relative to other modes. Thus in mode 2 the central mass remains stationary while the other two move in opposite directions, 180° out of phase, with m_3 always having twice the displacement of m_1. In mode 1 $\mathbf{p_1}$, corresponding to $\omega = 2 - \sqrt{3}$, the displacements of the

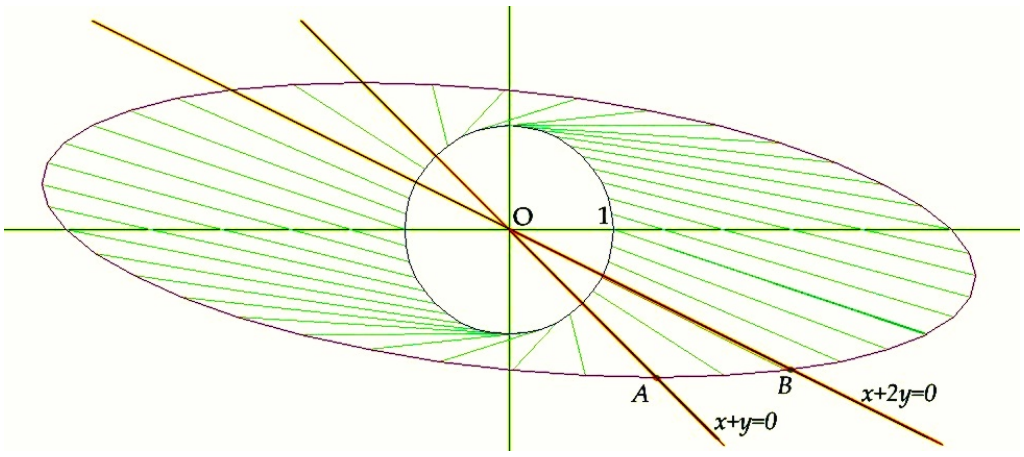

Figure 2: Two-dimensional illustration of a matrix transformation. The unit circle is mapped to an ellipse by $\begin{pmatrix} 4 & 2 \\ -1 & 1 \end{pmatrix}$ through the connecting lines. The eigenvectors are highlighted in red.

three masses are in the ratios $1 : 2(\sqrt{3}-1) : 2$, and $\mathbf{p_3}$ for $\omega_3 = 2+\sqrt{3}$ the ratios are $1 : -2(\sqrt{3}+1) : 2$. (That is $1 : 1\cdot 46 : 2$ and $1: -5\cdot 46 : 2$.)

When our 3-mass system vibrates purely in the ith mode, the equation of motion Eq 1 is $\mathbf{K}.\mathbf{p}_i = \omega_i^2\,\mathbf{M}.\mathbf{p}_i$ where $\mathbf{p_i}$ are the eigenvectors, $i = 1, 2, 3$. The symmetry of both $\mathbf{M}$ and $\mathbf{K}$ leads to the eigenvectors being orthogonal in the sense that $\mathbf{p_i}^T.\mathbf{M}.\mathbf{p_j}$ and $\mathbf{p_i}^T.\mathbf{K}.\mathbf{p_j}$ are zero unless $i = j$. Proof of this uses the property of transposes of any two matrices, $\mathbf{A}$ and $\mathbf{B}$, that $(\mathbf{A}.\mathbf{B})^T = \mathbf{B}^T.\mathbf{A}^T$. First pre-multiply the jth equation of motion $\mathbf{K}.\mathbf{p}_j = \omega_j^2\,\mathbf{M}.\mathbf{p}_j$ by $\mathbf{p_i}^T$:

$$\mathbf{p_i}^T\mathbf{K}.\mathbf{p}_j \;=\; \omega_j^2\,\mathbf{p_i}^T\mathbf{M}.\mathbf{p_j} \tag{5a}$$

Similarly premultiply the equivalent equation for the ith mode by $\mathbf{p_j}^T$:

$$\mathbf{p_j}^T(\mathbf{K}.\mathbf{p_i}) \;=\; \omega_i^2\,\mathbf{p_j}^T(\mathbf{M}.\mathbf{p_i})$$

Now transpose twice in turn:

$$(\mathbf{K}.\mathbf{p_i})^T\mathbf{p_j} \;=\; \omega_i^2\,(\mathbf{M}.\mathbf{p_i})^T.\mathbf{p_j}$$
$$\mathbf{p_i}^T\mathbf{K}^T\mathbf{p_j} \;=\; \omega_i^2\,\mathbf{p_i}^T\mathbf{M}^T.\mathbf{p_j}$$

But $\mathbf{K}^T = \mathbf{K}$ and $\mathbf{M}^T = \mathbf{M}$ so

$$\mathbf{p_i}^T\mathbf{K}.\mathbf{p}_j = \omega_i^2\,\mathbf{p_i}^T\mathbf{M}.\mathbf{p_j} \tag{5b}$$

which is Eq 5a with ω_i instead of ω_j. Because these two frequencies are distinct, Eqs 5a, b can be equal only if both sides are 0. If $i = j$, we have $\mathbf{p_j}^T\mathbf{K}.\mathbf{p}_j \;=\; \omega_j^2\,\mathbf{p_j}^T\mathbf{M}.\mathbf{p_j}$. The left side of this is proportional to the potential energy in the springs and the right side to the kinetic energy in the masses.

Amongst users of finite element analysis it is usual to normalise the eigenvectors by choosing the scaling constants c so that $(\mathbf{p})^T.\mathbf{M}.(\mathbf{p}) = 1$. This is called 'mass normalisation'.

- For the first eigenvector $c_1 = 1/\sqrt{8[3-\sqrt{3}]} = 0\cdot 3140$,
- for the second $c_2 = 1/\sqrt{8} = 0\cdot 3536$,
- for the third, $c_3 = 1/\sqrt{8[3+\sqrt{3}]} = 0\cdot 1625$.

Mass normalisation allows some simplification. For instance in the equation of motion for the j^{th} normal mode, $\mathbf{p_j}^T\mathbf{K}.\mathbf{p}_j \;=\; \omega_j^2\,\mathbf{p_j}^T\mathbf{M}.\mathbf{p_j}$, the right side is now just ω_j^2. More generally

$$\text{If}\quad \mathbf{P}^T.\mathbf{M}.\mathbf{P} = \mathbf{I} \qquad \text{then} \qquad \mathbf{P}^T.\mathbf{K}.\mathbf{P} \;=\; \text{diag}(\omega_1^2, \omega_2^2, \omega_3^2) \;=\; \mathbf{\Omega}\,. \tag{6}$$

Texts of linear algebra prove that a square matrix such as $\mathbf{E}$ whose eigenvalues are all distinct can be mapped into an equivalent or conjugate diagonal matrix. This is a remarkable and very useful property since when the matrix form is diagonal, the equations of motions $(\mathbf{E}-\omega^2\,\mathbf{I})$ for the N degrees of freedom become uncoupled into N separate, independent equations, a much simpler description. The transformation which diagonalises a matrix A is called a 'similarity' transformation. We say that square matrices $\mathbf{A}$ and $\mathbf{D}$ are similar if there exists an invertible matrix $\mathbf{P}$ such that $\mathbf{P}.\mathbf{D} = \mathbf{A}.\mathbf{P}$, or $\mathbf{D} = \mathbf{P}^{-1}\mathbf{A}.\mathbf{P}$. $\mathbf{A}$ and $\mathbf{D}$ have the same eigenvalues and these appear explicitly as diagonal elements of $\mathbf{D}$. Such a matrix $\mathbf{P}$ is readily constructed by making its columns the eigenvectors of $\mathbf{A}$.

Now apply this to $\mathbf{E}$. We will follow the convention of finite element analysis (FEA) and have the eigenvectors $\mathbf{p_j}$ mass-normalised. Recall that in our 3-mass example, $c_1 = 0\cdot 314$, $c_2 = 0\cdot 3536$, $c_3 = 0\cdot 1625$. The transformation matrix made from these eigenvectors is

$$\mathbf{P} \;=\; \begin{pmatrix} c_1 & c_2 & c_3 \\ 2c_1(\sqrt{3}-1) & 0 & -2c_3(\sqrt{3}+1) \\ 2c_1 & -2c_2 & 2c_3 \end{pmatrix} \;=\; \begin{pmatrix} 0\cdot 3140 & 0\cdot 3536 & 0\cdot 1625 \\ 0\cdot 4597 & 0 & -0\cdot 8881 \\ 0\cdot 6280 & -0\cdot 7071 & 0\cdot 3251 \end{pmatrix}. \qquad (7a)$$

We will also need the inverse of $\mathbf{P}$ which is

$$\mathbf{P}^{-1} \;=\; \begin{pmatrix} 1\cdot 2559 & 0\cdot 4597 & 0\cdot 6280 \\ 1\cdot 4142 & 0 & -0\cdot 7071 \\ 0\cdot 6501 & -0\cdot 8881 & 0\cdot 3251 \end{pmatrix}. \qquad (7b)$$

As direct calculation will verify, $\mathbf{P}$ will map $\mathbf{E}$ into the diagonal matrix $\mathbf{\Omega}$ whose elements are the eigenvalues

$$\mathbf{P}^{-1}.\mathbf{E}.\mathbf{P} \;=\; \mathrm{diag}(\omega_1^2, \omega_2^2, \omega_3^2) \;=\; \mathbf{\Omega}\,. \qquad (8)$$

In the diagonalised matrix equation of motion each row is a separate, independent equation in a new variable, η_1, η_2, η_3 respectively. (η seems to be the widely used notation.) These are the 'modal' or 'normal co-ordinates'. In general in a system with N degrees of freedom there are N normal modes and N co-ordinates. The orthogonal property ensures that they are independent – motion in one mode cannot affect motion in any of the others. Hence they form a basis for describing any small amplitude vibration of the system. In normal co-ordinates we have simple harmonic motion:

$$\ddot{\boldsymbol{\eta}} + \mathbf{\Omega}\boldsymbol{\eta} \;=\; 0\,. \qquad (9)$$

The general solution for the i^{th} mode is $\eta_i = C_i\cos\omega_i t + D_i\sin\omega_i t$. Only one ω features in each modal solution, meaning that in this mode all masses and springs oscillate at this one frequency. Each normal co-ordinate is a linear combination of the space co-ordinates x_1, x_2, x_3. It is the matrix $\mathbf{P}$ which transforms between the two co-ordinate systems:

$$\mathbf{x} \;=\; \mathbf{P}\,\boldsymbol{\eta} \quad \text{and conversely} \quad \boldsymbol{\eta} \;=\; \mathbf{P}^{-1}\,\mathbf{x}\,. \qquad (10)$$

This is readily seen by comparing equivalent ways of writing the equations of motion:

$$\mathbf{E}\mathbf{x} \;=\; -\ddot{\mathbf{x}}$$

$$\mathbf{\Omega}\boldsymbol{\eta} \;\equiv\; \mathbf{P}^{-1}\mathbf{E}\mathbf{P}\boldsymbol{\eta} \;=\; -\ddot{\boldsymbol{\eta}}$$

$$\mathbf{E}\mathbf{P}\boldsymbol{\eta} \;=\; -\mathbf{P}\ddot{\boldsymbol{\eta}}$$

$$\text{so} \quad \mathbf{P}\boldsymbol{\eta} \;=\; \mathbf{x} \quad \text{and} \quad \mathbf{P}\ddot{\boldsymbol{\eta}} \;=\; \ddot{\mathbf{x}}\,.$$

Eqs 9 and 10 are key results. The linear combination of x_1, x_2, x_3 which are equivalent to each of the normal co-ordinates can be read directly from the $\mathbf{P}^{-1}$. Bearing in mind that only ratios of amplitudes are significant,

$$\begin{aligned} \eta_1 &= 1\cdot 256x_1 + 0\cdot 460x_2 + 0\cdot 628x_3\,, \\ \eta_2 &= 2x_1 - x_3\,, \\ \eta_3 &= 0\cdot 650x_1 - 0\cdot 888x_2 + 0\cdot 325x_3 \end{aligned} \qquad (11)$$

or any multiple of these is a set of normal co-ordinates. Specific values determine modal displacements.

2.1 Example: Given initial conditions

I close this section with an example of how free motion after an initial disturbance can be described by a sum of normal modes. Whilst carefully selected initial conditions will cause only one mode to be excited, in general all three will be excited to some degree. Suppose mass 3 is given an initial displacement of $0\cdot05$ m and released from rest, the other masses being held for that moment in their undisturbed positions[5]. The subsequent motion will be a sum of normal modes and we must now find their weightings. Using matrix $\mathbf{P}$

$$x_1 \;=\; 0\cdot314(C_1\cos\omega_1 + D_1\sin\omega_1 t) \;+\; 0\cdot354(C_2\cos\omega_2 + D_2\sin\omega_2 t) \;+\; 0\cdot163(C_3\cos\omega_3 t + D_3\sin\omega_3 t)$$

and similarly for x_2, x_3. At $t = 0$ the displacement and velocity are

$$x_1(0) \;=\; 0\cdot314C_1 + \;0\cdot354C_2 + 0\cdot163C_3 \;=\; 0$$

$$\dot{x_1}(0) \;=\; 0\cdot314D_1 + \;0\cdot354D_2 + \;0\cdot163D_3 \;=0\,.$$

Similarly

$$x_2(0) \;=\; 0\cdot46C_1 - \;0\cdot888C_3 \;=\; 0$$

$$\dot{x_2}(0) \;=\; 0\cdot46D_1 - \;0\cdot888D_3 \;=0\,.$$

$$x_3(0) \;=\; 0\cdot628C_1 - \;0\cdot707C_2 + 0\cdot325C_3 \;=\; 0\cdot05$$

$$\dot{x_1}(0) \;=\; 0\cdot628D_1 - \;0\cdot707D_2 + \;0\cdot325D_3 \;=0\,.$$

The initial velocities can all be made zero simply by setting $D_1 = D_2 = D_3 = 0$. The remaining equations are

$$\mathbf{P}.\begin{pmatrix}C_1\\C_2\\C_3\end{pmatrix} \;=\; \begin{pmatrix}0\\0\\0\cdot05\end{pmatrix}$$

with solution

$$\begin{pmatrix}C_1\\C_2\\C_3\end{pmatrix} \;=\; \mathbf{P}^{-1}.\begin{pmatrix}0\\0\\0\cdot05\end{pmatrix} \;=\; \begin{pmatrix}0\cdot03140\\-0\cdot03536\\0\cdot01625\end{pmatrix},$$

numbers remarkably similar to those defining x_1. The displacements are therefore

$$\begin{aligned} x_1 \;&= 0\cdot00986\cos\omega_1 t - 0\cdot01250\cos\omega_2 t + 0\cdot00264\cos\omega_3 t\,,\\ x_2 \;&= 0\cdot01443\cos\omega_1 t - 0\cdot01443\cos\omega_3 t\,,\\ x_3 \;&= 0\cdot01972\cos\omega_1 t + 0\cdot02500\cos\omega_2 t - 0\cdot00528\cos\omega_3 t \qquad (12)\\ \omega_1 \;&=\; 0\cdot518, \qquad \omega_2 \;= 1\cdot000, \qquad \omega_1 \;=\; 1\cdot932\,. \end{aligned}$$

In matrix form

$$\mathbf{x}(t) \;=\; \mathbf{P}.\begin{pmatrix}C_1\cos\omega_1 t\\C_2\cos\omega_2 t\\C_3\cos\omega_3 t\end{pmatrix}.$$

[5] These mechanics textbook questions are quite contrived. To achieve a displacement of mass 3 alone would require a force equal and opposite to the tension in spring 3 to be applied to mass 2 to hold it in position, a situation of initial internal stress. Release of mass 3 would require simultaneous release of the constraint on mass 2.

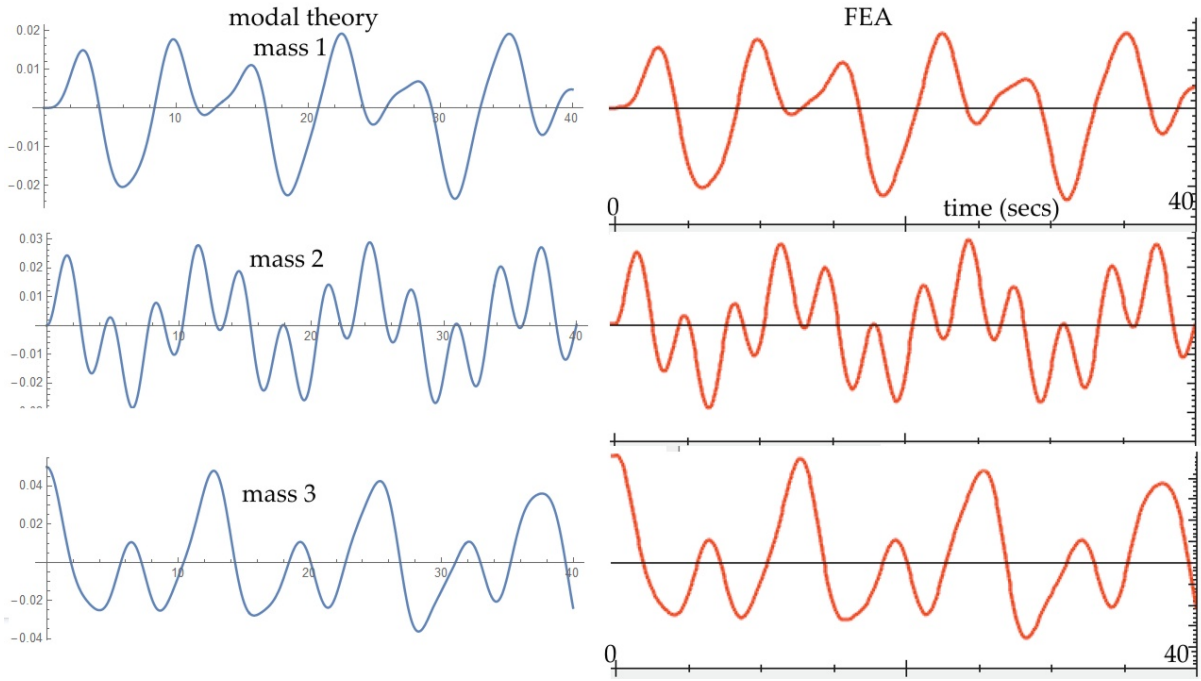

Figure 3: Displacement of the three mass in Figure 1 after m_3 is given initial displacement of $0 \cdot 05$ m. Left panel: sum of normal modes, Eq 11. Right : FEA results from Mecway 3.

The wave forms of the three masses for the first 40 seconds are plotted in the left panel of Figure 3 from Eqs 11. I also used the finite element program Mecway 3 to calculate the response and its results are in the right panel. This used a time step of 1/20 sec. and the initial condition was approached by letting the equal and opposite forces on masses 2 and 3 increase linearly and very slowly (over 80 secs) from zero before being switched off. There is close agreement with the displacement, though less so with the velocities. None of the masses move periodically because the values of ω_1, ω_2 and ω_1 have no common factor.

To round off this section, here is a list of the main properties which characterise normal modes:

1. A normal, characteristic or free mode is a pattern of motion encompassing all particles of the system and occurs in the absence of external disturbances.

2. In a normal mode all particles move sinusoidally at the same frequency.

3. In each normal mode the relative amplitudes of the particles remain constant. Their absolute amplitudes depend on the initial disturbance which set the mode in motion.

4. All free motions of the system can, within the linear approximation, be compounded as a superposition of normal modes.

3 Periodic forced oscillations

We now examine how each modal pattern contributes to more complicated motion under an external driving force. External forces can act on one or more masses, or by causing prescribed motion of the support to which the springs are attached. I am ultimately interested in the motion of the top plate of a violin under the action of forces applied at the two feet of the bridge, which in turn is driven by a string oscillating under the slip-stick drag of the bow hairs. Strictly the whole system should be modelled rather than just the wooden plate because the applied forces under the bridge will be modified by reaction of the plate back on the bridge. This would be too complicated, however, so I must settle for prescribing some plausible periodic, non-harmonic forces applied simultaneously at two positions. Such forces can be specified in essentially two ways:

- as functions of time in which $F(t)$ is given by an analytic expression or as a sequence of point values each separated by a time step h,
- as a spectrum of continuous sinusoidal forces, following Fourier's theorem.

The temporal approach will assume that the system starts from rest at time $t = 0$ and displacements will grow with time after the forces are switched on. The spectral approach assumes that the forces have been operating sufficiently long that a steady state has been reached.

It is well known that the most general solution of the equation

$$\mathbf{M}\,\ddot{\mathbf{x}} + \mathbf{K}\,\mathbf{x} \;=\; \mathbf{F}(t) \tag{13}$$

has two parts

- a 'complementary function' $\mathbf{x}_c$ which solves $\mathbf{M}\,\ddot{\mathbf{x}}_c + \mathbf{K}\,\mathbf{x}_c = 0$ and so describes the transients when the forces are switched on and immediately after they have been switched off,
- a 'particular solution'. To find this one usually substitutes a trial $\mathbf{x}(t)$ with the same type of structure as $\mathbf{F}(t)$. This often works because the driven system tends to follow the applied forces.

In this study I am interested mainly in the particular solution. To deal with the transients, I notionally introduce weak attenuation through a damping term Δ. The true matrix equation of motion is therefore

$$\mathbf{M}\,\ddot{\mathbf{x}} + \boldsymbol{\Delta}\,\dot{\mathbf{x}} + \mathbf{K}\,\mathbf{x} \;=\; \mathbf{F}(t)$$

though by taking $\boldsymbol{\Delta}$ very small the equation to be solved remains Eq 13.

The equations for the individual masses contained within Eq 13 will in general be coupled and hence difficult to solve as such. The diagonalisation which separates Eq 13 into independent normal modes can be applied here and the relation $\mathbf{x} = \mathbf{P}\,\eta$ of Eq 10 still holds. Let $\mathbf{P}$ be mass normalised. If Eq 13 is now multiplied on the left by $\mathbf{P}^T$, Eq 6 can be used to obtain

$$\ddot{\boldsymbol{\eta}} + \boldsymbol{\Omega}\,\boldsymbol{\eta} \;=\; \mathbf{P}^T\,\mathbf{F}(t) \;=\; \mathbf{f}(t)\,.$$

$\mathbf{f}(t)$ are called 'modal forces'; they distribute the applied forces across the three modes in proportion the relative displacements in each mode. At this stage I wish to change the notation for the modal displacement from $\boldsymbol{\eta}$ to $\boldsymbol{\xi}$. I will keep $\boldsymbol{\eta}$ for the free modes in which the relative displacements of the masses in the j^{th} normal mode are given by the respective eigenvector p_j. We have yet to assess the meaning of modal displacement when the motion is forced. Accordingly we will work with the modal equation of motion in the form

$$\ddot{\boldsymbol{\xi}} + \boldsymbol{\Omega}\,\boldsymbol{\xi} \;=\; \mathbf{P}^T\,\mathbf{F}(t) \;=\; \mathbf{f}(t)\,. \tag{14}$$

3.1 Sinusoidal forces

If the applied forces are strictly sinusoidal, Eq 14 represents a set of independent equations of driven SHM type. For example, if there are three applied sinusoidal forces with frequencies μ_1, μ_2, μ_3 applied at three separate points of the system, each modal force f_j might have the form

$$a_j \sin \mu_1 t + b_j \sin \mu_2 t + c_j \cos \mu_3 t \,.$$

The particular solution to the equation

$$\ddot{\xi}_j + \omega_j^2 \xi \;=\; a_j \sin \mu_1 t + b_j \sin \mu_2 t + c_j \cos \mu_3 t$$

$$\text{is} \qquad \xi_j \;=\; \frac{a_j \sin \mu_1 t}{\omega_j^2 - \mu_1^2} \;+\; \frac{b_j \sin \mu_2 t}{\omega_j^2 - \mu_2^2} \;+\; \frac{c_j \cos \mu_3 t}{\omega_j^2 - \mu_3^2} \,. \tag{15}$$

Particular solutions always have this form, with each sine or cosine in the expression for the force producing respectively a sine or cosine term in the solution. The solution states that each mass moves as the sum of the imposed sine waves, the amplitudes of which are modulated not just by the strength of the applied forces, but by the proximity of the forcing frequencies to the natural frequencies. Clearly the amplitude of motion increases in a singular way if any of the applied frequencies μ_k approaches the modal frequency ω_j. This is the well known condition for resonance. In practice the amplitudes of vibration are limited only by resistive damping. Once the motion in modal co-ordinates $\boldsymbol{\xi}$ has been determined, the displacements x_j can be found as before from Eq 10, namely $\mathbf{x} = \mathbf{P}\boldsymbol{\xi}$. A numerical example based on the 3-mass-3-spring system of Figure 1 will demonstrates the mathematical procedure.

Suppose therefore that in the 3-mass-3-spring example of Figure 1 a force $F_1 = A_1 \sin \mu_1 t$ is applied to mass m_1 and $F_3 = A_3 \sin \mu_3 t$ to m_3. The forces started from time $t = 0$, sufficiently long ago that the complementary solutions due to the force switching on have died away. The modal forces are

$$\mathbf{P}^T\mathbf{F} \;=\; \mathbf{P}^T \begin{pmatrix} A_1 \sin \mu_1 t \\ 0 \\ A_3 \sin \mu_3 t \end{pmatrix} \quad \rightarrow \quad \begin{pmatrix} 0\cdot 314\, A_1 \sin \mu_1 t \;+\; 0\cdot 628\, A_3 \sin \mu_3 t \\ 0\cdot 356\, A_1 \sin \mu_1 t \;-\; 0\cdot 707\, A_3 \sin \mu_3 t \\ 0\cdot 163\, A_1 \sin \mu_1 t \;-\; 0\cdot 325\, A_3 \sin \mu_3 t \end{pmatrix} \;=\; \mathbf{f}(t) \,. \tag{16}$$

Take $A_1 = 0{\cdot}1$ units, $\mu_1 = 0{\cdot}6$ radians/sec, $A_3 = -0{\cdot}2$, $\mu_3 = 1{\cdot}6$. Thus μ_1 is fairly close to the resonant frequency at $0\cdot 518$ and μ_3 is between the natural frequencies at 1 and $1\cdot 93$ rads/sec but well away from both. We can anticipate that motion at $\mu_1 = 0\cdot 6$ will be amplified through the denominator of Eq 15. With these values the modal forces are

$$\mathbf{f} \;=\; \begin{pmatrix} 0{\cdot}0314 \sin 0{\cdot}6t \;-\; 0{\cdot}126 \sin 1{\cdot}6t \\ 0{\cdot}0354 \sin 0{\cdot}6t \;+\; 0{\cdot}141 \sin 1{\cdot}6t \\ 0{\cdot}0163 \sin 0{\cdot}6t \;-\; 0{\cdot}065 \sin 1{\cdot}6t \end{pmatrix}.$$

The solution for modal co-ordinate ξ_1 is

$$\xi_1 \;=\; \frac{0{\cdot}0314 \sin \mu_1 t}{\omega_1^2 - \mu_1^2} \;-\; \frac{0{\cdot}126 \sin \mu_3 t}{\omega_1^2 - \mu_3^2} \;=\; -0{\cdot}341 \sin 0{\cdot}6t \;+\; 0{\cdot}0548 \sin 1{\cdot}6t \,. \tag{17}$$

Including the other two modes in a similar way gives

$$\mathbf{x} \;=\; \mathbf{P}\boldsymbol{\xi} \;=\; \mathbf{P}. \begin{pmatrix} -0{\cdot}3411 \sin 0{\cdot}6t \;+\; 0{\cdot}0548 \sin 1{\cdot}6t \\ 0{\cdot}0552 \sin 0{\cdot}6t \;-\; 0{\cdot}0907 \sin 1{\cdot}6t \\ 0{\cdot}0048 \sin 0{\cdot}6t \;-\; 0{\cdot}0555 \sin 1{\cdot}6t \end{pmatrix}$$

$$\mathbf{x} \;=\; \begin{pmatrix} -0{\cdot}0868\sin 0{\cdot}6t \;-\; 0{\cdot}0239\sin 1{\cdot}6t \\ -0{\cdot}1611\sin 0{\cdot}6t \;+\; 0{\cdot}0744\sin 1{\cdot}6t \\ -0{\cdot}2517\sin 0{\cdot}6t \;+\; 0{\cdot}0805\sin 1{\cdot}6t \end{pmatrix}. \tag{18}$$

As expected, the coefficient $0\cdot3412$ of $\sin(0\cdot6t)$ in mode 1 is much larger than any other coefficient. It has been augmented through the proximity of $0\cdot6$ to $\omega_1 = 0\cdot52$ rads/sec. Figure 4 plots the displacements of the three masses from $t = 0$ to 220 seconds[6]. The displacement of m_3 is far the largest. All three graphs are quasi-periodic with 21 cycles in 220 seconds, a frequency of $0\cdot6$ rad/sec. The impressed force at the higher frequency adds only decoration, despite being twice as strong (amplitude $0\cdot2$ compared with $0\cdot1$ at $0\cdot6$ rad/sec).

3.2 Driven modes

The mathematical machinery has produced the mode-like quantities $\mathbf{f}$ and $\boldsymbol{\xi}$ so it is fair to ask to what extent modes can be recognised in periodic forced oscillation. $\boldsymbol{\xi}$ is the counterpart of the normal co-ordinates (modal displacements) $\boldsymbol{\eta}$ of free motion. As a working term I will call these 'forced modes' or 'driven modes'. To start let us determine conditions in which only one such mode is excited. Suppose this one mode has frequency μ. From Eq 14 $\mathbf{F(t)} = (\mathbf{P}^T)^{-1}\mathbf{f}$. There are three possibilities:

$$\text{mode } \xi_1: \qquad (\mathbf{P}^T)^{-1}\begin{pmatrix}\sin\mu t\\0\\0\end{pmatrix} \;=\; 0\cdot628\begin{pmatrix}2\\\sqrt{3}-1\\1\end{pmatrix}\sin\mu t\,,$$

[6] I accept that the complementary functions would need to be added to $\boldsymbol{\xi}$ if we were concerned about the actual behaviour near $t = 0$. However, all that need be illustrated here is the general form of the displacements under the applied periodic forces.

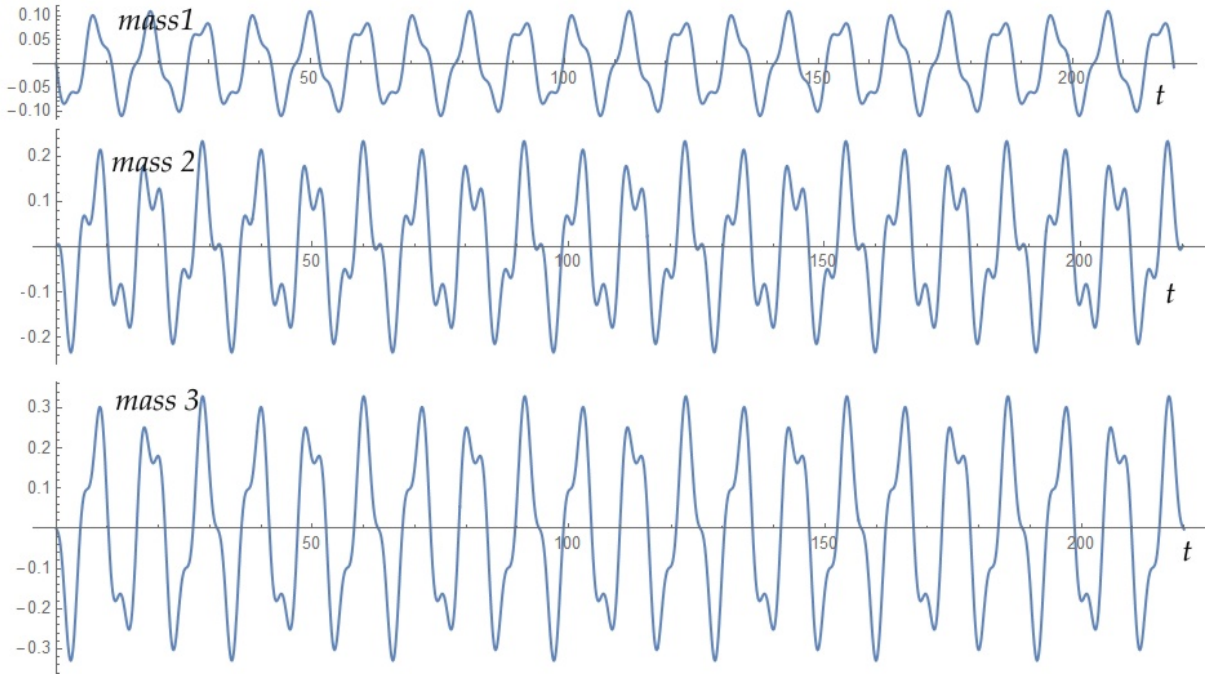

Figure 4: Displacements of the 3 masses of Figure 1 under forces $0{\cdot}1\sin 0{\cdot}6t$ on mass 1 and $-0{\cdot}2\sin 1{\cdot}6t$ on mass 3.

$$\text{mode } \xi_2: \qquad (\mathbf{P}^T)^{-1}\begin{pmatrix}0\\ \sin\mu t\\ 0\end{pmatrix} = 0\cdot 707\begin{pmatrix}2\\ 0\\ -1\end{pmatrix}\sin\mu t\,, \tag{19}$$

$$\text{mode } \xi_3: \qquad (\mathbf{P}^T)^{-1}\begin{pmatrix}0\\ 0\\ \sin\mu t\end{pmatrix} = 0\cdot 325\begin{pmatrix}2\\ -\sqrt{3}-1\\ 1\end{pmatrix}\sin\mu t\,.$$

Referring back to the value of $\mathbf{P}$ at Eq 7a, the modal displacements ξ_j and physical displacements $\mathbf{x}$ corresponding to these single modal forces are respectively

$$\xi_1 = \begin{pmatrix}\frac{\sin\mu t}{\omega_1^2-\mu^2}\\ 0\\ 0\end{pmatrix} \quad \text{giving} \quad \mathbf{x} = \frac{c_1\sin\mu t}{\omega_1^2-\mu^2}\begin{pmatrix}1\\ 2(\sqrt{3}-1)\\ 2\end{pmatrix}, \qquad c_1 = \frac{1}{\sqrt{8(3-\sqrt{3})}},$$

$$\xi_2 = \begin{pmatrix}0\\ \frac{\sin\mu t}{\omega_2^2-\mu^2}\\ 0\end{pmatrix} \quad \text{giving} \quad \mathbf{x} = \frac{c_2\sin\mu t}{\omega_2^2-\mu^2}\begin{pmatrix}1\\ 0\\ -2\end{pmatrix}, \qquad c_2 = \frac{1}{\sqrt{8}}, \tag{20}$$

$$\xi_3 = \begin{pmatrix}0\\ 0\\ \frac{\sin\mu t}{\omega_3^2-\mu^2}\end{pmatrix} \quad \text{giving} \quad \mathbf{x} = \frac{c_3\sin\mu t}{\omega_3^2-\mu^2}\begin{pmatrix}1\\ -2(\sqrt{3}+1)\\ 2\end{pmatrix}, \qquad c_3 = \frac{1}{\sqrt{8(3+\sqrt{3})}}.$$

Observe that the ratios of mass displacements are the same as the ratios in the corresponding free normal mode, and these ratios are independent of μ.

In addition the three ratios of force amplitudes in Eq 19 are characteristic of the system. Forces applied to the three masses in any of these ratios will produce displacements which are affected by only one mode of the structure. I have confirmed these predictions numerically using FEA with Mecway. In one case, for instance, apply the forces $F(t) = (0\cdot 2, 0\cdot 0732, 0\cdot 1)\sin 1\cdot 02\,t$ units to the masses (m_1, m_2, m_3) respectively. This frequency is very close to the resonance at $\omega_2 = 1$ so we might intuitively expect extremely large amplitudes, as would occur if only one force were applied. In fact the three forces restrain each other and the structure, as the following calculation shows.

$$\mathbf{f} = \begin{pmatrix}0\cdot 159\sin(1\cdot 02\,t)\\ 0\\ 0\end{pmatrix}, \qquad \boldsymbol{\xi} = \begin{pmatrix}-0\cdot 206\sin(1\cdot 02\,t)\\ 0\\ 0\end{pmatrix}$$

on dividing by $\omega_1^2-\mu^2$. Finally

$$\mathbf{x} = \mathbf{P}\boldsymbol{\xi} = -0\cdot 0647\sin(1\cdot 02\,t)\begin{pmatrix}1\\ 1\cdot 464\\ 2\end{pmatrix}, \qquad 1\cdot 464 = 2(\sqrt{3}-1)\,.$$

All displacements are finite – resonance has been blocked. Similarly, the ξ_2 force set in Eq 19 will block resonances at ω_1 and ω_3, and ξ_3 will block resonances at ω_1 and ω_2.

Here is a general proof of these important points. Suppose only one modal force $f_j\sin\mu t$ is applied so only the j^{th} modal displacement is non-zero. Let σ_j stand for $\omega_j^2-\mu^2$. The particular

solutions of the equations of motion are $\xi_j = f_j/\sigma_j \sin\mu t$, and $\xi_k = 0, k \neq j$. The particle displacements are

$$\mathbf{x} = \begin{pmatrix} p_{11} & p_{21} & \cdots & p_{j1} & \cdots \\ p_{12} & p_{22} & \cdots & p_{j2} & \cdots \\ \cdots & \cdots & \cdots & \cdots & \cdots \\ p_{1j} & p_{2j} & \cdots & p_{jj} & \cdots \\ \cdots & \cdots & \cdots & \cdots & \cdots \end{pmatrix} \begin{pmatrix} 0 \\ 0 \\ \cdots \\ f_j/\sigma_j \\ \cdots \end{pmatrix} \sin\mu t = \frac{f_j}{\sigma_j} \begin{pmatrix} p_{j1} \\ p_{j2} \\ \cdots \\ p_{jj} \\ \cdots \end{pmatrix} \sin\mu t = \frac{f_j}{\sigma_j} \mathbf{p_j} \sin\mu t\,,$$

$\mathbf{p_j}$ being the eigenvector of the j^{th} free mode, as used in the construction of $\mathbf{P}$.

In summary, it is reasonable to speak of 'driven modes' where each mode represents both

1. the amplitude ratios of a set of sinusoidal forces, all at the same frequency μ, applied at the various masses such that the motion of the particles is modulated by only one of the natural frequencies of the system, and
2. the resulting amplitude ratios of the masses, this being the same as in the corresponding free mode.

The relative displacements are *independent of the applied frequency* μ. The absolute displacements are determined by the magnitude of the applied forces and by the proximity of μ to the natural frequency ω_j through the denominator $\omega_j^2 - \mu^2$. The linear relation $\mathbf{f} = \mathbf{P}^T\mathbf{F}(t)$ ensures that any applied force $\mathbf{F}$ can be represented as a sum of modal forces, and hence the resulting motion as a sum of modal displacements $\boldsymbol{\xi}$. This runs parallel to the behaviour of a free system where any free motion can be represented as a sum of normal modes matched to the initial conditions. All this considered, driven modes are essentially the same as natural modes except that the natural frequency ω is replaced by the driving frequency μ.

3.3 Frequency response spectra

It is common to show the response of an oscillating system to an applied sinusoidal force by plotting the displacement amplitude and phase as functions of the frequency μ. With a one-mass system the amplitude spectrum is just a single graph with a spike at the single resonance frequency, but with our 3-mass-3-spring system a single force can be applied to any of the masses and the displacements of each plotted. Figure 5 shows the displacements of the three masses when a unit force $\sin\mu t$ is applied to mass 1 (top panel), mass 2 (centre) or to mass 3 (bottom). The singularities are at the three resonant frequencies, $\omega_1 = 0 \cdot 518$ rad/sec, $\omega_2 = 1$, $\omega_3 = 1 \cdot 93$. It is notable that when the force is on the middle mass m_2, there is no resonance at $\omega_2 = 1$; indeed, the displacement of m_2 at $\mu = 1$ is zero.

There is a second way in which frequency response can be considered, in terms of modal forces and modal displacements rather than forces on masses and displacement of masses as in Figure 5. Bear in mind that the scheme of calculation progresses through the sequence

$$\text{force } \mathbf{F} \text{ on masses} \rightarrow \text{modal forces } \mathbf{f} \rightarrow \text{modal displacements } \boldsymbol{\xi} \rightarrow \text{ mass displacements } \mathbf{x}.$$

There is only one modal displacement $\boldsymbol{\xi}_j$ for a single modal force $\mathbf{f}_j$ and its graph has one singularity at $\mu = \omega_j$. The corresponding x displacements for unit modal force are plotted in Figure 6. The graphs in Figure 5 are a sum of these, weighted according to $\mathbf{f} = \mathbf{P}^T\mathbf{F}$.

Let us now place this in the context of the 3-mass system radiating musical sounds. In a practical mechanical arrangement the masses could be metal plates stacked parallel to each other

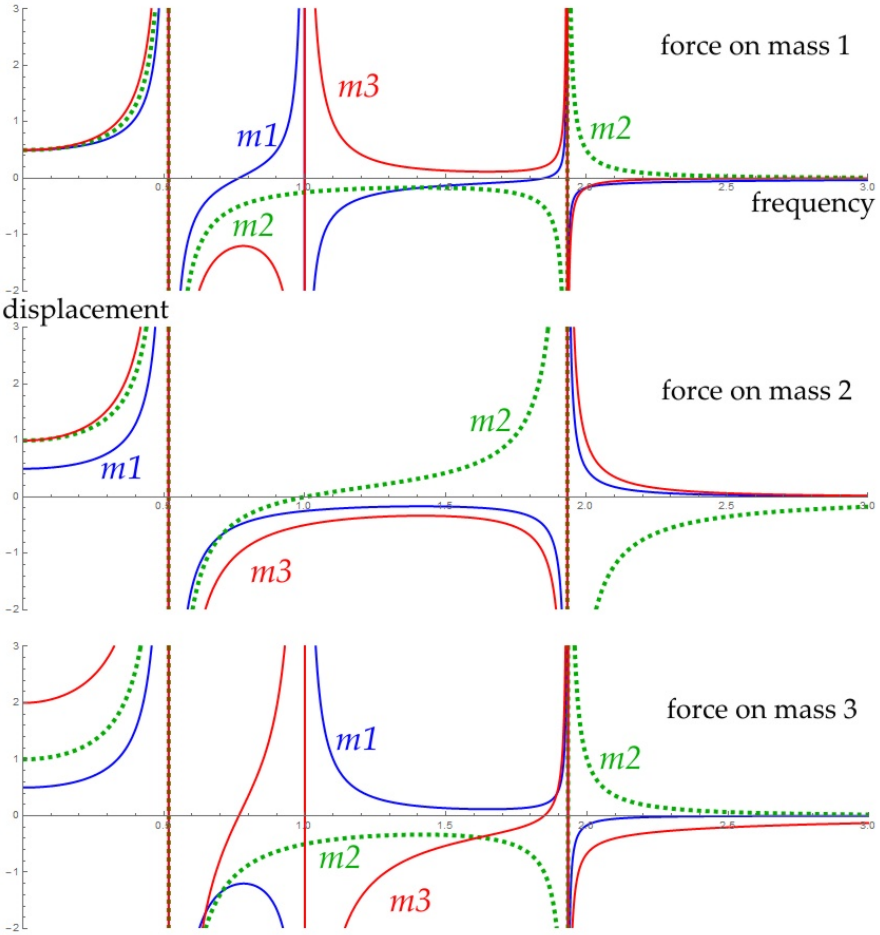

Figure 5: Frequency responses of 3-mass-3-spring system of Figure 1 to single unit force $\sin \mu t$ applied to each mass in turn. Blue: displacement amplitude of mass 1. Green dashed: displacement of mass 2. Red: displacement of mass 3.

and joined by fairly short springs. We assume that the frequencies are at musical pitch. The interval between ω_1 and ω_3 is about 1 semitone less than two octaves – say C below middle C to B above middle C. The listener is positioned in the far field in the direction of the line of springs, normal to the plates. We also assume that the plates do not mask one another yet are sufficiently close compared with the smallest wavelength of interest that all the sound can be regarded as coming from the same position. Then the phase differences between the three sources are determined solely by the + or − signs shown in Figure 6. We can further suppose that the emitted sound amplitude is proportional to the product of its area and its velocity, and that the area of each plate is proportional to its mass. The sound wave at the listener due to motion in mode j is then proportional to the algebraic sum over the three plates

$$\mu \cos(\mu t) \left(m_1 x_{j1} + m_2 x_{j2} + m_3 x_{j3}\right). \tag{21}$$

(The factor μ comes from $d \cos \mu t/dt$ to obtain the velocity.) Figure 7 plots the spectrum of this combined sound amplitude when each mode separately is driven by unit modal force at frequency μ. The formulae for these curves for modes 1, 2, 3 respectively are

$$\frac{2 \cdot 34\mu}{0 \cdot 268 - \mu^2}, \qquad \frac{0 \cdot 707\mu}{1 - \mu^2}, \qquad \frac{0 \cdot 087\mu}{3 \cdot 732 - \mu^2}. \tag{22}$$

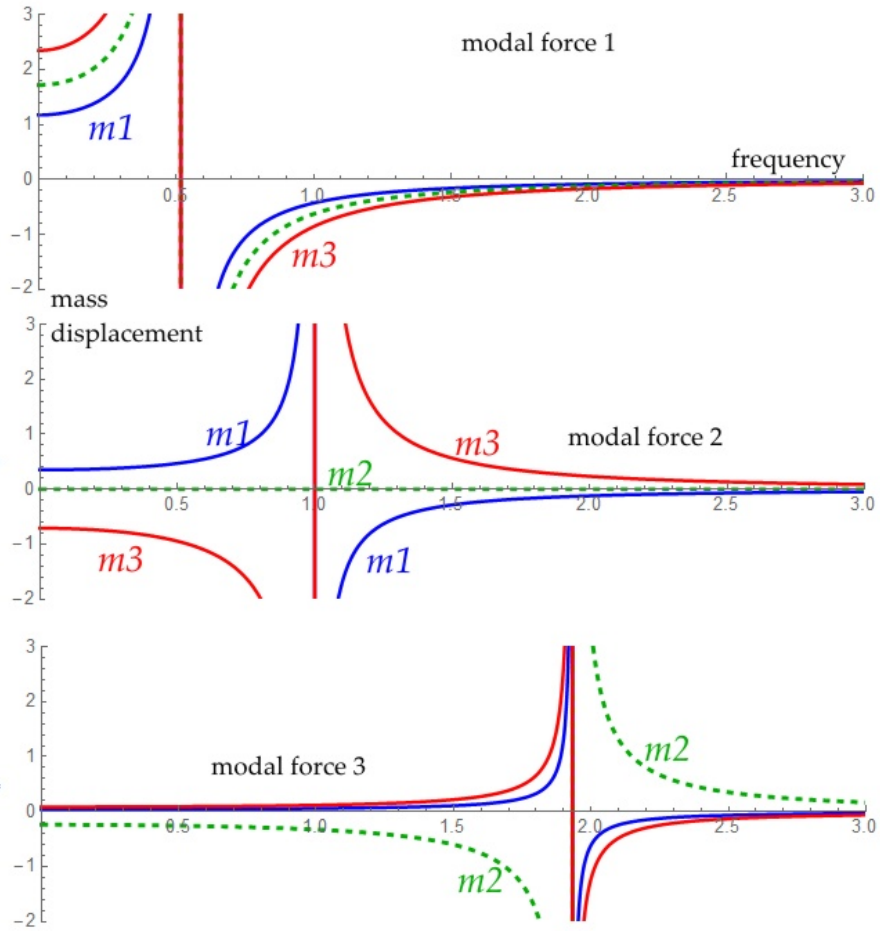

Figure 6: Frequency response of masses to unit modal force $\mathbf{f}_j$, $j = 1, 2, 3$. Blue: displacement amplitude of mass 1. Green dashed: displacement of mass 2. Red: displacement of mass 3.

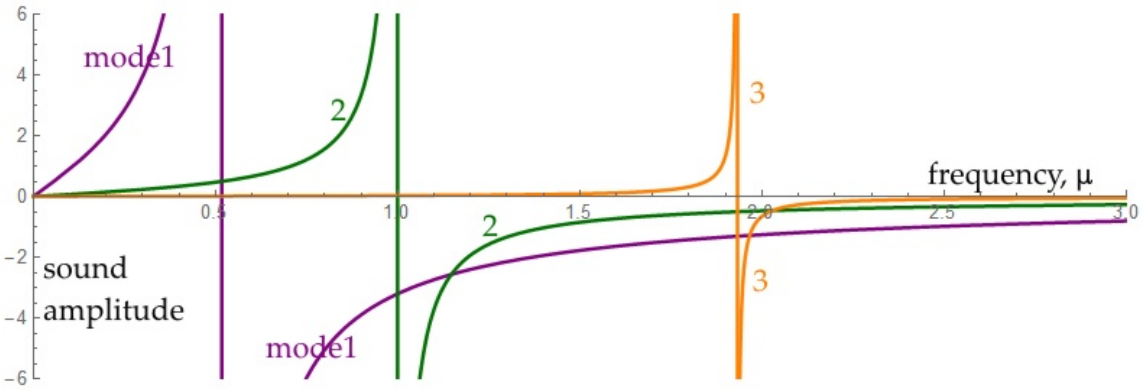

Figure 7: Spectrum of sound in response to unit modal force $\mathbf{f}_j$ applied to 3-mass-3-spring system.

The large mass 1 (4 units) has a much bigger effect than the two smaller masses, $m_2 = m_3 = 1$. Despite the weighting of the graphs by the linearly increasing factor μ, the low frequency mode 1 dominates, with the high frequency mode 3 contributing little except at frequencies close to $\mu = 1{\cdot}93$. In mode 2 the sound is coming only from masses 1 and 3.

4 Spectrum of sine waves forces

In the numerical example in §3.1 a sinusoidal force oscillating at $0 \cdot 6$ radians/sec was applied to mass 1 of Figure 1 and a force at $1 \cdot 6$ rad/sec to mass 3. In this section this theme of applying several sinusoidal forces at the same time is developed to account for the response of a structure to periodic but non-sinusoidal forces. We shall use the fact that periodic waveforms that occur in practice can be represented as a Fourier series of sinusoidal waves at multiples of a fundamental frequency μ.

Suppose that the force on mass m_3 is

$$F(t) \;=\; \sum_{s=1}^{S} a_s \sin(s\mu t) \qquad \text{or} \qquad \sum_{s=1}^{S} b_s \cos(s\mu t)\,. \tag{23}$$

Suppose also that the values a_s, b_s are such that the fundamental frequency is μ and the period of the applied force[7] is $2\pi/\mu$. It is a property of some waveforms that only a small number of terms from their Fourier series can represent them quite well. Four examples are given in Figure 8. The series for the sawtooth shown is

$$\sin t - \tfrac{1}{2}\sin 2t + \tfrac{1}{3}\sin 3t - \tfrac{1}{4}\sin 4t + \tfrac{1}{5}\sin 5t \tag{24}$$

and for the spikes is the six terms

$$0 \cdot 968\cos t + 0 \cdot 875\cos 2t + 0 \cdot 737\cos 3t + 0 \cdot 573\cos 4t + 0 \cdot 405\cos 5t + 0 \cdot 255\cos 6t\,.$$

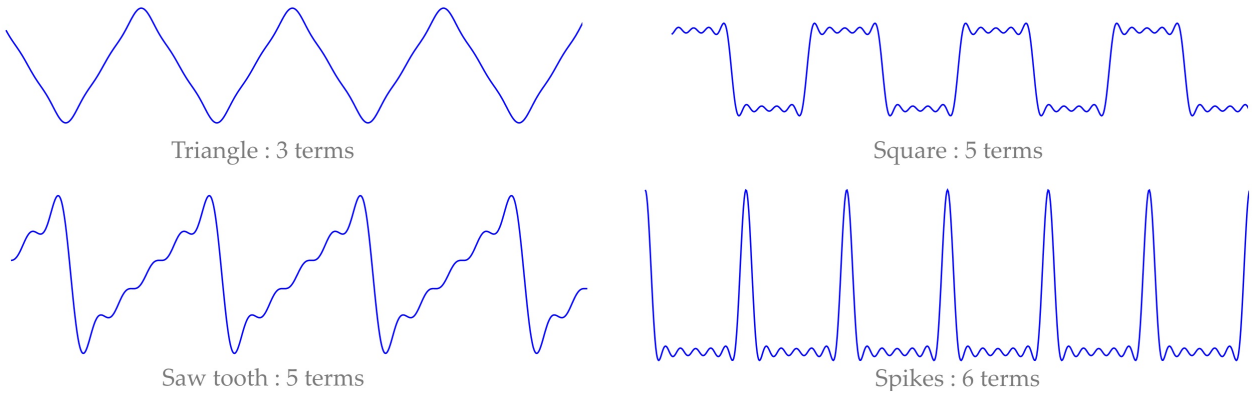

Figure 8: Four periodic waveforms generated from six or fewer terms of a Fourier sine or cosine series.

If one of the series in Eq 23 is substituted into Eq 14, the modal forces are found each to have the same series structure. There is nothing essentially new in this mathematical working; it is just more involved because of the many terms in the Fourier series. With force on m_3 only

$$\mathbf{P}^T\mathbf{F}(t) \;=\; \mathbf{P}^T\begin{pmatrix} 0 \\ 0 \\ \sum_{s=1}^{S} a_s \sin(s\mu t) \end{pmatrix} \;\rightarrow\; \begin{pmatrix} 0 \cdot 628 \sum_{s=1}^{S} a_s \sin(s\mu t) \\ -0 \cdot 707 \sum_{s=1}^{S} a_s \sin(s\mu t) \\ 0 \cdot 325 \sum_{s=1}^{S} a_s \sin(s\mu t) \end{pmatrix} \;=\; \mathbf{f}(t)\,. \tag{25}$$

[7] This condition is applied because the periodicity of the composite waveform is given by the greatest common divisor of the non-zero constituent frequencies, not just the lowest frequency. The perceived pitch of a musical note made of various overtones is demonstrated on *www.mathstudio.co.uk/pitch_perception.htm*.

The modal multiplying factors $0\cdot628$ *etc.* can be incorporated into a new set of coefficients a'_s so we are presented with solving for each driven mode an ODE of the form

$$\ddot{\xi} + \omega^2 \xi \;=\; \sum_{s=1}^{S} a'_s \sin(s\mu t)\,. \tag{26}$$

Following Eq 15 the general solution is

$$\xi_j \;=\; C_j \cos\omega_j t \;+\; D_j \sin\omega_j t \;+\; \sum_{s=1}^{S} \frac{a'_s \sin(s\mu t)}{\omega_j^2 - (s\mu)^2}\,, \tag{27}$$

where the cosine and sine terms in $\omega_j\, t$ determine the transients and can be ignored in steady state.

To illustrate the method apply the sawtooth force of Eq 24 to mass m_3 only. Our main interest is in how the coefficients of the sine waves are changed from the impressed force to the displacements of the masses. One can use computer algebra software to evaluate $\mathbf{f}$, then $\boldsymbol{\xi}$ and finally $\mathbf{x}$. Here is a similar scheme by which the coefficients of $\mathbf{x}$ can be determined without carrying round the associated $\sin s\mu t$ factors. Introduce $\mathcal{S}$ as the column matrix of sines:

$$\mathcal{S} \;=\; \begin{pmatrix} \sin\mu t \\ \sin 2\mu t \\ \sin 3\mu t \\ \sin 4\mu t \\ \sin 5\mu t \end{pmatrix}.$$

Now use $\mathbf{f} = \mathbf{P}^T\mathbf{F}(t)$ from Eq 14 to calculate the column matrix of coefficients of modal force in the jth mode, $\mathbf{A}_j$. Paralleling Eq 25 we find[8]

$$\mathbf{A}_1 \;=\; \begin{pmatrix} 0\cdot628 \\ -0\cdot628/2 \\ 0\cdot628/3 \\ -0\cdot628/4 \\ 0\cdot628/5 \end{pmatrix}, \qquad \mathbf{A}_2 \;=\; \begin{pmatrix} -0\cdot707 \\ 0\cdot707/2 \\ -0\cdot707/3 \\ 0\cdot707/4 \\ -0\cdot707/5 \end{pmatrix}, \qquad \mathbf{A}_3 \;=\; \begin{pmatrix} 0\cdot325 \\ -0\cdot325/2 \\ 0\cdot325/3 \\ -0\cdot325/4 \\ 0\cdot325/5 \end{pmatrix}.$$

These correspond to the a'_s in Eq 26. In the j^{th} mode $\mathbf{A}_j^T\mathcal{S} = a_{j1}\sin\mu t + ... + a_{j5}\sin 5\mu t$. Each of these coefficients must now be divided by a factor of form $\omega^2 - (s\mu)^2$ as in Eq 27. Define three diagonal matrices, one for each driven mode $j = 1, 2, 3$

$$\mathbf{W}_j \;=\; \mathrm{diag}\left(\frac{1}{\omega_j^2 - \mu^2},\; \frac{1}{\omega_j^2 - 4\mu^2},\; , \frac{1}{\omega_j^2 - 9\mu^2},\; \frac{1}{\omega_j^2 - 16\mu^2},\; \frac{1}{\omega_j^2 - 25\mu^2} \right).$$

The column matrix $\mathbf{g}_j = \mathbf{W}_j\mathbf{A}_j$ is equivalent to the series of $a'_s/[\omega_j^2 - s^2\mu^2]$ in Eq 27. Now form the 3-by-5 matrix $\mathbf{G}$ whose rows are the transposes of $\mathbf{g}_1$, $\mathbf{g}_2$ and $\mathbf{g}_3$:

$$\mathbf{G} \;=\; \begin{pmatrix} \frac{0\cdot628}{0\cdot2679-\mu^2} & \frac{-0\cdot0785}{0\cdot0670-\mu^2} & \frac{0\cdot0233}{0\cdot0298-\mu^2} & \frac{-0\cdot00981}{0\cdot0167-\mu^2} & \frac{0\cdot00502}{0\cdot0107-\mu^2} \\ \\ \frac{-0\cdot707}{1-\mu^2} & \frac{0\cdot088}{0\cdot25-\mu^2} & \frac{-0\cdot0262}{0\cdot111-\mu^2} & \frac{0\cdot0110}{0.0625-\mu^2} & \frac{-0\cdot00566}{0\cdot04-\mu^2} \\ \\ \frac{0\cdot325}{3\cdot7321-\mu^2} & \frac{-0\cdot0406}{0\cdot9330-\mu^2} & \frac{0\cdot0120}{0\cdot4147-\mu^2} & \frac{-0\cdot00501}{0\cdot2333-\mu^2} & \frac{0\cdot00260}{0\cdot1493-\mu^2} \end{pmatrix}. \tag{28}$$

[8] If a spectrum of sine wave forces had also been applied to m_1 and m_2, the column matrix would be longer, having as many rows as sines. Compare with Eq 16.

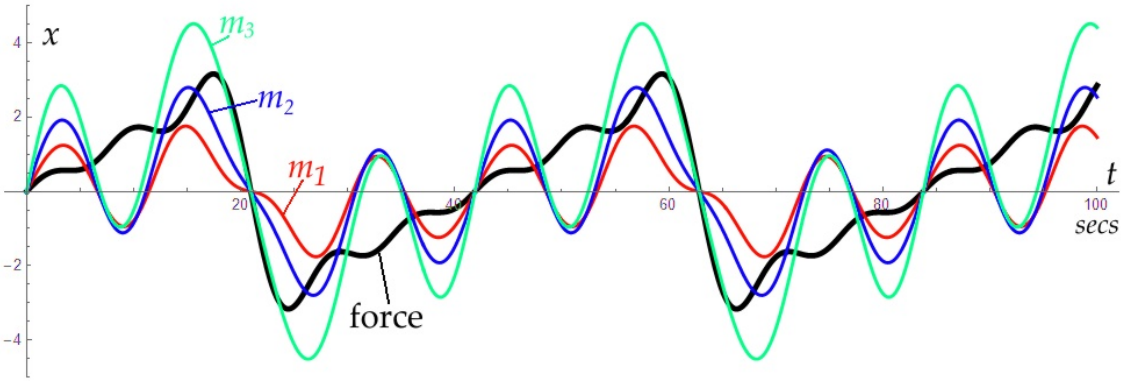

Figure 9: Displacements of three masses in Figure 1 under a quasi-saw-tooth driving force (black curve from Eq 24) applied to m_3 at $\mu = 0 \cdot 15$.

This gives the coefficients of the modal displacement vector $\boldsymbol{\xi}$; the time dependence of the modal displacements are in the vector $\mathbf{G}\,\mathcal{S}$. From this $\mathbf{P}\,\boldsymbol{\xi}$ gives $\mathbf{x}$, the physical displacements of the masses.

Recall that the natural frequencies are $\omega_1 = 0{\cdot}518$, $\omega_2 = 1$, $\omega_3 = 1{\cdot}932$ rad/sec. Any component of the applied force which is near one of these will be exaggerated in the response of the system. At a frequency well below the lowest resonance all masses try to follow the applied force. For example, at $\mu = 0 \cdot 15$ rad/sec the modal displacement is much larger in the ω_1 mode than in the other two:

$$\boldsymbol{\xi} \;=\; \begin{pmatrix} 2{\cdot}56\sin(0{\cdot}15t) - 1{\cdot}76\sin(0{\cdot}3t) + 3{\cdot}20\sin(0{\cdot}45t) + 1{\cdot}71\sin(0{\cdot}6t) - 0{\cdot}42\sin(0{\cdot}75t) \\ -0{\cdot}72\sin(0{\cdot}15t) + 0{\cdot}39\sin(0{\cdot}3t) - 0{\cdot}30\sin(0{\cdot}45t) + 0{\cdot}28\sin(0{\cdot}6t) - 0{\cdot}32\sin(0{\cdot}75t) \\ 0{\cdot}09\sin(0{\cdot}15t) - 0{\cdot}04\sin(0{\cdot}3t) + 0{\cdot}03\sin(0{\cdot}45t) - 0{\cdot}02\sin(0{\cdot}6t) + 0{\cdot}02\sin(0{\cdot}75t) \end{pmatrix}.$$

In mode 1 the three masses move in the same direction with amplitude ratios roughly $1 : 1\frac{1}{2} : 2$. The coefficient matrix for the mass displacements is

$$\mathbf{x} \;=\; \begin{pmatrix} 0{\cdot}562 & -0{\cdot}424 & 0{\cdot}905 & 0{\cdot}629 & -0{\cdot}245 \\ 1{\cdot}098 & -0{\cdot}771 & 1{\cdot}443 & 0{\cdot}805 & -0{\cdot}214 \\ 2{\cdot}147 & -1{\cdot}397 & 2{\cdot}227 & 0{\cdot}868 & -0{\cdot}0325 \end{pmatrix}$$

meaning, for example, that m_3 has displacement

$$2{\cdot}147\,\sin(0{\cdot}15t) - 1{\cdot}397\,\sin(0{\cdot}3t) + 2{\cdot}227\,\sin(0{\cdot}45t) + 0{\cdot}868\,\sin(0{\cdot}6t) - 0{\cdot}0325\,\sin(0{\cdot}75t)\,.$$

The motions of the three masses at $\mu = 0 \cdot 15$ rads/sec are plotted in Figure 9. The approximated saw-tooth driving force from Eq 24 is also sketched. Clearly all three masses, though having a period equal to that of the applied force $(40\pi/3)$, also have a strong tendency to oscillate at about $3\frac{1}{2}$ times this rate, that is at $\omega_1 = 0 \cdot 518$. Assuming that μ were increased to an audible frequency, the fundamental frequency of the saw-tooth would probably not be heard over the tone at ω_1.

If the sawtooth frequency is increased to $\mu = 0 \cdot 26$, the second harmonic excites the ω_1 resonance. The mode 1 displacement is

$$\boldsymbol{\xi_1} \;=\; 3{\cdot}1\sin(0{\cdot}26t) + \mathbf{128{\cdot}1}\sin(0{\cdot}52t) - 0{\cdot}6\sin(0{\cdot}78t) + 0{\cdot}2\sin(1{\cdot}04t) - 0{\cdot}1\sin(1{\cdot}3t)\,.$$

When μ is above the highest resonance, masses 1 and 3 move contrary to the force, but do not move a great distance because the structure cannot respond rapidly enough. At $\mu = 2$, just above

the top ω_3 resonance, only the fundamental in the driving force causes any significant displacement:

$$\mathbf{x} = \begin{pmatrix} -\frac{1}{6} & 9\times10^{-5} & -4\times10^{-6} & 5\times10^{-7} & -1\times10^{-7} \\ 1 & -0\cdot0026 & 3\times10^{-4} & -7\times10^{-5} & 2\times10^{-5} \\ -\frac{2}{3} & 0\cdot0335 & -0\cdot0095 & 0\cdot0040 & -0\cdot00202 \end{pmatrix}$$

As we saw in Figures 5, 6, and 7, when $\mu = 4$, even the main contributions to the displacement are small:

$$\mathbf{x} = \begin{pmatrix} -0\cdot040\sin 4t + ... \\ 0\cdot047\sin 4t + ... \\ -0\cdot026\sin 4t + ... \end{pmatrix}$$

To check these results I have plugged the calculated values of x_1, x_2, x_3 into the three equations of motion, Eq 1 for $\mu = 0\cdot15$ and 2 and found that they do indeed satisfy them.

The example illustrates further how the applied forces are in part filtered, in part selectively amplified by the natural tendencies of the system. Knowing the particle displacement ratios in the normal modes, we can 'read' the pattern of particle motion from the modal displacement matrix **G**, Eq 28. Each of the two panels in Figure 10 plots as dots the sound amplitude (according to the sum over mass × velocity of Eq 21) of the fundamental frequency μ and its four harmonics when mass 3 is driven by the sawtooth force of Eq 24. The three sets of points in each panel are for pitches one semitone apart. I arbitrarily took $\mu = 1\cdot15$ as the pitch c above middle C. The left panel is for the notes E, F and F♯ about $\frac{2}{3}$ octave below Middle C. The right panel is for c, the b a semitone below and the c♯ above[9]. The amplitudes of the higher harmonics vary little with pitch, but in the right panel particularly the fundamental amplitude changes significantly for just a semitone change. In this right panel the fundamental changes phase as well. We can therefore expect the b, c and c♯ to sound different in timbre from each other. Extending this to a violin plate being driven through the saw-tooth slip-stick action of the moving bow hairs, we can in principle calculate how the natural frequencies of the wooden box will modulate the driving force and hence affect the timbre of the sound radiated to a listener.

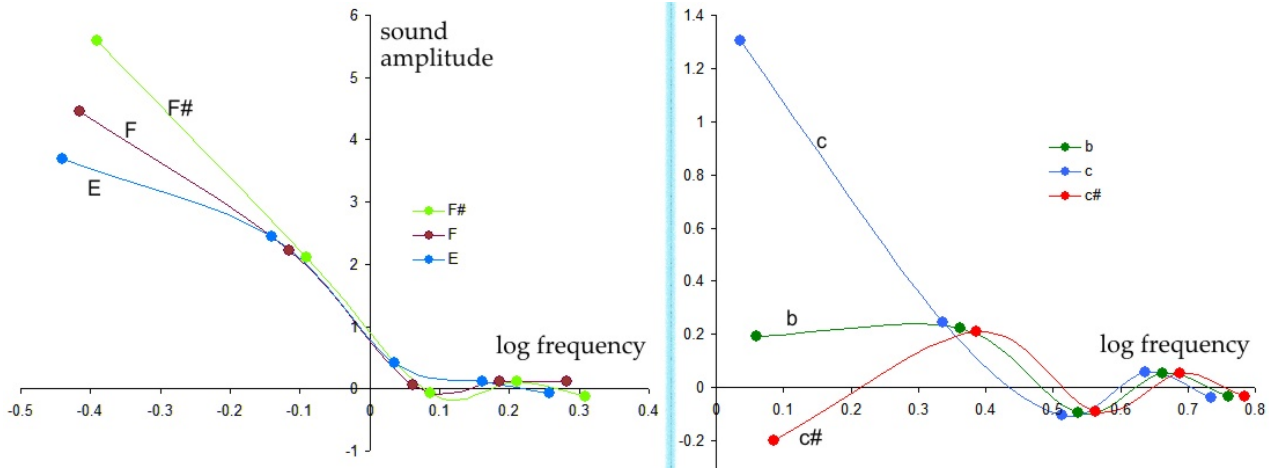

Figure 10: Frequency spectra of sound amplitude for two sets of three notes one semitone apart when sawtooth force at frequency μ is applied to mass 3. Left panel: low pitch. Right: higher pitch.

[9] The μ values are: E=0·362, F=0·384, F♯=0·407, b=1·085, c=1·15, c♯=1·22.

5 Damped vibrations

Any model of a vibrating system would not be realistic unless some allowance for energy loss were included, for otherwise at the resonant frequencies the displacement amplitudes would grow without limit. Resistive damping, through sound radiation, friction in the moving joints and internal friction within the material, blunts the resonances. With a structure like a violin or 'cello which is intended to be resonant, the effects of damping will be most significant close to the resonances and at high frequencies. Near resonances damping will decrease the peak amplitude but spread it over a wider range of frequencies, and this will be mirrored in the timbre of the instrument. I consider first the discrete 3-mass-3-spring example of Figure 1 with discrete dashpots added. The scheme follows the same path as before, namely

force $\mathbf{F}$ on masses $\rightarrow$ modal forces $\mathbf{f}$ $\rightarrow$ modal displacements $\boldsymbol{\xi}$ $\rightarrow$ mass displacements $\mathbf{x}$.

We shall find that damping couples modes which otherwise would be independent. Moreover, there is not an easy link between the coefficients which describe the dashpots' energy losses and the coefficients which describe damping of the resonant modes.

5.1 Masses, springs and dashpots

One common model of physical damping is a dashpot of viscous fluid fitted in parallel with the spring. The fluid applies a velocity-dependent force which always opposes motion of the attached masses. Suppose there are three such dashpots with viscosity coefficients δ_1, δ_2, δ_3 fitted in parallel across the springs k_1, k_2, k_3 as shown in Figure 11. In the each spring-dashpot pair the forces add so the equations of motion for the masses in the absence of a driving force are

$$\begin{aligned} -k_1x_1 + k_2(x_2 - x_1) - \delta_1\dot{x_1} + \delta_2(\dot{x_2} - \dot{x_1}) &= m_1\,\ddot{x}_1 \\ -k_2(x_2 - x_1) + k_3(x_3 - x_2) - \delta_2(\dot{x_2} - \dot{x_1}) + \delta_3(\dot{x_3} - \dot{x_2}) &= m_2\,\ddot{x}_2 \\ -k_3(x_3 - x_2) - \delta_3(\dot{x_3} - \dot{x_2}) &= m_3\,\ddot{x}_3\,. \end{aligned}$$

In matrix form the above simultaneous equations are $\mathbf{M}\,\ddot{\mathbf{x}} + \boldsymbol{\Delta}\,\dot{\mathbf{x}} + \mathbf{K}\,\mathbf{x} = 0$ where

$$\boldsymbol{\Delta} = \begin{pmatrix} \delta_1 + \delta_2 & -\delta_2 & 0 \\ -\delta_2 & \delta_2 + \delta_3 & -\delta_3 \\ 0 & -\delta_3 & \delta_3 \end{pmatrix}$$

and $\mathbf{K}$ and $\mathbf{M}$ are as at Eq 1. Assuming a harmonic form for each x, the equation of motion is

$$-\omega^2\mathbf{M}\mathbf{x} + i\omega\boldsymbol{\Delta}\mathbf{x} + \mathbf{K}\,\mathbf{x} = 0 \qquad \text{or} \qquad -\omega^2\mathbf{M}\mathbf{x} + i\omega\boldsymbol{\Delta}\mathbf{x} + \mathbf{K}\,\mathbf{x} = \mathbf{F}(t) \tag{29}$$

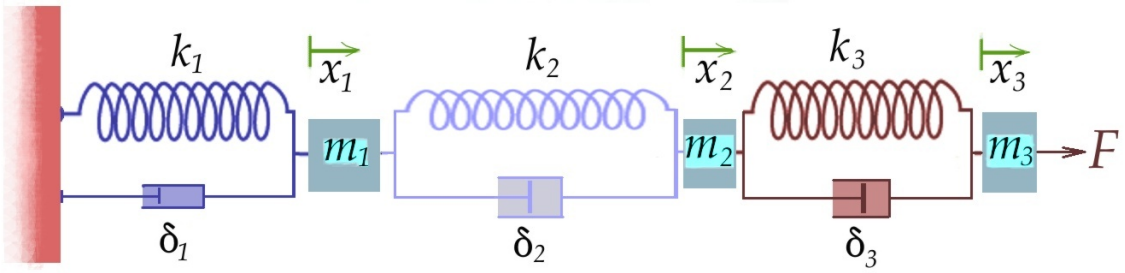

Figure 11: 3-mass-3-spring system with viscous dashpots in parallel with each spring and a force F on mass 3.

if there are applied forces. The force-free equation of motion does not have the standard form of an eigenvalue equation. The complex number represents phase quadrature since the damped motion always lags behind an applied force.

Various approaches have been employed over the years to cope with this complication[10]. In musical instruments damping is light so the first step is to take all the δ to be zero and find the eigenvalues and eigenvectors of the undamped system. From there the eigenvectors are mass-normalised and the transformation matrix $\mathbf{P}$ constructed as in §2. The orthogonality of $\mathbf{M}$ and $\mathbf{K}$ then apply, as in Eqs 5 and 6. Recall that $\mathbf{P}$ is scaled so that $\mathbf{P}^T\boldsymbol{M}\mathbf{P} = \mathbf{I}$, the identity matrix, and simultaneously $\mathbf{P}^T\boldsymbol{K}\mathbf{P} = \boldsymbol{\Omega} = \mathbf{diag}(\omega_1^2, \omega_2^2, ..., \omega_N^2)$. Applying the same operation to $\boldsymbol{\Delta}$ creates the modal damping matrix $\mathbf{R} = \mathbf{P}^T\boldsymbol{\Delta}\mathbf{P}$, but in general this will *not* be diagonal. Therefore the equations of motion do not separate into independent modes; damping couples the modes. As an example, suppose in Figure 11 that $\delta_1 = 0 \cdot 3$, $\delta_2 = 0 \cdot 1$, $\delta_3 = 0 \cdot 2$. Then

$$\mathbf{R} \;=\; \frac{1}{230}\begin{pmatrix} 8 \cdot 59 & 1 & 9 \cdot 38 \\ 1 & 34 \cdot 5 & -26 \cdot 9 \\ 9 \cdot 38 & -29 \cdot 9 & 94 \cdot 8 \end{pmatrix}$$

where the diagonal elements are the largest but the off diagonal $26 \cdot 9$ is hard to ignore. Decreasing all the δ_j by the same factor h, say, reduces R overall by h but does not change the relative values of its elements – R does not become 'more diagonal'. The only two matrices which are diagonal under $\mathbf{P}$ are $\mathbf{M}$ and $\mathbf{K}$, so $\mathbf{R}$ will only be diagonal when it is some linear combination of $\mathbf{M}$ and $\mathbf{K}$. This was spotted by that brilliant Victorian amateur theoretical physicist, Lord Rayleigh. 'Rayleigh damping' sets

$$\boldsymbol{\Delta}_{Rayleigh} \;=\; \alpha\mathbf{M} + \beta\mathbf{K} \tag{30}$$

where α and β are constants chosen to make the damped vibration of the structure resemble its observed behaviour. However, this is at best a fudge because in general the viscosity coefficients δ_j cannot be unambiguously identified with the elements of $\boldsymbol{\Delta}_{Rayleigh}$. To see this consider the example $\alpha = 0 \cdot 1$, $\beta = 0 \cdot 2$ and $\mathbf{M}$ and $\mathbf{K}$ have the values of §2 at Eq 4. We find

$$\boldsymbol{\Delta}_{Rayleigh} \;=\; \frac{1}{10}\begin{pmatrix} 12 & -4 & 0 \\ -4 & 7 & -2 \\ 0 & -2 & 3 \end{pmatrix}.$$

Comparing this with the above expression for $\boldsymbol{\Delta}$, we might conclude that $\delta_2 = 0 \cdot 4$ and $\delta_1 = 0 \cdot 8$, but what of δ_3? Is it $0 \cdot 2$ or $0 \cdot 3$? We should not be surprised at these inconsistencies. If $\boldsymbol{\Delta}$ were truly diagonal, the equations of motion would separate and describe genuinely independent modes. But that contradicts our practical experience that damped modes do interact.

In a lumped system (one with discrete elements) the viscosity δ of each dashpot can in principle be measured by removing it from the system and subjecting it to controlled forces while measuring the velocity of the piston relative to the casing. Suppose that $\delta_1 = 0 \cdot 3$, $\delta_2 = 0 \cdot 1$, $\delta_3 = 0 \cdot 2$ are actual measured values. To use the Rayleigh model of damping one would need to determine α and β to give a best fit. The matrix of differences is

$$\alpha\mathbf{M} + \beta\mathbf{K} - \boldsymbol{\Delta} \;=\; \begin{pmatrix} 4\alpha + 4\beta - 0 \cdot 4 & -2\beta + 0 \cdot 1 & 0 \\ -2\beta + 0 \cdot 1 & \alpha + 3\beta - 0 \cdot 3 & -\beta + 0 \cdot 2 \\ 0 & -\beta + 0 \cdot 2 & \alpha + \beta - 0 \cdot 2 \end{pmatrix}.$$

[10] A comprehensive review with proposals for sophisticated ways of dealing with damping in vibration studies can be found in the Ph D thesis of Sondipon Adhikari, 'Damping Models for Structural Vibration', Cambridge Univ. , September 2000, available on the internet.

A least squares scheme would minimise the sum of squares of these elements with respect to α and β. The sum of squares is $18\alpha^2 + 40\alpha\beta - 4\cdot2\alpha + 36\beta^2 - 7\beta + 0\cdot39$ and the derivatives with respect to α and β are respectively $36\alpha + 40\beta - 4\cdot2$, $40\alpha + 72\beta - 7$. These are simultaneously zero when $\alpha = 0\cdot0226$, $\beta = 0\cdot0847$. The fitted matrix is

$$\mathbf{\Delta}_{Rayleigh} = \begin{pmatrix} 0\cdot429 & -0\cdot169 & 0 \\ -0\cdot169 & 0\cdot277 & -0\cdot085 \\ 0 & -0\cdot085 & 0\cdot107 \end{pmatrix}, \qquad \mathbf{\Delta}_{Actual} = \begin{pmatrix} 0\cdot4 & -0\cdot1 & 0 \\ -0\cdot1 & 0\cdot3 & -0\cdot2 \\ 0 & -0\cdot2 & 0\cdot2 \end{pmatrix}.$$

Whether this is a close enough fit it a matter of judgement. We might also ponder whether it is physically realistic to have a frequency dependence to the modal damping coefficients R. Consider that when transformed to the modal domain,

$$\mathbf{P}^T \mathbf{\Delta}_{Rayleigh} \mathbf{P} = \mathbf{R}_{Rayleigh} = \mathbf{P}^T (\alpha\mathbf{P} + \beta\mathbf{K}) \mathbf{P} = \alpha\mathbf{I} + \beta\mathbf{\Omega}. \tag{31}$$

In a structure like a violin made of continuous components, there are no dashpots but instead energy loss is through sound radiation and friction, both at joints and internal to the material. Though a Rayleigh damping model could be contrived, it seems more natural to look at the damping of the resonances – that is, to look at damping in the frequency domain. This is the subject of the next sub-section.

5.2 Modal damping

Assume that the first stage in the chain of calculation has been carried out and we have modal equations of motion, the counterpart for Eq 14

$$\ddot{\boldsymbol{\xi}} + \mathbf{R}\dot{\boldsymbol{\xi}} + \mathbf{\Omega}\,\boldsymbol{\xi} = \mathbf{P}^T \mathbf{F}(t) = \mathbf{f}(t). \tag{32}$$

For a periodic force the j^{th} modal equation of motion is the damped version of Eq 26:

$$\ddot{\xi}_j + R_j\dot{\xi}_j + \omega_j^2\xi_j = \sum_{s=1}^{S} a'_{js} \sin(\mu_s t). \tag{33}$$

μ_s will eventually be set to $s\mu$, but for the present is kept general. As the subscript indicates, R_j is the resistive damping coefficient for the mode under consideration and will generally be different for each mode.

To develop some understanding of the structure of the damped solution, take first the case of only one sine term in the driving force. A full account is given in Appendix 2, so here I just pick out some central points. The general solution of

$$\ddot{\xi} + R\dot{\xi} + \omega^2\xi = F\sin\mu t \quad \text{is}$$

$$\xi = e^{-t/\tau}\,(C_1 \sin\omega_d t + C_2 \cos\omega_d t) + F\,\frac{(\omega^2 - \mu^2)\,\sin\mu t - R\mu\cos\mu t}{(\omega^2 - \mu^2)^2 + R^2\mu^2} \tag{34}$$

where ω is the natural frequency, $\omega_d = \sqrt{\omega^2 - R^2/4}$ and $\tau = 2/R$, a time constant. The first term of the expression with the two adjustable constants C_1, C_2 is the complementary solution, describing the exponentially attenuated natural oscillation at the slightly reduced frequency of ω_d. τ is the time constant for its decay. The second term is the particular solution describing the driven motion once the transient has fully died away. This differs in two respects from the particular solution in the undamped case, Eq 15:

1. the $\frac{\sin\mu t}{\omega^2-\mu^2}$ has been replaced by $\frac{\sin\mu t}{\omega^2-\mu^2+\frac{R^2\mu^2}{\omega^2-\mu^2}}$, ensuring that the amplitude can never become infinite,

2. there is a second term with time variation $\cos\mu t$. This is a reactive term, 90° out of phase with the driving force. The whole solution for ξ could be written in the form $A\sin(\mu t+\beta)$ where β is a phase shift.

The absolute value of displacement is

$$|\xi| \;=\; \frac{1}{\sqrt{(\omega^2-\mu^2)^2+R^2\mu^2}}\,. \tag{35}$$

If the driving frequency μ were to scan through a resonance at ω, maximum displacement would occur when $\mu^2 = \omega^2 - R^2/2$ which is very close to the undamped resonant frequency. The value of this maximum is almost $F/(R\omega)$ for R small and the full width at half height (FWHH) of the peak is about $2\sqrt{3}\,R\omega = 3\cdot 46R\omega$. So if R is constant across all modes the damping will affect the high frequency modes most. This is important for the sound quality produced by a violin-family instrument. The resonances of the structure are responsible for the change in the spectrum of frequency response from semitone to semitone. Mechanisms which dampen the resonances lessen the variation and so rob the instrument of the rich tonal subtleties essential to a lively, interesting sound. On the other hand, almost zero damping (as would probably occur with a non-standard violin made entirely of aluminium or steel) would probably make the instrument so sensitive to pitch variations that its timbre could vary wildly making it difficult for the player to control.

Now generalise to non-sinusoidal periodic forced oscillations of a damped system. As with the undamped response of Eqs 26 and 27, it turns out that when the driving force is a sum of sinusoidal components, the modal displacement is a corresponding superposition of sinusoidal oscillations, each with the form of Eq 33. Specifically, the particular solution of Eq 32 is

$$\xi_j \;=\; \sum_s^S \frac{a'_s}{D_s}\left\{(\omega_j^2-\mu_s^2)\sin\mu_s t \;-\; R\mu_s\cos\mu_s t\right\}, \qquad D_s \;=\; (\omega_j^2-\mu_s^2)^2+R^2\,\mu_s^2\,. \tag{36}$$

The matrix manipulations of §4 are readily extended by adding a second matrix representing the reactive component and containing the coefficients of the cosines. Let $\mathcal{C}$ be the matrix of cosines equivalent to $\mathcal{S}$, and $\mathbf{h}_j$ the matrix of their coefficients $-a'_sR\mu_s/D_s$. Also let $\mathbf{g'}_j$ be the coefficient column matrix for the sine terms, equivalent to the $\mathbf{g}_j$ of §4; these have form $a'_s(\omega^2-\mu_s^2)/D_s$. The displacement in the jth mode is therefore $\mathbf{g'}_j^T\mathcal{S}+\mathbf{h}_j^T\mathcal{C}$. Following §4, form the matrices $\mathbf{G'}$ and $\mathbf{H}$ whose rows are the transposes of $\mathbf{g'}_j$ and $\mathbf{h}_j$ respectively. The modal displacement matrix $\boldsymbol{\xi} = \mathbf{G'}\mathcal{S}+\mathbf{H}\mathcal{C}$. The physical displacements $\mathbf{x}$ are again given by $\mathbf{P}\boldsymbol{\xi}$. We only require the coefficients of the sine and cosine components of $\mathbf{x}$ and these are given respectively by $\mathbf{PG'}$ and $\mathbf{PH}$. The result is remarkable in that no approximation is involved and the formulae hold for any R provided that it represents under-damping in all modes, that is $R<2\omega_j$ for all j.

In §9.2 of Appendix 2 I describe experiments to determine R_j values for a 'cello body (no string vibration) by measuring the transient decay time constant τ. The principal method is to excite the 'cello at one of its natural frequencies using by a vibrating electromagnetic exciter, suddenly remove the exciter and record the decay in recorded sound. This sounds simple and straightforward, but in practice I did not get consistent results at all resonances, as can be seen the in scattered points plotted in Figure 12. The problem probably lies in the interaction of resonances which are close together in pitch. I consider the points plotted in blue to be more reliable than those in

orange, though that hardly excuses the discrepancies amongst the three values each at 97 Hz and 177 Hz. In Figure 12 the frequency is on a logarithmic scale to be proportional to musical pitch. Several reference pitches are indicated by the small red triangles. Even if there were no experimental uncertainty, there is no reason to expect the time constants τ to vary monotonically with resonant frequency. That said, there is a slight trend for τ to decrease with pitch as $\tau \approx 180 - 42 \log_{10} \omega$ milliseconds, ω in radian/sec, or as $\tau \approx 147 - 42 \log_{10} f$ milliseconds, f in Hz; that is, about 13 msec per octave.

It is of interest to see how well these measured values for the 'cello can be made to fit with a Rayleigh damping scheme $R_j = \alpha + \beta\omega_j^2$ for the j^{th} mode where $R_j = 2/\tau_j$. Figure 13 replots the data of Figure 12 as $R = 2/\tau$ against ω^2 (ω in radians /sec). The straight line is the Rayleigh model, but is hardly a good fit. Its equation is $R \approx 44 \cdot 4 + 1 \cdot 36 \times 10^{-6}\omega^2$ per second.

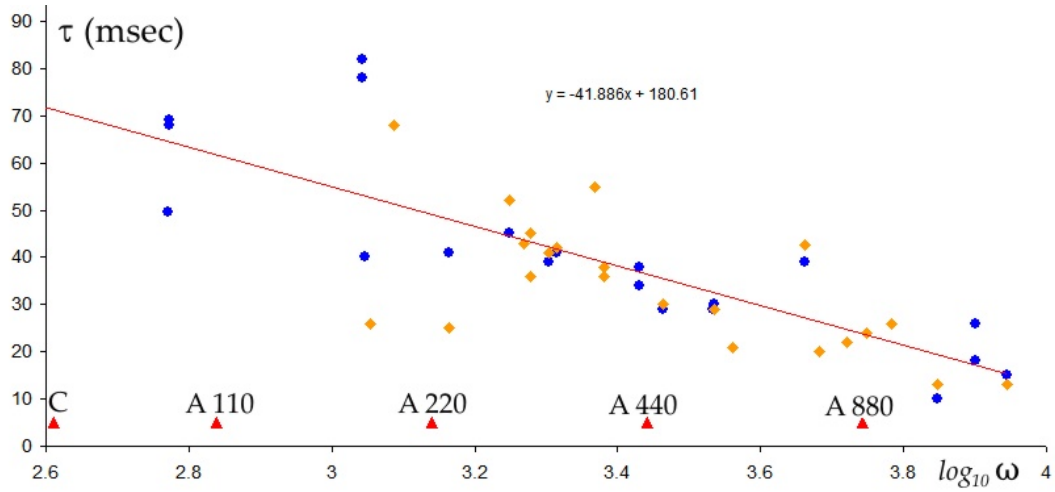

Figure 12: Experimental measurement of resonance decay time constant τ plotted against pitch of resonance for a 'cello. ω is in radians/sec.

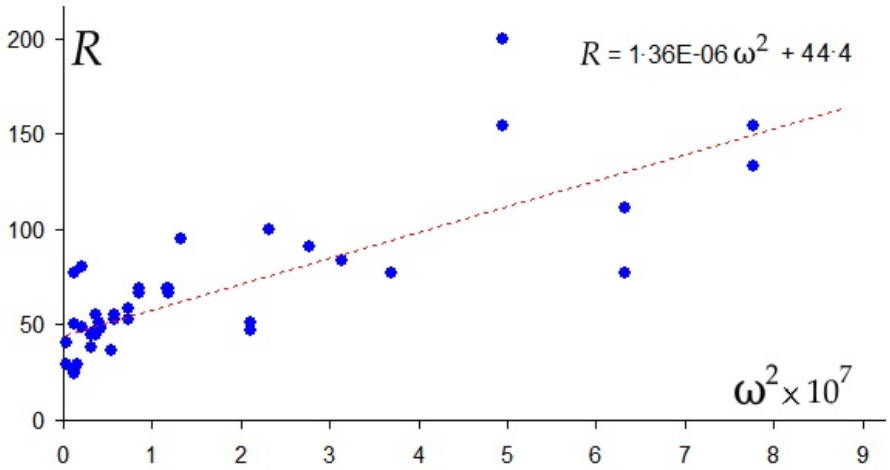

Figure 13: $R = 2/\tau$ sec^{-1} for 'cello resonances against ω^2 to test fit to Rayleigh damping formula.

6 Time integration for non-periodic forces

This section is partly in preparation for the next, §7, in which I compare modal analysis with the numerical output from the Mecway finite element program's Dynamic Response 3D facility. Dynamic Response is programmed to deal with arbitrarily varying applied forces which are specified in a table of values at given times t. This is much more general than is required for calculating the spectral response of a resonant musical instrument. By the same token it is unnecessarily complicated for spectral analysis and does not output its results as functions of frequency but as the displacement at each node in the mesh. In the course of understanding how Mecway and its precursor LISA function I have looked into the mathematical background of numerical integration schemes for solving second order differential equations of motion. This section relates some of this background and draws substantially on the book by S S Rao, sections 7.4.7 and 12.1.

Suppose that the time period of interest – which includes but may be longer than the time during which the force is applied – is divided into many equal small intervals of duration h, and that the force on a mass at successive time steps has the values $F(0)$, $F(h)$, $F(2h)$, ... The force can vary in almost any chosen way and several masses or mesh nodes can have different forces. Suppose also that the mass-normalised transformation matrix $\mathbf{P}$ for the undamped state is known and the modal force $f(t)$ at each time step has been calculated for each vibrational mode. This produces a time sequence $f(0)$, $f(h)$, $f(2h)$, $f(3h)$, ... of modal forces for each mode. I will now write these as f_0, f_1, f_2, ... where the subscript is an index of the time step. The idea behind the family of algorithms is to solve analytically the equation of motion for each time interval in turn using a suitable approximation to the force acting during that interval. Being a second order differential equation, there will be two freely adjustable parameters, C_1, C_2, by which the solution ξ can be matched to ξ_0 and $\dot{\xi}_0$ at the beginning of the time interval. The analytical solution then gives the values at the end of the interval, which is the beginning of the next. Therefore, if $\xi(t = 0)$ and $\dot{\xi}(t = 0)$ at the very start are both given, solution values can be propagated interval by interval through to the end. The numerical challenge is to describe the system's behaviour over a long time span without accumulating unacceptable errors. Accuracy will be determined by how well the varying force can be approximated by piecewise segments. It is inevitable that approximation and rounding errors will be pushed to later times.

6.1 Algorithms neglecting damping

I will first outline the algorithm by neglecting damping and assuming that the modal force changes stepwise every time increment h. $f(t)$ is therefore approximated by a single representative constant value f_c within each step, which could be the average $(f_n + f_{n+1})/2$. The equation of motion at the i^{th} time step and its solution are

$$\ddot{\xi} + \omega^2 \xi \;=\; f_c\,, \qquad \xi \;=\; \frac{f_c}{\omega^2} + C_1 \cos\omega t + C_2 \sin\omega t\,, \quad \dot{\xi} \;=\; \omega(-C_1 \sin\omega t + C_2 \cos\omega t)\,. \tag{37}$$

t is here the local time within the interval, not the absolute time since the sequence was started. Choose C_1, C_2 to fit ξ and $d\xi/dt$ at the beginning of the time step in question, which spans data points f_n to f_{n+1}. Put $t = 0$ to select the beginning and obtain

$$\xi_n \;=\; \frac{f_c}{\omega^2} + C_1 \quad \text{from which} \quad C_1 = \xi_n - \frac{f_c}{\omega^2}\,.$$

Similarly at $t = 0$, $\dot{\xi} = \omega C_2$ from which C_2 can be found provided we have an estimate of $\dot{\xi}_n$ at 0. Then ξ and its derivative at the end of the interval are

$$\xi_{n+1} \;=\; \frac{f_c}{\omega^2} + \left(\xi_n - \frac{f_c}{\omega^2}\right)\cos\omega h + \frac{\dot{\xi}_n}{\omega}\sin\omega h\,, \tag{38a}$$

$$\dot{\xi}_{n+1} \;=\; \dot{\xi}_n \cos\omega h - \omega\left(\xi_n - \frac{f_c}{\omega^2}\right)\sin\omega h\,. \tag{38b}$$

How good is this scheme? It is similar to the rectangle rule for integrating a function because it divides the global force function $f(t)$ into a sequence of flat-topped steps. For this reason I will call it the 'rectangle approximation'. One might suppose that a trapezium-type rule would give a better answer because of its closer fit to most smooth force functions. A trapezoidal approximation can be constructed by taking $f(t) = At + B = (f_{n+1} - f_n)t/h + f_n$ over the time between data points n and $n+1$. The solution of

$$\ddot{\xi} + \omega^2\xi \;=\; At + B \quad \text{is} \quad \xi \;=\; \frac{At+B}{\omega^2} + C_1\cos\omega t + C_2\sin\omega t \tag{39}$$

with derivative

$$\frac{d\xi}{dt} \;=\; \frac{A}{\omega^2} + \omega[-C_1\sin\omega t + C_2\cos\omega t]\,. \tag{40}$$

Putting $t = 0$, corresponding to data point n, gives

$$C_1 \;=\; \xi_n - \frac{B}{\omega^2} \quad \text{and} \quad C_2 \;=\; \frac{\dot{\xi}_n}{\omega} - \frac{A}{\omega^3}\,.$$

The recursive scheme is therefore

$$\xi_{n+1} \;=\; \frac{Ah+B}{\omega^2} + \left(\xi_n - \frac{B}{\omega^2}\right)\cos\omega h + \left(\frac{\dot{\xi}_n}{\omega} - \frac{A}{\omega^3}\right)\sin\omega h\,. \tag{41}$$

$$\dot{\xi}_{n+1} \;=\; \frac{A}{\omega^2} \;+\; \left(\dot{\xi}_n - \frac{A}{\omega^2}\right)\cos\omega h \;-\; \left(\omega\xi_n - \frac{B}{\omega}\right)\sin\omega h\,. \tag{42}$$

The analogy with the rectangular and trapezium rules for integration should not be taken too literally. In integration, if the function is linear, then both give the same answer provided the midpoint value is taken in the rectangle rule. Here, however, if $f(t)$ is linear and $f_c = Ah/2 + B$, the difference "rectangle–trapezium" in estimates of ξ_{n+1} is

$$\xi_{n+1,rect} - \xi_{n+1,trap} \;=\; -\frac{Ah}{2\omega^2}(1+\cos\omega h) + \frac{A}{\omega^3}\sin\omega h\,, \qquad A = \frac{1}{h}(f_{n+1} - f_n)\,; \tag{43}$$

that is, it increases almost proportionally with the step length h and with the rate of change A of the force. This quantifies the improvement in using the trapezium-linear approximation to force instead of the rectangular-flat one.

6.2 Damping and more accurate schemes

These schemes are readily modified to include a damping term, though of course the expressions are more involved. The solution of the damped rectangular approximation $\ddot{\xi} + R\dot{\xi} + \omega^2\xi = f_c$ is

$$\xi \;=\; \frac{f_c}{\omega^2} + e^{-Rt/2}\left(C_1\cos\omega_d t + C_2\sin\omega_d t\right)\,,$$

$$\dot{\xi} \;=\; e^{-Rt/2}\left[\left(C_2\omega_d - \tfrac{1}{2}C_1R\right)\cos\omega_d t - \left(C_1\omega_d + \tfrac{1}{2}C_2R\right)\sin\omega_d t\right]\,,$$

$$C_1 \;=\; \xi_n - \frac{f_c}{\omega^2}\,, \qquad C_2 \;=\; \frac{1}{2\omega_d}(2\dot{\xi}_n + C_1R)\,, \qquad f_c \;=\; \tfrac{1}{2}(f_n + f_{n+1})\,, \qquad \omega_d = \tfrac{1}{2}\sqrt{4\omega^2 - R^2}\,. \tag{44}$$

Explicitly the next-step values for the damped rectangular approximation are

$$\xi_{n+1} \;=\; \frac{f_c}{\omega^2} + e^{-Rh/2}\Big[\;\Big(\xi_n - \frac{f_c}{\omega^2}\Big)\cos\omega_d h \;+\; \frac{1}{2\omega_d}\Big(\xi_n R + 2\dot{\xi_n} - \frac{f_c R}{\omega^2}\;\Big)\sin\omega_d h\;\Big]\,,$$

$$\dot{\xi}_{n+1} \;=\; e^{-Rh/2}\Big[\dot{\xi_n}\cos\omega_d h \;-\Big\{\omega_d\Big(\xi_n - \frac{f_c}{\omega^2}\Big) + \frac{R}{4\omega_d}\Big(\xi_n R + 2\dot{\xi_n} - \frac{f_c R}{\omega^2}\Big)\Big\}\sin\omega_d h\;\Big]\,.$$

When $R = 0$ these reduces to Eq 38.

When damping is included, the 'trapezium' approximation, using a linear fit to the force function within the interval, has the following equation and solution:

$$\ddot{\xi} + R\dot{\xi} + \omega^2\xi \;=\; At + B$$

$$\text{where}\quad \xi \;=\; \frac{At+B}{\omega^2} - \frac{AR}{\omega^4} + e^{-Rt/2}\,[C_1\cos\omega_d t + C_2\sin\omega_d t]\,, \qquad \omega_d = \tfrac{1}{2}\sqrt{4\omega^2 - R^2}\,. \tag{45a}$$

Put $t = 0$ to find ξ_n and hence

$$C_1 \;=\; \xi_n + \frac{AR}{\omega^4} - \frac{B}{\omega^2}\,.$$

Differentiate and again put $t = 0$ to find $\dot{\xi}_n$:

$$\frac{d\xi}{dt} \;= \frac{A}{\omega^2} + \omega_d\, e^{-Rt/2}[C_2\cos\omega_d t - C_1\sin\omega_d t] - \tfrac{1}{2}\,R\,e^{-Rt/2}[C_1\cos\omega_d t + C_2\sin\omega_d t]\,;$$

$$\dot{\xi}_n \;=\; \frac{A}{\omega^2} + \omega_d C_2 - \frac{R}{2}C_1 \quad\text{so}\quad C_2 \;=\; \frac{1}{\omega_d}\left(\dot{\xi}_n + \frac{R\xi_n}{2} - \frac{(2A+BR)}{2\omega^2} + \frac{AR^2}{2\omega^4}\right). \tag{45b}$$

ξ_{n+1} and $\dot{\xi}_{n+1}$ are found by putting $t = h$. These reduce to Eq 42 when $R = 0$.

An even more sophisticated approximation would use a parabola fitted to three consecutive data points, as is done in Simpson's rule. The mathematics of this is as follows. In this case I assume that $f(t)$ is given as an explicit formula which can be evaluated at any chosen t, particularly at the centre of an interval of length $2h$. Alternatively, $f(t)$ can be tabulated at even spacing h and intervals taken in pairs. The method will give the exact answer of ξ_{n+2}, $\dot{\xi}_{n+2}$ if the force varies quadratically with time.

The equation of the parabola through three consecutive force values is $At^2 + Bt + C$ where

$$C \;=\; f_n\,, \qquad B \;=\; \frac{1}{2h}(-3f_n + 4f_{n+1} - f_{n+2})\,, \qquad A \;=\; \frac{1}{2h^2}(f_n - 2f_{n+1} + f_{n+2})\,. \tag{46}$$

The solution of

$$\ddot{\xi} + R\dot{\xi} + \omega^2\xi \;=\; At^2 + Bt + C \quad \text{is}$$

$$\xi \;=\; \frac{At^2+Bt+C}{\omega^2} \;-\; \frac{2A(Rt+1)\;+\;BR}{\omega^4} \;+\; \frac{2AR^2}{\omega^6} \;+\; e^{-Rt/2}\,[\mathcal{C}_1\cos\omega_d t + \mathcal{C}_2\sin\omega_d t]\,. \tag{47a}$$

with derivative

$$\frac{d\xi}{dt} \;=\; \frac{2At+B}{\omega^2} - \frac{2AR}{\omega^4} \;+\; \omega_d\, e^{-Rt/2}[\mathcal{C}_2\cos\omega_d t - \mathcal{C}_1\sin\omega_d t] - \tfrac{1}{2}\,R\,e^{-Rt/2}[\mathcal{C}_1\cos\omega_d t + \mathcal{C}_2\sin\omega_d t]\,. \tag{47b}$$

and ω_d as before at Eq 44. Putting $t = 0$

$$\mathcal{C}_1 \;=\; \xi_n - \frac{1}{\omega^6}(2AR^2 - (2A+BR)\omega^2 + C\omega^4)\,, \qquad \mathcal{C}_2 \;=\; \frac{1}{\omega_d}\left(\dot{\xi}_n + \tfrac{1}{2}\mathcal{C}_1 R + \frac{2AR}{\omega^4} - \frac{B}{\omega^2}\right). \tag{47c}$$

ξ_{n+2} and $\dot{\xi}_{n+2}$ are obtained by putting $t = 2h$. These formulae are modest elaborations of Eq 45 and reduce to Eq 45 when $A = 0$, $B \to A$, $C \to B$. In a calculation which advances in steps of h this parabola scheme will use each tabulated value of f thrice, once for $f(n+2)$ then for $f(n+1)$ and then for $f(n)$.

To illustrate the accuracy of the rectangle, trapezium and parabola approximations I have evaluated them when the force function is $f(t) = 43 \sin 10t$ and $R = 2$, and compared them with the exact solution. The peak force amplitude of 43 was chosen to normalise the peak displacement to 1 unit. Figure 14 is for $h = \pi/(3\mu)$ which gives force values every 60° of the cycle, though not at the peaks. This is arguably the coarsest sample spacing able to represent a sine wave with fair precision. The left panel shows the predicted amplitude for t from 0 to 2 seconds, whilst the right panel is the error for t from 2 to 4 seconds. The accuracy improves from rectangle to trapezium and then to parabola, as expected. The mean absolute errors were respectively $0 \cdot 095$, $0 \cdot 049$, $0 \cdot 010$ units– $9 \cdot 5\%$, $4 \cdot 9\%$ and $1 \cdot 0\%$ of the peak displacement amplitude. The rectangle and trapezium see the force function as flat-topped from 60° to 120° of each cycle, but the parabola interpolates a higher peak at an intermediate position. With 8 points per cycle, $h = \pi/(4\mu)$, the peak force values are given explicitly in the table of $f(nh)$ and the mean errors decrease significantly to $0 \cdot 057$, $0 \cdot 029$, $0 \cdot 006$, about 60% of the respective errors with only 6 points per cycle.

The trapezium method give about half the error of the rectangle, and the parabola almost a tenth. There could be benefit from using the parabola approximation where the force varies smoothly but rapidly, as in the sine wave here.

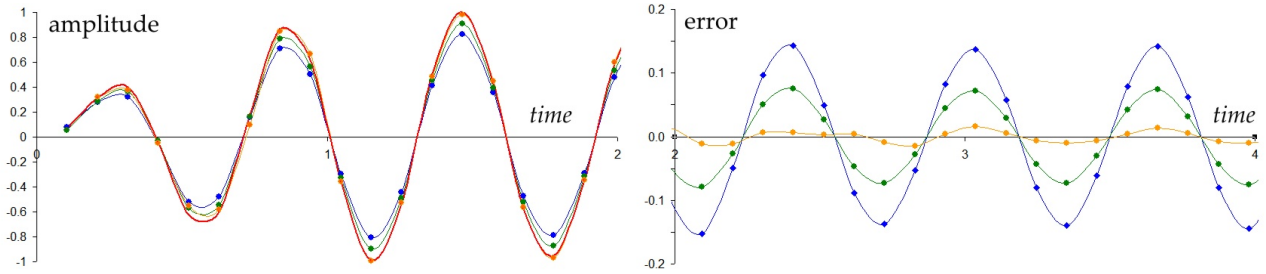

Figure 14: Comparison of the rectangle (blue), trapezium (green) and parabola (orange) schemes at calculating amplitude for force $43 \sin 10t$. Resonant frequency $\omega = 12$, $R = 2$, $h = \pi/30$ secs.

7 Finite element modelling of vibrating plate.

In this final section I move a step closer towards modelling the forced vibration of a thin wooden plate, a very simple counterpart of the top surface of a violin, viola or 'cello. I use the Mecway v4 software which grew out of the LISA 8 program so the presentation in LISA will probably be similar.

7.1 Comparison with Mecway FEA

Discussion is based around the example illustrated in Figure 15 of a rectangular plate 500 mm by 200 mm, 2 mm thick, made of isotropic elastic material with Young's modulus 100 kPa, Poisson's ratio zero, and density 2000 kg/m^3. It is modelled as a quad8 finite element with the standard node numbering shown. This is a shell/plate bending element, suitable for modelling thin sections in which internal through-thickness deformation can be neglected. To limit the model to only 4 degrees of freedom (DoF) – sufficient for an example – heavy constraints are applied at all 8 nodes.

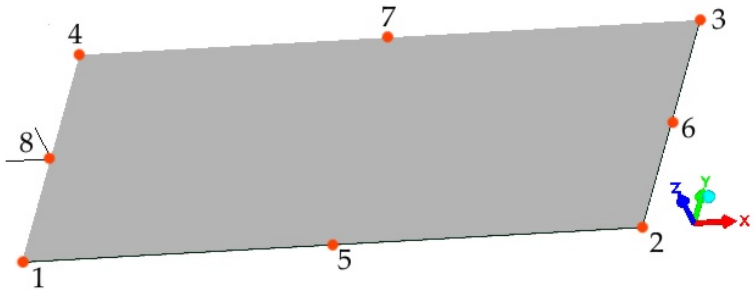

Figure 15: Quad8 shell element used in example. Nodes shown in red. Dimensions 500 mm in x, 200 mm in y, 2 mm in z. Only nodes 2, 6, 3, 7 can move, and then only in z (out of plane).

Unrestricted, each node would have 6 DoF, being 3 for translation and 3 for rotation. Here all nodes are totally restricted to zero rotation, zero translation in x and zero in y. Nodes 4, 8, 1, 5 also have zero z displacement, so the only available DoF are the z displacements at nodes 2, 6, 3, 7. These allow four normal modes of vibration. These are calculated by Mecway and illustrated in the panels of Figure 16. The Modal Analysis 3D facility in Mecway gives the displacements illustrated in Figure 16. However, absolute displacement is not meaningful in this context; the node displacements illustrated in each panel are really the components of the mass-normalised eigenvectors of that particular mode. The element has quadratic variation in displacement across its surface and the contours accordingly show smooth change between all nodes. We should be able to express the response of the plate to a periodic force applied to any of the four mobile nodes in terms of these eigenvectors. The example developed below shows how this is done and compares the results with the time-step numerical integration scheme described in §6 above and carried out in Mecway's Dynamic Response 3D facility.

We do not need concern ourselves with how Mecway calculates the mass and stiffness matrices. This is deep inside the structure of the finite elements. The variation in displacement over each element is described by quadratic shape functions. The actual mass of the element is 400 grams, but no mass is allocated to the immobile nodes. Fortunately Mecway 4 allows the mass and stiffness matrices to be printed to file. There values are

$$\mathbf{M} = \frac{1}{225}\begin{pmatrix} 3 & 1 & -3 & -3 \\ 1 & 3 & -4 & -3 \\ -3 & -4 & 16 & 10 \\ -3 & -3 & 10 & 16 \end{pmatrix}, \qquad \mathbf{K} = \frac{1}{9}\begin{pmatrix} 1450 & 810 & -70 & -1960 \\ 810 & 1450 & -410 & -1960 \\ -70 & -410 & 1640 & 0 \\ -1960 & -1960 & 0 & 4160 \end{pmatrix}.$$

I have retained the row order used by Mecway, which is nodes 3, 2, 7, 6; that is, the displacement vector is $(z_3, z_2, z_7, z_6)^T$. The mass matrix has non-zero off-diagonal elements, quite unlike the discrete case in §2. The matrix

$$\mathbf{E} = \mathbf{M}^{-1}\mathbf{K} = \frac{50}{141}\begin{pmatrix} 35363 & 12745 & 3830 & -40344 \\ 21345 & 43755 & -2250 & -58440 \\ 17084 & 16900 & 11810 & -36192 \\ -8681 & -8605 & -7085 & 22428 \end{pmatrix}$$

from which we obtain the characteristic equation and roots

$$\lambda^4 - 40197\lambda^3 + 3 \cdot 91335\,10^8\,\lambda^2 - 1 \cdot 1668\,10^{12}\,\lambda + 7 \cdot 7438\,10^{14}$$

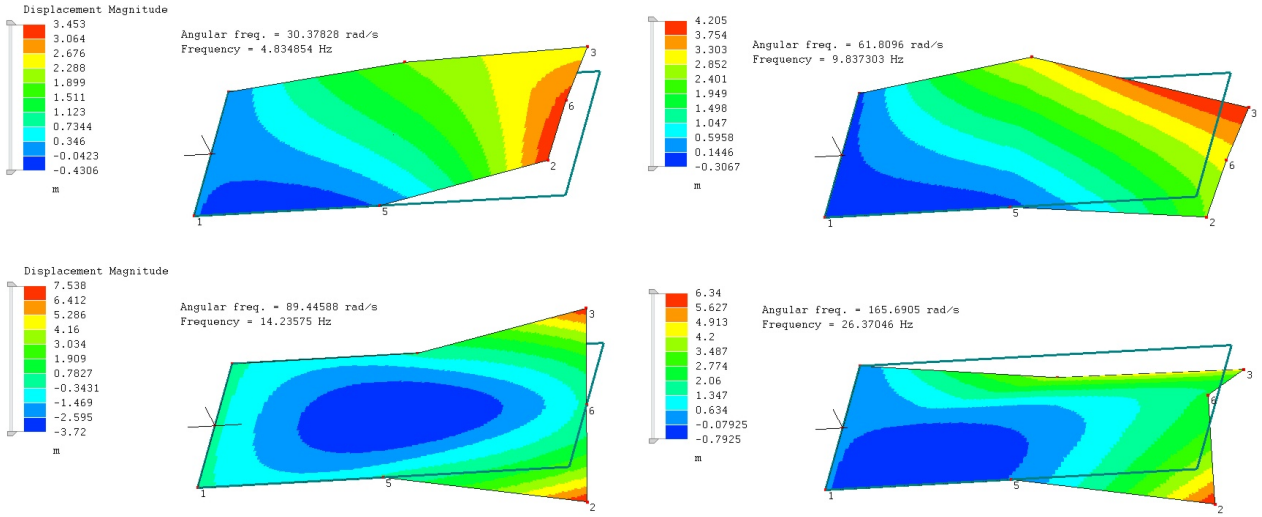

Figure 16: Four normal modes of quad8 membrane element. The undeformed shape is shown in outline. Contours and scales show relative displacement in z (out of plane) direction.

$\lambda = \omega^2$	ω (radians/sec)	frequency (Hz)
$922 \cdot 84$	$30 \cdot 38$	$4 \cdot 83$
$3820 \cdot 4$	$61 \cdot 81$	$9 \cdot 84$
$8000 \cdot 6$	$89 \cdot 45$	$14 \cdot 24$
$27453 \cdot 33$	$165 \cdot 69$	$26 \cdot 37$

These are the values obtained by Mecway and printed in the output in Figure 16. The eigenvectors are found as in §2. I state them as ratios and in the mass-normalised version, as the latter is what Mecway outputs (within a factor of ±1).

$$\omega_1 = 30 \cdot 38: \qquad \mathbf{p_1} = z_3 \begin{pmatrix} 1 \\ 1 \cdot 421 \\ 0 \cdot 786 \\ 1 \cdot 336 \end{pmatrix} = \begin{pmatrix} 2 \cdot 425 \\ 3 \cdot 445 \\ 1 \cdot 906 \\ 3 \cdot 238 \end{pmatrix}$$

$$\omega_2 = 61 \cdot 81: \qquad \mathbf{p_2} = z_3 \begin{pmatrix} 1 \\ 0 \cdot 583 \\ -0 \cdot 744 \\ 0 \cdot 723 \end{pmatrix} = \begin{pmatrix} 4 \cdot 205 \\ 2 \cdot 453 \\ -3 \cdot 130 \\ 3 \cdot 041 \end{pmatrix}$$

$$\omega_3 = 89 \cdot 45: \qquad \mathbf{p_3} = z_3 \begin{pmatrix} 1 \\ -1 \cdot 013 \\ 0 \cdot 005 \\ -0 \cdot 002 \end{pmatrix} = \begin{pmatrix} 7 \cdot 444 \\ -7 \cdot 538 \\ 0 \cdot 034 \\ -0 \cdot 016 \end{pmatrix}$$

$$\omega_4 = 165 \cdot 69: \qquad \mathbf{p_4} = z_3 \begin{pmatrix} 1 \\ 1 \cdot 442 \\ 0 \cdot 908 \\ -0 \cdot 501 \end{pmatrix} = \begin{pmatrix} 4 \cdot 395 \\ 6 \cdot 340 \\ 3 \cdot 991 \\ -2 \cdot 200 \end{pmatrix}$$

Notice how in mode 3 only nodes 3 and 2 experience any significant displacement. This means that a force applied at either node 6 or 7 would struggle to excite this mode.

Pressing on, the matrix $\mathbf{P}$ of columns is formed:

$$\mathbf{P} = \begin{pmatrix} 2\cdot4246 & 4\cdot2054 & 7\cdot4441 & 4\cdot3954 \\ 3\cdot4451 & 2\cdot4532 & -7\cdot5375 & 6\cdot3398 \\ 1\cdot9062 & -3\cdot1300 & 0\cdot0340 & 3\cdot9913 \\ 3\cdot2382 & 3\cdot0410 & -0\cdot0159 & -2\cdot2002 \end{pmatrix},$$

The Rayleigh damping parameters used in Mecway also need to be specified. The measurements on the 'cello in Figure 13 and Appendix 2, §9.3 show a modest shortening of the transient time constant τ with increasing resonant frequency. Suppose therefore that at ω_1 we want $\tau = 1$ sec but only $0\cdot3$ sec at ω_4. Solving the two simultaneous equations gives $\alpha = 1\cdot838$, $\beta = 0\cdot0001769$. With these values the two intermediate resonances have $\tau_2 = 0\cdot8$, $\tau_3 = 0\cdot62$ sec. The corresponding damping coefficients are $R_1 = 2\cdot0$, $R_2 = 2\cdot51$, $R_3 = 3\cdot245$, $R_4 = 6\cdot667$. That completes definition of the structure.

The next step is to specify an oscillating force on one or more nodes and calculate the response for comparison with the results of Mecway which uses modal analysis then numerical integration over time steps as described in §6. As a first case let a force $\mathbf{F} = (\sin\mu t, 0, 0, 0)^T$ of 1 N amplitude be applied to node 3 in the $\pm z$ direction. From Eq 14 the modal force vector is

$$\mathbf{f} = \begin{pmatrix} 2\cdot4246 \\ 4\cdot2054 \\ 7\cdot4441 \\ 4\cdot3954 \end{pmatrix} \sin\mu t\,.$$

From Eq 34 the steady state modal displacements can be written immediately. In vector form

$$\boldsymbol{\xi} = \begin{pmatrix} \frac{2.425\,(922.9-\mu^2)}{4.00\mu^2+(922.94-\mu^2)^2} \\ \frac{4.205\,(3820.5-\mu^2)}{6.30\mu^2+(3820.48-\mu^2)^2} \\ \frac{7.444\,(8001.3-\mu^2)}{10.53\mu^2+(8001.3-\mu^2)^2} \\ \frac{4.395\,(27453.2-\mu^2)}{44.44\mu^2+(27453.2-\mu^2)^2} \end{pmatrix} \sin\mu t \;-\; \begin{pmatrix} \frac{4.849\mu}{4.00\mu^2+(922.94-\mu^2)^2} \\ \frac{10.55\mu}{6.29847\mu^2+(3820.48-\mu^2)^2} \\ \frac{24.16\mu}{10.53\mu^2+(8001.3-\mu^2)^2} \\ \frac{29.30\mu}{44.44\mu^2+(27453.2-\mu^2)^2} \end{pmatrix} \cos\mu t\;. \qquad (48)$$

Since the columns in the matrix $\mathbf{P}$ and hence the modal displacements are only determined to within a factor of -1, it is not meaningful combine the ξ_j values. The modulus of ξ for each of the four modes is plotted in Figure 17 up to $\mu = 200$. The four resonances are very apparent.

To compare a few numerical values with Mecway I have chosen the four forcing frequencies of $\mu = 40$, 80, 120 and 160 rads/sec. Eq 48 has been evaluated at these and the values are listed in Table 1. The enhancement at the ω_4 resonance can be seen in the last row. The last column is the corresponding values of modulus from Mecway, obtained as described below.

My understanding of Mecway[11] is that it uses the same modal analysis modal analysis that gave Eq 48 at each time step, and applies the trapezium scheme of §6 to move to the next time step. Mecway calculates the response to an applied force defined at a finite number of time steps and thereby calculates the total time response, including the start and end transients. These transients,

[11] I am most grateful to Mr Victor Kemp of Mecway for his explanations and for use of a non-standard version of the program which writes the mode weighting factors at each time step to file.

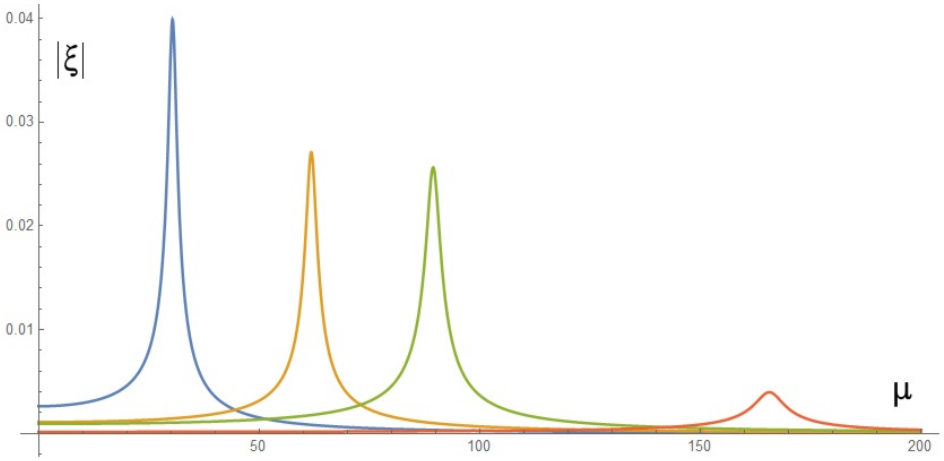

Figure 17: Modal displacement in each of the four vibrational modes when force is on mesh node 3.

	μ	sine	cosine	theory modulus	Mecway modulus
mode 1	40	$-353\cdot1$	$-41\cdot7$	$355\cdot6$	$350\cdot8$
$30\cdot38$ r/s	80	$-44\cdot2$	$-1\cdot3$	$44\cdot2$	$44\cdot7$
$4\cdot83$ Hz	120	$-18\cdot0$	$-0\cdot3$	$18\cdot0$	$18\cdot0$
	160	$-9\cdot8$	$-0\cdot1$	$9\cdot8$	$9\cdot6$
mode 2	40	$189\cdot0$	$-8\cdot5$	$189\cdot2$	$186\cdot6$
$61\cdot81$ r/s	80	$-162\cdot0$	$-12\cdot6$	$162\cdot5$	
$9\cdot84$ Hz	120	$-39\cdot7$	$-1\cdot1$	$39\cdot7$	$39\cdot3$
	160	$-19\cdot3$	$-0\cdot4$	$19\cdot3$	$19\cdot3$
mode 3	40	$116\cdot3$	$-2\cdot4$	$116\cdot3$	$114\cdot7$
$89\cdot45$ r/s	80	$453\cdot2$	$-73\cdot5$	$459\cdot1$	$455\cdot4$
$14\cdot24$ Hz	120	$-115\cdot9$	$-7\cdot1$	$116\cdot1$	
	160	$-42\cdot3$	$-1\cdot2$	$42\cdot3$	42.0
mode 4	40	$17\cdot0$	$-0\cdot2$	$17\cdot0$	$16\cdot8$
$165\cdot69$ r/s	80	$20\cdot9$	$-0\cdot5$	$20\cdot9$	
$26\cdot37$ Hz	120	$33\cdot5$	$-2\cdot1$	$33\cdot6$	$33\cdot4$
	160	$178\cdot2$	$-102\cdot5$	$205\cdot5$	$204\cdot1$

Table 1: Modal displacements $\times10^5$ calculated from Eq 48 at four selected forcing frequencies. Force on mesh node 3 only. Last column lists values from Mecway.

however, are of no interest to steady state spectrum analysis and deliberately ignored. To compare Mecway's values with Table 1 it is necessary to model the oscillating force for long enough that the transients have died away, and then select a sample of cycles from the end of the steady state, just before the force ceases and the end transient starts. Thus in Figure 18 this sample would be from about $5\cdot9$ to $6\cdot2$ seconds. The program will list the mode contributions at each time step, which means they are in the form $f_j \sin(\mu t_n + \beta)_j$ at step n. An example of these is plotted in Figure 19 for $\mu = 80$; the numbers denote the mode. To find the modulus from these I have taken the difference in ξ between an adjacent peak and trough. Moreover, to estimate the true peak, rather than just use

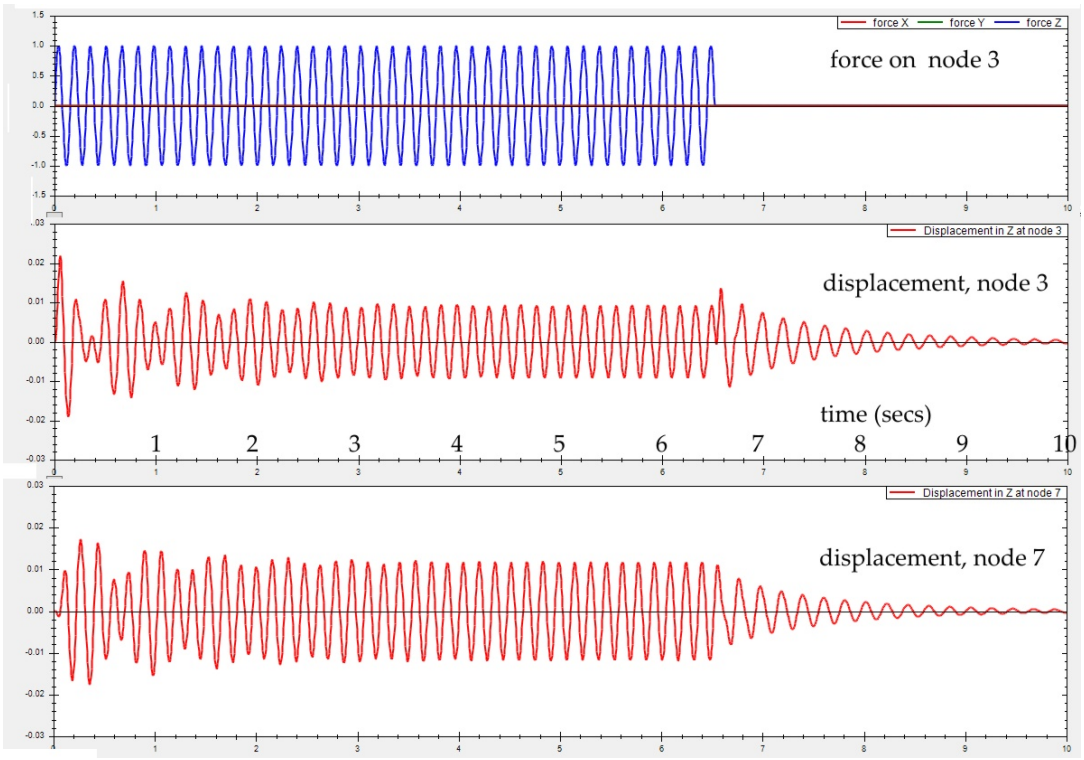

Figure 18: Graphical output from Mecway FEA showing applied force burst at $\mu = 40$ rad/sec (top panel) and the z displacements at mesh nodes 3 and 7.

the largest value in the tabulated output, I fitted a parabola to the three points which straddle the maximum (or minimum)[12]. The twelve values in the last column of Table 1 were produced in this way. They are sufficient to show good agreement with Eq 48 across all modes and resonant frequencies. This confirms the inner workings of Mecway and points to how the steady state frequency spectrum of structure under forced vibration might be more readily calculated.

[12] Given three equally spaced values of a function f, the fitted parabola $At^2 + Bt + C$ has coefficients given by Eq 46 and interpolated extreme value $C - B^2/(4A)$.

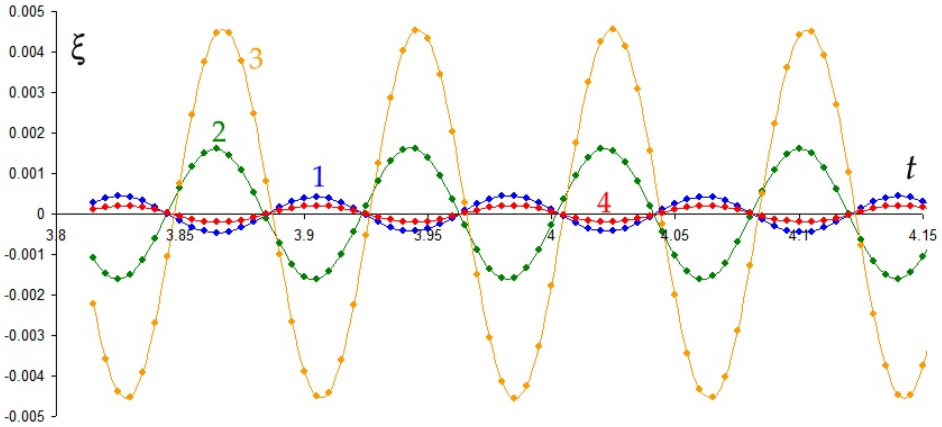

Figure 19: Mode weighting factors at 5 msec time steps for $\mu = 80$ rad/sec as produced by Mecway.

7.2 Mode excitation and sound radiation

To conclude this article I wish to touch on the implications of this steady state (non-transient) modal description of vibration for the behaviour of violin-family instruments. I have written at length on various aspects of violin acoustics in articles published on *www.mathstudio.co.uk*, including charting the vibrational modes of wooden plates and boxes, and the radiation of sound to the listener. The first aim of an integrated model would be to relate the modal spectrum to the sound a listener would hear if the instrument were playing long even notes. The radiated sound field is determined through sound interference of the wavelets from all the vibrating elements of the surface of the wooden box. (The strings contribute almost nothing directly.) At any driving frequency the input to a radiation model will be the steady state displacement of the surface. Where finite element calculations determine the surface displacement, this will be a representative transverse (normal to surface) displacement value of each mesh element, averaged over its nodes, with due recognition of phase. The model would not be limited to harmonic driving forces since the modal spectra can be used to find the response to sawtooth and other periodic forces by the Fourier superposition method described in §4. With these modelling techniques taken together we come quite close to modelling the sound from a vioin, viola or 'cello from a finite element model of its wooden belly when the bow and string impose a complex saw-tooth type of periodic force on the bridge.

One aspect of instrument design which it would be worth modelling would be the effect of changing the position of the feet of the bridge. It is well established that the wooden box-like belly of a viola, say, has many vibrational modes, but the only ones that can affect the sound are those which are excited by the forces applied through the two feet of the bridge. It may be that some less good quality instruments fail to produce a rich, interesting sound because there are wide regions of the spectrum over which there are no active resonances to enhance the loudness and so support the tone. In principle this could be corrected by moving the modal patterns so that a vibrational node line (locus of zero displacement as revealed in Chladni figures) is no longer under a bridge foot. Another option might be an alternative bridge design which places the applied force so that previously stagnant modes are excited.

Recall that the calculation will proceed as follows:

1. Set up the mesh model and material parameters and run the finite element program to find the mass and stiffness matrices. Finding the matrices $\mathbf{M}$ and $\mathbf{K}$ is the only part of the calculation requiring finite elements – the rest is just matrix linear algebra.

2. Find the eigenvalues (natural frequencies) and eigenvectors over N relevant modes. Mass normalise the eigenvectors and form the transformation matrix $\mathbf{P}$.

3. Decide upon the coefficients of Rayleigh damping α, β to give the desired transient decay time constant as a function of resonant frequency. Alternatively input R_j of each mode j from a table.

4. Select which node or nodes at which the force will be applied. Define the vector $\mathbf{F}$ and the calculate the modal force vector $\mathbf{f} = \mathbf{P}^T\,\mathbf{F}$.

5. Choose a driving frequency μ and build the matrices of sine and cosine components of modal displacement $\boldsymbol{\xi}$ as at Eqs 34, 48. If a symbolic mathematics program is being used, μ can be retained as a parameter.

6. Transform to mesh node displacements by $\mathbf{x_{sin}} = \mathbf{P}\,\boldsymbol{\xi}_{sin}$ and $\mathbf{x_{cos}} = \mathbf{P}\,\boldsymbol{\xi}_{cos}$.

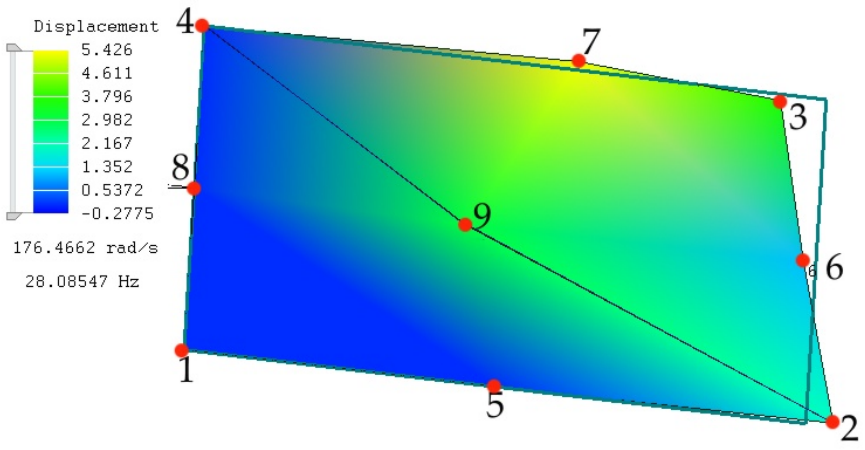

Figure 20: Plate of Figure 15 redefined as two tri6 finite elements showing 5 degrees of freedom.

The result will be two matrices giving the sine and cosine components of displacement in each of the directions x, y, z at the specified frequency driving μ.

In this form the data are well matched to the input requirements of the program I wrote to calculate the radiation of sound from a vibrating surface [13]. That program models the surface as a mesh of triangular tiles and sums the elementary waves radiated from each to the listening point, taking account of amplitude, phase and path differences, using either the Kirchhoff or Rayleigh-Sommerfeld formulation. The input to the program includes the lists of triangular elements, the co-ordinates of the vertices, and the surface amplitude and phase of each. The displacement of each surface element can be taken to be the algebraic mean of the displacements of its constituent nodes. The sound radiation calculation, such as by the Kirchhoff model, will also involve the area of each element and its position and orientation with respect to the listening position.

Figure 20 illustrates how the thin rectangular plate of Figure 15 may be modelled as two tri6 elements through the introduction of a new node, number 9, in the centre of the diagonal. Even with this very small model there are 9×6 potential degrees of freedom so the eigenvalues which form the columns of $\mathbf{P}$ will have 54 rows. If there are no constraints on movement, there will be 54 normal modes, generating $\mathbf{P}$ as a 54 by 54 matrix. The imposed force $\mathbf{F}$ will be a vector with 54 rows, all but one or two of which will be zero. In a less contrived structure it may be desirable to limit the size of the matrices by i) imposing constraints on the nodes which set the corresponding rows in the eigenvectors to zero, and ii) limiting the number of vibrational modes included to $m < 6n$ where n is the number of mesh nodes. $\mathbf{P}$ then reduces to a $6n$ by m matrix. Clearly any such truncating of the matrices must be done with engineering judgement. Sound is generated only by transverse motion of the plate, so modes which are predominantly in-plane motion can be disregarded. It would be reasonable to constraint the structure to move only out-of-plane provided checks show that this constraint does not lead to non-physical movement. For instance, applying zero-rotation about the z (plate normal) axis in Figure 20 will suppress 9 vibrational modes without much affecting the vibration. However, preventing hinge-like rotation at the edge of a plate will change the boundary conditions from simply-supported to fully encastré, and that will push the resonant frequencies up greatly – a very different situation. I would like to explore the practical implementation of steady state modal vibration in a future article on *www.mathstudio.co.uk*.

[13] See §6.2 and §7 of 'Physics of sound wave radiation from vibrating surfaces' published on *www.mathstudio.co.uk*.

The calculation just outlined will give the displacement at each mesh node at frequency μ. There is a second, complementary way to present the information – as the frequency spectrum of the average node displacement. This is a quicker calculation – even rough and ready – which just takes the algebraic averages of transverse (out-of-plane) displacements over all mesh nodes and presents this as a table or graph against μ. When the object is a flat or almost flat plate, and the mesh nodes are evenly distributed over the plate surface so that the density of nodes is uniform, this average has a physical interpretation; when multiplied by the area of the plate, it approximates the sound amplitude radiated by the plate in a direction normal to its plane, taking into account the amplitude and phase differences over the whole surface. Though not as precise as using the sound radiation program, it would provide a quick, flexible way of seeing the effect on the sound spectrum of design changes to the structure. The reason the calculation would be quick is that it would not be necessary to calculate the physical displacements $\mathbf{x}$. Instead, form a one-row matrix $\mathcal{P}_{av}$ whose elements are the averages of the columns of $\mathbf{P}$. Then the average displacement of the whole structure is $Z_s \sin \mu t + Z_c \cos \mu t$ where Z_s is the one-element matrix $\mathcal{P}_{av}(\mu)\, \boldsymbol{\xi_s(\mu)}$, and similarly Z_c. From these components calculate the modulus $Z_t(\mu) = \sqrt{Z_s^2 + Z_c^2}$ and phase $\arctan(Z_c/Z_s)$. The user could make a rapid survey of design options using this quick, approximate calculation and then decide where the more exact but more complicated sound radiation program is needed.

To illustrate the sort of result that would be obtained, Figure 21 plots the spectra $Z_t(\mu)$ for the rectangular thin hex8 plate element when an oscillating force of 1 newton peak is applied to various mesh nodes[14]. The top four panels have the whole force applied at one node only, whilst the central bottom panel has the force shared, $0 \cdot 5 \sin \mu t$ N on node 2 and the same, in phase, on node 7. These spectra approximate the sound amplitude close to the surface. What is most striking is the inability to get any sound from vibrational mode 3. A glance at Figure 16 shows why – two corners of the rectangle are reciprocating and form an acoustic dipole in which the sound disturbances at each corner of the plate cancel out within a short distance above the surface. The bottom panel shows a similar effect where the equal, in-phase forces on nodes 2 and 7 jam mode 2 which wants to have these two nodes move out of phase. The third notable feature is the dominance of mode 1 however the plate is driven. It is likely that similar effects are happening in all violin-family instruments – many resonant modes of the wooden box exist, but some cannot be excited from the positions of the bridge feet, and others that can be excited radiate little sound. In principle finite element modelling can be applied as described above to study this and hopefully prompt thoughts on how to harness the resonances more efficiently.

John Coffey, Cheshire, England, January 2016

[14] The values are not strictly the mean Z_t but just the sum. They are therefore 8 times larger than Z_t.

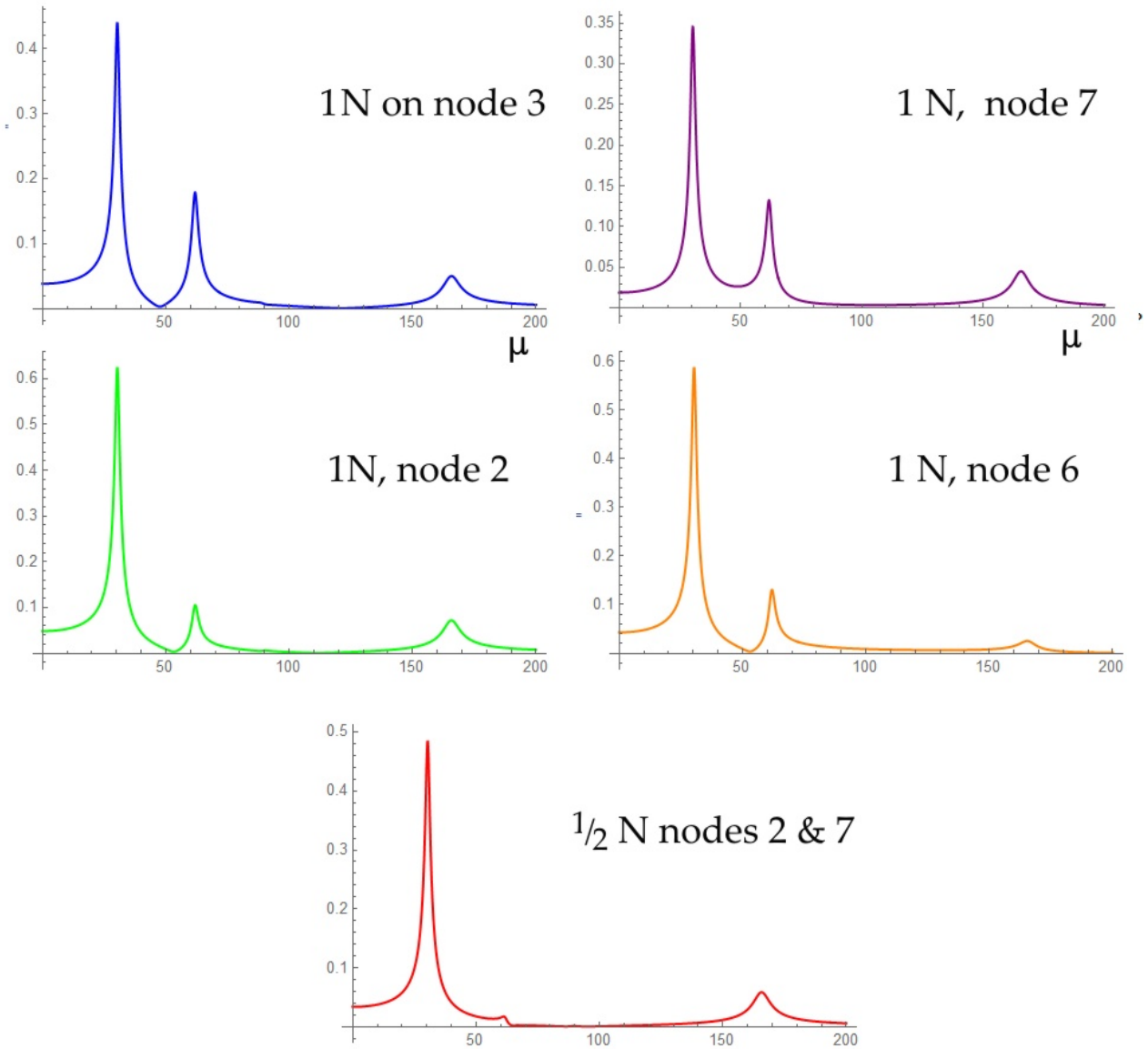

Figure 21: Spectra of net z displacement of plate of Figure 15 for force 1 $\sin \mu t$ N applied in five positions.

8 Appendix 1: Linear approximation

This Appendix illustrates what is involved in making the linear approximation to a vibrating system, using an example. The case examined is a pendulum with one mass, but with a spring or elastic chord in place of the usual 'inextensible string'. I first derive the exact equations of motion using Lagrange's equation and then eliminate all terms that are not linear in the two variables x and θ or their time derivatives. In this reduced form the equations of motion separate and two normal modes are readily identified.

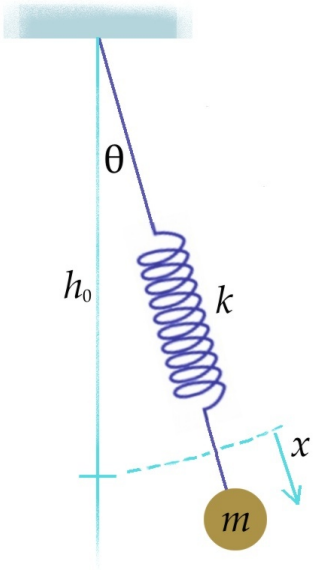

Figure 22: The spring-and-mass pendulum.

The system is shown in Figure 22. All motion is confined to the plane. The spring has negligible mass, stiffness constant k and natural length h_0, and remains straight at all times. The length at time t is $H(t) = h_0 + x(t)$, x being the instantaneous extension. At the vertical equilibrium position the length of the spring under the weight of the bob is $h = h_0 + mg/k$. There are two degrees of freedom and we use co-ordinates x and θ.

Lagrange's method[15] is a protocol for determining the equations of motion. If $q_j,\ j = 1, 2$ are the generalised co-ordinates and T and V are respectively the total kinetic and potential energies, then

$$\frac{d}{dt}\left(\frac{\partial T}{\partial \dot{q}_j}\right) - \frac{\partial T}{\partial q_j} + \frac{\partial V}{\partial q_j} = 0\,. \qquad (A1)$$

The co-ordinate derivatives here have a peculiar interpretation; they are performed as if q and $\dot{q}$ were independent variables. In our case $q_1 = x(t)$ and $q_2 = \theta(t)$.

The potential energy is the work done in moving to its current configuration from some reference state. Take the reference state, V zero, to be when the spring is unstretched, hanging vertically downwards without the bob attached. The potential energy has a contribution from elastic strain and another from gravity when the bob is not at the level h_0. Thus

$$V = \tfrac{1}{2}kx^2 + mg(h_0 - [h_0 + x]\cos\theta)\,.$$

[15] See again the book by Douglas Gregory, 'Classical Mechanics' page 339.

$$\frac{\partial V}{\partial x} \;=\; kx - mg\cos\theta \qquad \text{and} \qquad \frac{\partial V}{\partial \theta} \;=\; mgH\sin\theta\,. \tag{A2}$$

The instantaneous velocity of the bob has components along and at right angles to the line of the spring. The total kinetic energy is

$$T \;=\; \tfrac{1}{2}m(\dot{x}^2 + H^2\dot{\theta}^2) \tag{A3}$$

so that

$$\frac{\partial T}{\partial x} \;=\; mH\dot{\theta}^2\,, \qquad \frac{\partial T}{\partial \dot{x}} \;=\; m\dot{x}\,,$$
$$\frac{\partial T}{\partial \theta} \;=\; 0\,, \qquad \frac{\partial T}{\partial \dot{\theta}} \;=\; mH^2\,\dot{\theta}\,.$$

These quantities have physical meanings. $mH\dot{\theta}^2$ is the centrifugal force, $m\dot{x}$ is the linear momentum along the line of the spring and $mH^2\,\dot{\theta}$ is the angular momentum. For the time derivatives of $\partial T/\partial\dot{x}$ and $\partial T/\partial\dot{\theta}$ we revert to the usual meaning of differentiation. Then

$$\frac{d}{dt}\left(\frac{\partial T}{\partial \dot{x}}\right) \;=\; m\ddot{x} \qquad \text{and} \qquad \frac{d}{dt}\left(\frac{\partial T}{\partial \dot{\theta}}\right) \;=\; mH^2\ddot{\theta} + 2mH\dot{x}\,\dot{\theta}\,.$$

The equations of motion are

$$m\ddot{x} - m(h_0 + x)\,\dot{\theta}^2 + kx - mg\cos\theta \;=\; 0\,, \tag{A4a}$$

$$(h_0 + x)\ddot{\theta} + 2\dot{x}\dot{\theta} + g\sin\theta \;=\; 0\,. \tag{A4}$$

These are a tangled pair of simultaneous ordinary differential equations probably incapable of closed form analytical solution. Note that the second equation states that the angular momentum is not constant; this is because gravity applies a torque about the support. The quantity $g\sin\theta$ is the horizontal component of gravitational acceleration.

The linearised versions of Eq A4 are obtained by assuming that the perturbations of the system are small. While we could choose the total extension $x = H - h_0$ as the small quantity, an even better approximation is obtained by using the extension relative to h, the length of the spring under the dead weight of the bob. Introduce $\epsilon = x - mg/k$ where mg/k is the extension when the bob is stationary below the support. In terms of ϵ the two equations of motions are

$$m\ddot{\epsilon} - m\left(h_0 + \frac{mg}{k} + \epsilon\right)\dot{\theta}^2 + k\epsilon + mg(1 - \cos\theta) \;=\; 0\,, \tag{A5a}$$

$$\left(h_0 + \frac{mg}{k} + \epsilon\right)\ddot{\theta} + 2\dot{\epsilon}\dot{\theta} + g\sin\theta \;=\; 0\,. \tag{A5b}$$

The linearised equations are now obtained by assuming that not only ϵ and θ are small, but also $\dot{\epsilon}$, $\ddot{\epsilon}$, $\dot{\theta}$ and $\ddot{\theta}$, so that all squares and products of these can be ruthlessly disregarded. Moreover $\cos\theta$ is replaced by 1 and $\sin\theta$ by θ. The two equation are approximated by

$$m\ddot{\epsilon} + k\epsilon \;=\; 0\,, \tag{A6a}$$

$$h\ddot{\theta} + g\theta \;=\; 0\,. \tag{A6b}$$

These are not coupled. Their solutions are

$$\epsilon \;=\; C_1\cos\omega_x t + C_2\sin\omega_x t\,, \qquad \omega_x = \sqrt{\frac{k}{m}}\,, \tag{A7a}$$

$$\theta \;=\; D_1 \cos\omega_\theta t + D_2 \sin\omega_\theta t\,, \qquad \omega_\theta = \sqrt{\frac{g}{h}} \qquad (A7b),$$

with arbitrary constants C and D. The ϵ solution describes oscillation of the bob about the constant extension under the weight of the bob. The solution for θ describes a simple pendulum with chord length $h = h_0 + mg/k$. These are the two normal modes, and are just what we would expect for small disturbances.

Knowing that we want linearised equations, we could have simplified the calculation by removing all except quadratic terms from V and T. Using the small angle approximations of cosine and sine, and $H \to h$ give

$$V \;\approx\; \tfrac{1}{2}kx^2 \,-\, mgx \,+\, \tfrac{1}{2}mgh\theta^2\,.$$

$$\frac{\partial V}{\partial x} \;\approx\; kx - mg\,, \qquad \text{and} \qquad \frac{\partial V}{\partial \theta} \;\approx\; mgh\theta\,.$$

$$T \;\approx\; \tfrac{1}{2}m[\dot{x}^2 + h^2\dot{\theta}^2]$$

$$\frac{\partial T}{\partial x} \approx 0\,, \qquad \frac{\partial T}{\partial \dot{x}} = m\dot{x}$$

$$\frac{\partial T}{\partial \theta} = 0\,, \qquad \frac{\partial T}{\partial \dot{\theta}} \approx mh^2\,\dot{\theta}\,,$$

and Eq A6a, b follow immediately.

Using the power of Mathematica 10 it is possible to obtain numerical solutions to the two coupled exact non-linear equations. Take h = 1 metre, $m = 0\cdot1$ kg, k = 4 N, $g = 9\cdot8$ m s^{-2}. The length h with the bob attached is $1\cdot245$ m. The left panel of Figure 23 plots ϵ and θ for small initial displacements, and the right panel for displacements which are 10 times larger. Reading from the graphs in the left panel I find that $\omega_x^2 = 39\cdot9$ to be compared with $4/0\cdot1 = 40$ rad^2/sec^2, and $\omega_\theta^2 = 7\cdot90$ compared with $9\cdot8/1\cdot245 = 7\cdot87$. These values are close enough to confirm Eq A7. At the larger displacements the non-linear coupling of the two modes is very clear.

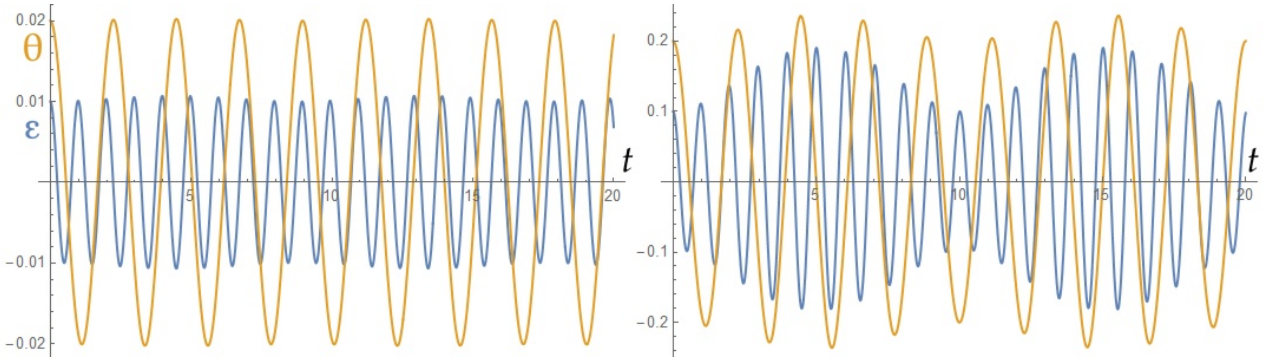

Figure 23: Oscillation displacement ϵ (blue) and angular position θ (orange) with time over 20 seconds after release from an initial position. Left: $x(0) = 0\cdot01$ m, $\theta(0) = 0\cdot02$ radians. Right: $x(0) = 0\cdot1$ m, $\theta(0) = 0\cdot2$ radians. $h_0 = 1$, $m = 0\cdot1$, $k = 4$ SI units.

In chapter 15 of his book on classical mechanics Gregory writes the linearised equations of motion in terms of matrices $\mathbf{T}$ and $\mathbf{V}$ which derive from the kinetic and potential energies respectively:

$$\mathbf{T}\ddot{\mathbf{q}} + \mathbf{V}\mathbf{q} = \mathbf{0}\,. \qquad (A8)$$

$$T \;= \dot{\mathbf{q}}^T\,\mathbf{T}\,\dot{\mathbf{q}}\,, \qquad V \;= \mathbf{q}^T\,\mathbf{V}\,\mathbf{q}\,.$$

Gregory's examples are all quadratic binary forms in the co-ordinate values. In our example $\mathbf{T}$ is a quadratic form, but to obtain the potential energy the constant $\frac{1}{2}mgx_0$ must be subtracted from $\mathbf{V}$ after the matrix multiplications have been carried out. This is on account of the chosen reference position for zero potential.

$$\mathbf{T} = \tfrac{1}{2}\begin{pmatrix} m & 0 \\ 0 & mh^2 \end{pmatrix}, \qquad \mathbf{V} = \tfrac{1}{2}\begin{pmatrix} k & 0 \\ 0 & mgh \end{pmatrix}, \qquad \mathbf{q} = \begin{pmatrix} \epsilon \\ \theta \end{pmatrix}.$$

$\mathbf{T}$ and $\mathbf{V}$ are the generalisation of $\mathbf{M}$ and $\mathbf{K}$ used in §2 and other analysis in this article.

9 Appendix 2: Experimental determination of mode damping in 'cello and viola

The damping in a resonant system manifests itself through the lowering and widening of the resonant peak as the frequency sweeps through the resonance, and in the rate of decay of oscillations after the system has been disturbed. I have examined many resonances of a 'cello body (no string vibration) and a few of a viola from both these points of view to obtain numerical values for the damping coefficients and to see if there is any trend with the resonant frequency. The experimental technique is similar to what I first used for exploring the Helmholtz resonance, as reported in the article 'The air cavity, *f*-holes and Helmholtz resonances of a violin and viola' 2013, published on the web site *www.mathstudio.co.uk*.

9.1 Mathematical foundation

Here I give a full account of the solution of the modal equation of motion Eq 32 to 34 because it is the foundation on which the experimental method is built. It is, of course, a conjecture and a mathematical convenience that the damping be described as directly proportional to the velocity of the vibrating mass. If instead it were proportional, say, to $\dot{\xi}^2$, we would have a non-linear equation soluble only numerically. So we assume a linear damping term $R\dot{\xi}$ and seek the general solution of

$$M\ddot{\xi} + R\dot{\xi} + K\xi \;=\; F\sin\mu t\,. \qquad (A2.1)$$

One can add to each side of this any expression which evaluates to zero, so if ξ_p is a solution, then so is $\xi_p+\xi_c$ where $M\ddot{\xi}_c+R\dot{\xi}_c+K\xi_c = 0$. ξ_p is the particular solution and ξ_c the complementary function, describing the motion when the force has ceased.

9.1.1 Solution of equation of motion

First solve for ξ_c. Treating differentiation as an operator $\mathcal{D} \equiv d/dt$, the complementary differential equation factors formally as

$$(\mathcal{D}-\lambda_+)(\mathcal{D}-\lambda_-)\,\xi \;=\; 0 \quad \text{where} \quad M\lambda_\pm^2 + R\lambda_\pm + K = 0\,.$$

The roots of this auxiliary equation are

$$\lambda_\pm \;=\; -\frac{R}{2M} \pm \frac{i}{2M}\sqrt{(4KM-R^2)}\,, \qquad 4KM > R^2\,.$$

$$\text{Thus} \quad \frac{d\xi}{dt} - \lambda_\pm\xi \;=\; 0 \quad \text{or} \quad \frac{d\xi}{\xi} \;=\; \lambda_\pm t\,.$$

Integrating and taking the exponential

$$\xi_\pm \;=\; C\,\exp\left(-\frac{Rt}{2M}\right)\left[\cos\omega_d t \pm i\sin\omega_d t\right], \qquad \omega_d = \frac{1}{2M}\sqrt{4KM-R^2}$$

where C is an arbitrary constant. There are two independent solutions here. A general linear combination of them is

$$\xi_c \;=\; e^{-t/\tau}\left[C_1\cos\omega_d t + C_2\sin\omega_d t\right], \qquad \tau = \frac{2M}{R}\,. \qquad (A2.2)$$

The selectable constants C_1, C_2 allow this complementary solution to match to any two given conditions such as values of $\xi(0)$ and $\dot{\xi}(0)$. This formula points directly to one potential method for

measuring the damping parameter; excite the system, then suddenly remove the force and measure the time for the wave envelope to fall to $e^{-1} = 36\%$ of its initial value. Unfortunately, this holds true only for a system with one degree of freedom. In general a system will have many modes and the transients can contain any mixtures of decaying modes depending on the precise displacement and velocity immediately when the force is switched on or off. Nevertheless we may hope to isolate single modes by driving it at a resonance using the frequency μ equal to the normal frequency ω. Then when the force is removed, hopefully only this mode will feature in the transient. My efforts to attain this happy state are described in §9.2 below.

To find the particular solution we try a function with form similar to the forcing term, so try $\xi_p = A\sin\mu t + B\cos\mu t$. Substituting in Eq A2.1, we find that A and B satisfy the matrix equation

$$\begin{pmatrix} K-\mu^2 M & -\mu R \\ \mu R & K-\mu^2 M \end{pmatrix} \begin{pmatrix} A \\ B \end{pmatrix} = \begin{pmatrix} F \\ 0 \end{pmatrix},$$

from which

$$\begin{pmatrix} A \\ B \end{pmatrix} = \frac{F}{\Delta}\begin{pmatrix} K-\mu^2 M \\ -\mu R \end{pmatrix}, \qquad \Delta = (K-\mu^2 M)^2 + \mu^2 R^2 .$$

Δ is the determinant of the coefficient matrix. The particular solution is therefore

$$\xi_p = \frac{F}{\Delta}[(K-\mu^2 M)\sin\mu t \; - \; \mu R\cos\mu t\,]. \qquad (A2.3a)$$

The sine and cosine can be combined to give

$$\xi_p = \frac{F}{\sqrt{\Delta}}\sin(\mu t-\psi) \quad \text{where} \quad \tan\psi = \frac{\mu R}{K-\mu^2 M} = \frac{2\mu}{\tau(\omega_0^2-\mu^2)}. \qquad (A2.3b)$$

There is a 180° phase shift as μ crosses the resonance.

For some purposes it is enlightening to express this solution in terms of frequencies rather than M, K and R. If $R = 0$ the undamped natural frequency is

$$\omega_0 = \sqrt{\frac{K}{M}}.$$

$$\text{Then} \quad \omega_d^2 = \frac{K}{M} - \left(\frac{R}{2M}\right)^2 = \omega_0^2 - \frac{1}{\tau^2} \qquad (A2.4)$$

$$\text{and} \quad \frac{\Delta}{M^2} = (\omega_0^2-\mu^2)^2 + \left(\frac{2\mu}{\tau}\right)^2. \qquad (A2.5)$$

$$\xi_p = \frac{F}{M}\,\frac{(\omega_0^2-\mu^2)\sin\mu t - \left(\frac{2\mu}{\tau}\right)\cos\mu t}{(\omega_0^2-\mu^2)^2 + \left(\frac{2\mu}{\tau}\right)^2}. \qquad (A2.6)$$

It follows immediately that the magnitude of the displacement is

$$|\xi_p| = \frac{F}{M}\,\frac{1}{\sqrt{(\omega_0^2-\mu^2)^2 + \left(\frac{2\mu}{\tau}\right)^2}} \qquad (A2.7)$$

which has its maximum value of

$$|\xi|_{peak} = \frac{FM}{R\omega_d} = \frac{F\tau}{2\,\omega_d} \quad \text{at} \quad \mu_m^2 = \omega_0^2 - \frac{2}{\tau^2}. \qquad (A2.8)$$

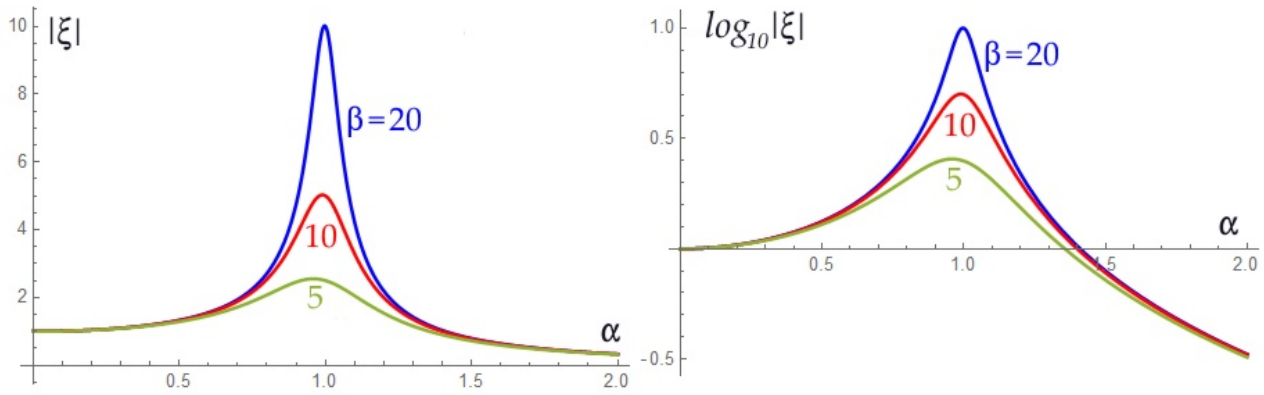

Figure 24: Relative amplitude as driven frequency sweeps through a damped resonance expressed in dimensionless parameters $\alpha = \mu/\omega_0$, $\beta = \tau\omega_0$. Left: linear amplitude scale. Right: logarithmic.

The full width of the peak at half height (FWHH) is $2\sqrt{3}R\omega_0$. μ_m is a third notable frequency to set alongside ω_0 and ω_d. To put some numbers on these, if $M = K = 1$ and $R = 1/5$ then $\omega_0 = 1$, $\omega_d = 0 \cdot 995$, $\mu_m = 0 \cdot 990$ and $\tau = 10$. So for R relatively small the peak occurs when the driving frequency μ almost coincides with the natural frequency ω_0.

There is a further way of expressing $|\xi_p|$ which used the dimensionless quantities $\alpha = \mu/\omega_0$ and $\beta = \tau\omega_0$. Since $\omega_0 = 2\pi/T$ where T is the period of the oscillations, β is 2π times the number of cycles for the amplitude of the oscillation to die to $e^{-1} = 36\%$ of its value when the force is suddenly switched off.

$$|\xi_p| = \frac{F}{\omega_0^2 M} \frac{1}{\sqrt{(1-\alpha^2)^2 + \left(\frac{2\alpha}{\beta}\right)^2}}.$$

$$\text{Then the peak amplitude is at } \alpha = \frac{\sqrt{\beta^2 - 2}}{\beta}, \quad \text{value } \frac{F}{\omega_0^2 M} \frac{\beta^2}{2\sqrt{\beta^2 - 1}}. \qquad (A2.9)$$

This form is usually used in textbooks to plot the relative amplitude as the driving frequency sweeps through a damped resonance. Figure 24 shows a family of such curves for three values of β. The trend to lower peak values can be seen in the curves for the most highly damped case, $\beta = 5$. The narrowing and sharpening of the peak at larger β is sometimes expressed in terms of a quality factor Q, usually defined at the ratio of power half width to peak centre frequency. Measuring the sharpness of a spectral peak is potentially a second method for quantifying the damping parameter R.

The parameter R was introduced into the equation of motion in terms of the resistive force $R\dot{\xi}$. R is also proportional to the rate of energy loss from the structure. To see this note that the work done when the force moves a distance $\delta\xi$ is $R\dot{\xi}\,\delta\xi$. Since the displacement $\xi = A\sin\mu t$ and $\delta\xi = \dot{\xi}\,\delta t$, the work done per cycle is

$$\int_0^{2\pi/\mu} R\mu^2 A^2 \cos^2(\mu t)\, dt \;=\; \pi A^2 R\mu\,. \qquad (A2.10)$$

Since there are $\mu/2\pi$ cycles per second, the rate of energy loss is $\frac{1}{2}\mu^2 A^2 R$ per second.

This analysis is all for the case of a single resonance. When there are multiple resonances the damping term in the equations of motion will lead to some limited interaction between resonances.

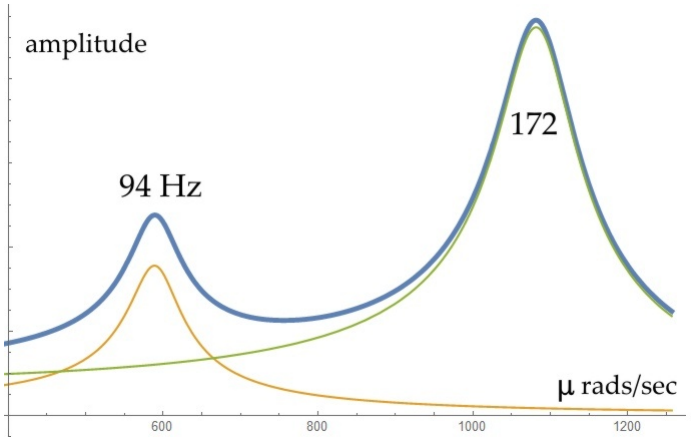

Figure 25: Simulation of the two 'cello resonance peaks at 94 and 172 Hz, by adding weighted responses curves as Eq A2.7. The individual curves are plotted feint.

The mathematics behind this is discussed in §5.1 of the main text. As a probably crude first approximation to the interaction we may simply add two curves, each given by Eq A2.7 but with different values of F, ω_0, and τ. As an example we shall see below that the 'cello has resonances close to 94 Hz and 172 Hz. Figure 25 is a simulation of what the combined spectrum might look like. There is little perturbation in the width and shape of each peak, but the flanks of the weaker one are significantly altered.

9.1.2 The rising transient

I continue the analysis to see what happens during the starting phase of a driven mode. This anticipates the experimental results which in most cases show a faster rise when a sine wave tone burst is applied to the musical instrument than fall when the tone burst abruptly ends. To solve this we must combine complementary and particular solutions of the equation of motion, choosing C_1 and C_2 in Eq A2.2 to match the initial conditions, which we take as $\xi(0) = 0$, $\dot{\xi}(0) = 0$. Setting $t = 0$ in either Eq A2.3a or A2.6 readily gives

$$C_1 \;=\; \frac{\mu F R}{\Delta} \;=\; \frac{2F\mu}{M\tau\Delta}\,. \qquad (A2.10a)$$

Differentiating with respect to t produces

$$\dot{\xi}(0) \;=\; C_2\,\omega_d - \frac{C_1}{\tau} + \frac{\mu F M}{\Delta}(\omega_0^2 - \mu^2)$$

from which

$$C_2 \;=\; -\frac{\mu F M}{\omega_d\,\Delta}\left(\omega_0^2 - \mu^2 - \frac{2}{\tau^2}\right). \qquad (A2.10b)$$

Measurement will be made nominally with μ at the peak of the resonance so $\mu = \mu_m \approx \omega_0 \approx \omega_d$. More precisely, $(\omega_0^2 - \mu_m^2) = 2/\tau^2$, $C_2 = 0$ and $\Delta = 4M^2(1 + \mu_m^2\,\tau^2)/\tau^4$ from which

$$\xi_{peak}(t) \;=\; \frac{F\tau^2}{2M\,(\mu_m^2\tau^2 + 1)}\left(e^{-t/\tau}\mu_m\tau\cos\omega_d t - \mu_m\tau\cos\mu_m t + \sin\mu_m t\right). \qquad (A2.11)$$

The structure of the rising amplitude from this formula is illustrated in Figure 26 for the quite heavily damped case of $F = M = K = 1$, $R = 1/5$. The expression evaluates to

$$\xi_{peak}(t) \;=\; 5e^{-t/10}\cos(0\cdot 995t) - 5\cos(0\cdot 990t) + 0\cdot 505\sin(0\cdot 990t)\,.$$

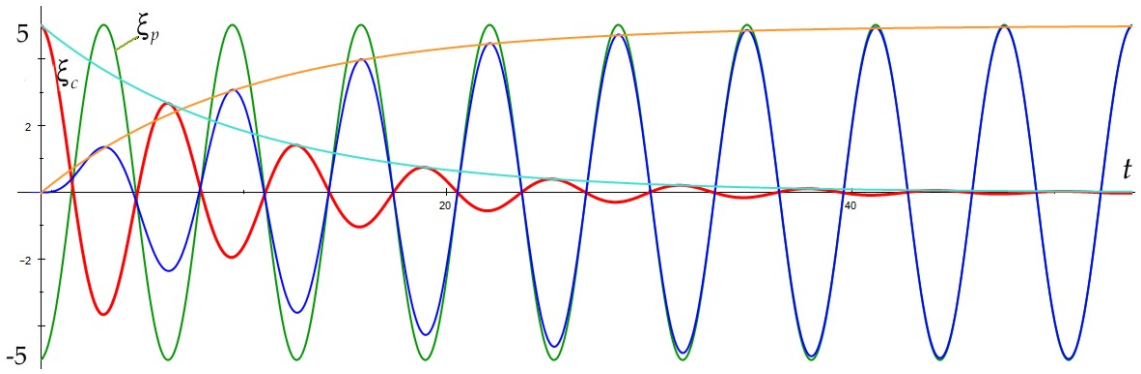

Figure 26: Structure of the increasing displacement ξ when the oscillating force is switched on with $\mu = \mu_{max}$. Red: ξ_c. Green: ξ_p. Blue: $\xi_c + \xi_p$,. Orange and cyan: envelopes. $F = M = K = 1$, $R = 0 \cdot 2$.

The steady state response (green curve) to the forcing term of $\sin(0 \cdot 990t)$ is heavily phase shifted, because $-5\cos(0 \cdot 990t) + 0 \cdot 505\sin(0 \cdot 990t) = 5 \cdot 025\sin(0 \cdot 990t - \psi)$ where $\tan\psi = -5/0 \cdot 505 = -9 \cdot 9$, $\psi = 84°$. Thus the steady state signal ξ_p is close to $-5 \cdot 025\cos(0 \cdot 990t)$ and at $t = 0$ this is exactly to the natural response $\xi_c = 5e^{-t/10}\cos(0 \cdot 995t)$ (red curve). These two waves cancel out exactly at $t = 0$, and the degree of cancellation falls with time constant $\tau = 10$. The sum $\xi_c(t) + \xi_p(t)$ is plotted as the blue curve. The envelope curve (orange) is $5 \cdot 025(1 - e^{t/10})$.

An important point to observe is that, provided the driving frequency is set to give maximum displacement, $\mu = \mu_m$, the same time constant $\tau = 2M/R$ describes this rise as describes the fall when the force is abruptly switched off. In other words, in an experiment we expect to see the same rates of change in the starting transient of a tone burst as in the trailing transient. However in any experiment with a musical instrument there may be some uncertainty as to which is exactly the peak frequency. The panels of numerical simulations in Figure 27 show how the structure of the rising pulse changes when the driving frequency is slightly off μ_m. The more rapid rise, and the oscillation in the envelope, are consequences of the interference between ξ_c and ξ_p – a type of beats. Indeed, the lower frequency structure in the envelope is at the beat frequency equal to the difference in frequencies of the two interfering waves; $\cos(X + \delta) + \cos(X - \delta) = 2\cos X\,\cos\delta$, but $|\cos\delta|$ has frequency 2δ, making the envelope oscillate with frequency δ. As an example, at $\mu = 0 \cdot 90$ $\delta = 1/20$ radians/sec so the period is $20\pi = 63$ secs, which is approximately the time delay between the peaks in the lower left panel of Figure 27. The increase in beat frequency with $\mu - \omega_0$ is apparent in this series of graphs.

Whatever shape the displacement envelope takes in response to the driving force starting, the complementary function has died to 2% of its starting value in a time 4τ. This, therefore, is one way of estimating τ and hence R. This is a convenient place to summarise all the potential methods for measuring the damping parameters, as suggested by the mathematics.

1. Look at either the rising or falling pulse and estimate when the disturbance has reached 2% of its steady state. The time interval since the driving pulse was switched on or off, as the case may be, is 4τ.

2. Measure the details of the falling pulse and fit the function $Ae^{-t/\tau}$.

3. Having checked that the driving frequency is as close as possible to μ_m, measure the details of the rising pulse and fit the function $A(1 - e^{-t/\tau})$.

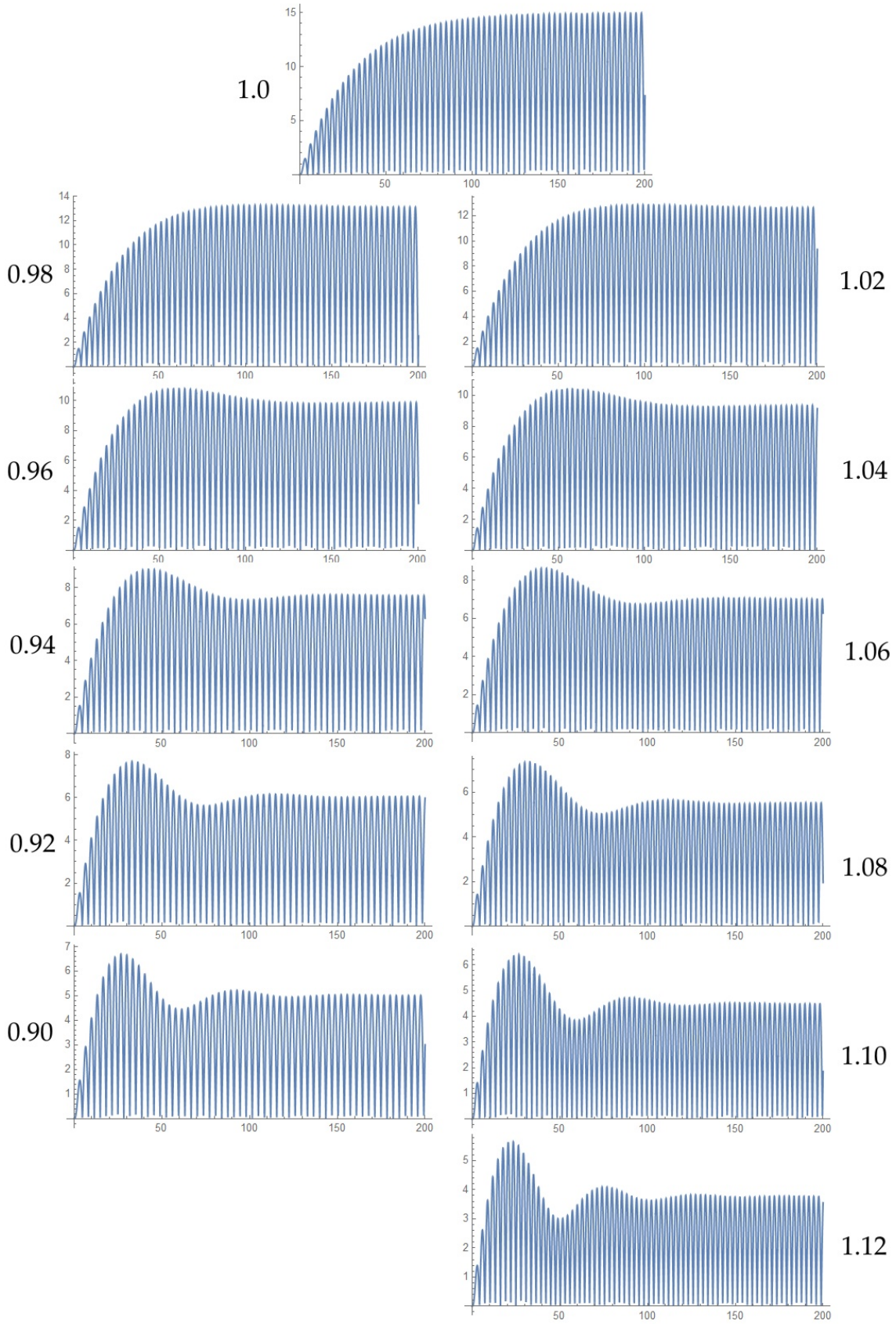

Figure 27: Change in shape and amplitude of rising tone burst pulse as the driving frequency μ deviates from resonance. $F = M = K = 1$, $R = 1/15$, $\omega_0 = 1$. Graphs labelled with μ.

4. Scan the frequency μ of the driving force through a selected resonance and measure the changing amplitude. Fit a function with the form of Figure 24, Eq A2.7 to the measurements, possibly with an added sloping background as in Figure 25.

In principle the difference between μ_m in ω_d in the transients should give a value of τ, but the difference will be two small to give any accuracy. Nevertheless, it will be a check on consistency to see whether $\mu_m < \omega_d$ as theory predicts, Eqs A2.4, A2.8. Clearly in any experiment one would hope that these four methods could all be applied and would give consistent results.

9.2 Experiment: equipment and preparatory observations

Here is a summary of the experimental arrangement. Measurements were made in a quiet room in a domestic house. Software (NCH tone generator or GoldWave wave editor) on a laptop computer generated a sinusoidal signal, either as a swept frequency continuous wave or in 2 or 3 second tone bursts at constant selected frequency. This was input to an acoustic power amplifier and thence to a hand held moving coil electromagnetic exciter, the latter being essentially a 40 mm diameter vibrating plate within a stator housing. The vibrating surface had a central boss of soft wood fixed to it so that, when held against a musical instrument, the vibrator did not scratch and the area of contact was no more that 1 square cm. In some experimental runs I placed the exciter against the body of the wooden box in the centre of the back of the instrument, while in others I held it against a corner of the bridge to simulate the action of the strings. In all cases the strings on the instrument were gently but firmly clamped with sponge and soft cloth so the vibrations were solely of the wooden belly. The sound emitted by the instrument under this controlled excitation was picked up by a good quality mono condenser microphone no more than half a metre distant, and fed via a conditioning unit into the laptop. There it was captured either at CD quality (44100 Hz sample rate) or, more economically, at 11025 Hz by the GoldWave editing program. Whole or selected sections of the monaural wave were stored as .wav files and spectral analysis of these was done using the Japanese program WaveSpectra. GoldWave also has the facility to output the stream of sampled amplitude values as numbers to a text file. I have written programs in BBC Basic to analyse these. These include measuring the frequency (as a check) from the number of zero crossings in a known time, and picking the local peak values at the carrier frequency of the waveform to give the wave envelope. I used Microsoft Excel to display these peak values and Excel's Solver facility to determine the parameter values which give nominally the best fit of a given function to the experimental data.

The aim has been to determine the time constant τ for a selection of the major resonance peaks in the responses of a 'cello and a viola at several frequencies. As part of developing an experimental procedure I made a number of preliminary observations of instrument response and some calibration measurements. This preliminary survey pointed out aspects that required refinement in the technique, which of course took extra effort.

1. I had to decide at which position on the instrument to apply the exciter. The two places used were i) the centre of the back, with the front (top) of the instrument turned towards the microphone, and ii) on the corner of the bridge. Figure 28 shows the spectrum for the 'cello when the exciter in on the back. Since I wanted to work with distinct, well separated peaks, I chose to excite the 'cello in the centre of its back. Spectral analysis quantified the main lower peak frequencies as 94, 172, 181, 194, 228, 282, 302, 320 and 372 Hz. All these values (at this stage) are to about ±2 Hz.

2. The room was in a domestic house, not an anechoic chamber. To assess the reverberation of the room I clapped together two medium sized pebbles to produce a sharp crack sound. The

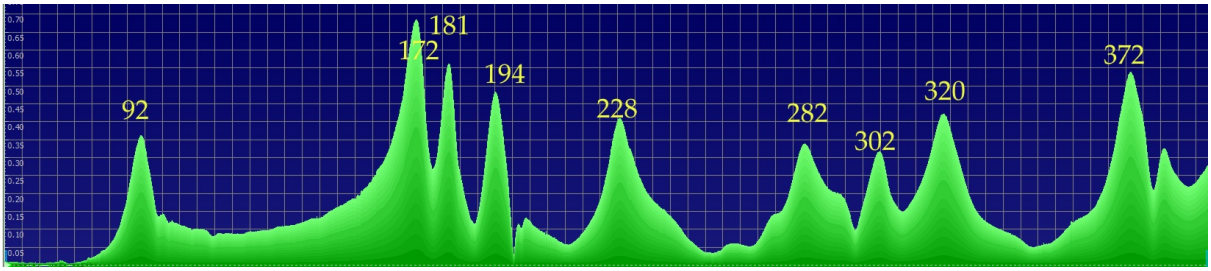

Figure 28: Spectrum of amplitude recorded from cello when driven by swept continuous sine wave from electro-mechanical exciter in centre of back plate, top plate facing microphone.

time for the recorded impulse to fall to 30% of its initial peak value was about 15 milliseconds, a figure to bear in mind when assessing the modal time constants of an instrument.

3. The frequencies in the trailing transients of different resonances were close to the driving frequency which gave the local peak response. This observation confirms the concept of modal damping; we are seeing the structure vibrating in one mode, and watching the decay of this one mode at its characteristic time constant.

4. I tried three ways of producing the tone bursts. The NCH generator produces a tone-burst with very abrupt start and finish – a strictly square topped envelope. To see whether the exciter itself rang on after the electrical signal had ceased, I drove it with this NCH burst while holding it close to the microphone (about 10 cm away) to record the weak sound emitted. There is a short high frequency ring at the start and end of the tone burst. Figure 29 shows the very start and end of the burst at 194 Hz. The higher amplitude, high frequency oscillation has a time constant τ less than 1 m sec and the resonant frequency of the exciter is about 3 kHz. The exciter, therefore, is quite highly damped and, apart from a slight abrupt jolt at the beginning and end of the tone burst, should itself introduce little spurious structure into the recorded waveform. However, the abrupt switching off can in some cases excite other resonances. These modulate the decay and make it difficult to estimate τ.

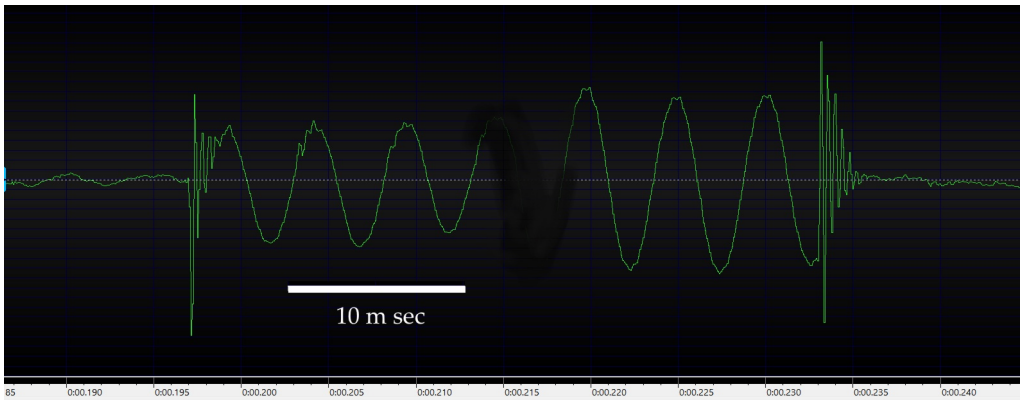

Figure 29: Start and end of tone burst at 194 Hz applied to exciter in absence of musical instrument.

5. As one alternative to using the abrupt NCH tone burst I did try driving the exciter with a continuous wave and creating the on-off stepped force by pressing the exciter by hand against the instrument, holding it steady for a couple of seconds, then lifting it off, the on and off being made as quickly as possible. This removes the short 3 kHz jolt from the exciter, but replaces it with the uncertainty of how quickly I could act in applying and removing the exciter. Figure

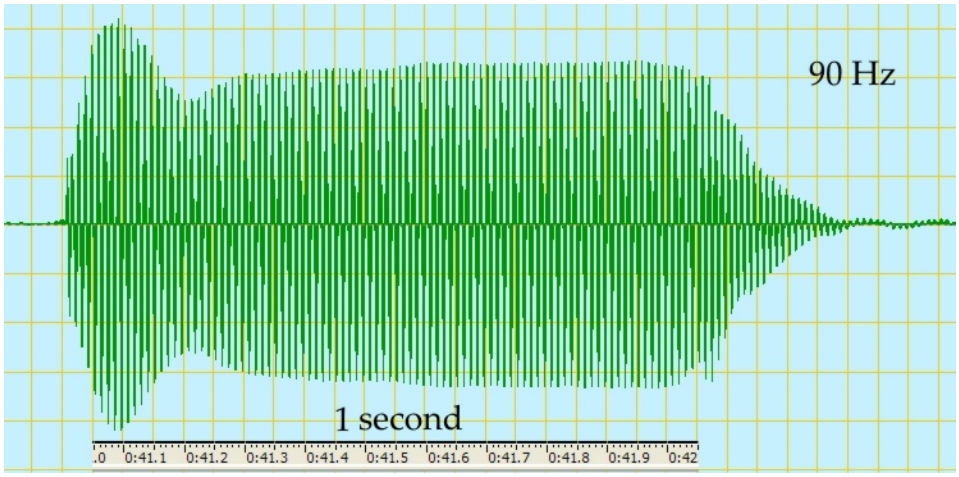

Figure 30: A tone burst on the 'cello at 90Hz produced by pressing the hand-held exciter to the 'cello's back for about one second. The peak response is at 94Hz.

30 shows a tone burst obtained in this way on the 'cello at 90 Hz. The driving frequency is about 5% lower than the resonance peak so we see the beating modulation of the rising pulse similar to that predicted by theory in Figure 27.

6. A third form of tone burst was obtained using GoldWave. This has a function evaluation facility by which I could create tone bursts with an exponential rise and decay, with controlled time constant τ_0. I chose τ_0 to be significantly shorter that τ for the 'cello. If then the measured value of time constant is τ_m, the actual time constant is $\tau_m - \tau_0$ or thereabouts. I found that in general this more gentle way of starting and ending the tone burst excited fewer other resonances that the NCH tone burst and gave the most exponential-like rise and decay. However, it was tedious to set up and leaves the uncertainty as to whether $\tau_m - \tau_0$ is a sufficiently good measure of τ. I only used it for a few measurements.

7. In some cases the sound received by the microphone rose and decayed in the exponential manner predicted by theory. Two examples are shown in Figure 31 for the cello at 94 and 543 Hz. However even when the rises and fall were monotonic and almost exponential, the rate of rise was in some cases quicker than the rate of fall. This could be an example of the effect predicted in Figure 27 where beating between natural and driven frequency on the rising edge appears, for small mismatch of frequencies, as a steepening of the leading edge. This points to the need to determine the peak frequency with precision. Looking back to the article on Helmholtz resonance on *www.mathstudio.co.uk*, it is clear from Figure 19 there, for a viola, that the rate of change, though exponential, is faster at the leading edge than at the trailing.

8. In several other resonances the envelopes of the rising and decaying transients were not exponential but significantly modulated. While the theory behind Figure 27 predicts beating between natural and driven frequency on the rising edge, no such modulation of the envelope is expected at the tail, when only the natural oscillation is present. Figure 32 shows the start and end of the tone burst at 181 Hz; note the subsidiary peak in the tail. This is probably caused by the abrupt ending of the driving force exciting other resonances. Indeed, subsequent close examination of the spectra showed that some peaks had a shoulder caused by an nearby weaker resonance *e.g.* in the 'cello at 320 (stronger) and 328 Hz (weaker). This modulation makes it difficult to state the time constant for the decay. In some of these cases I tried a different way of producing the tone burst.

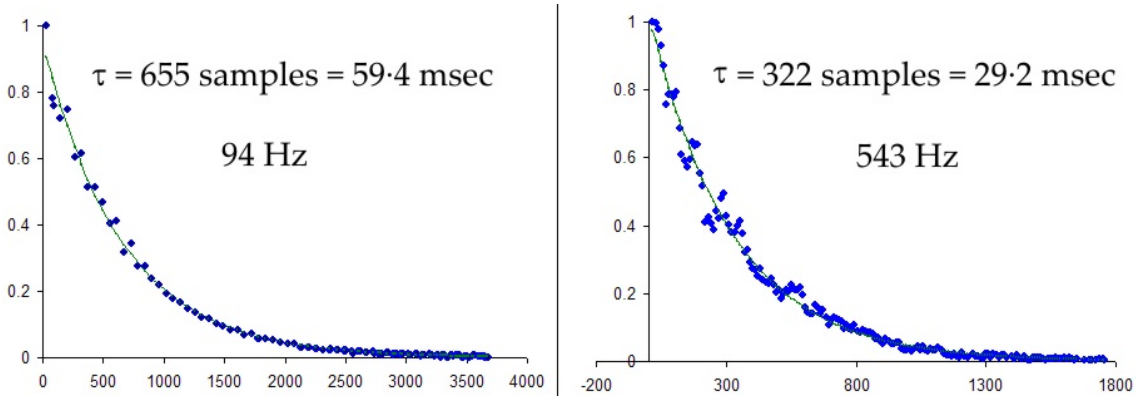

Figure 31: Two examples of exponential decay in the trailing transient of a tone burst. The fitted exponential is the thin green curve.

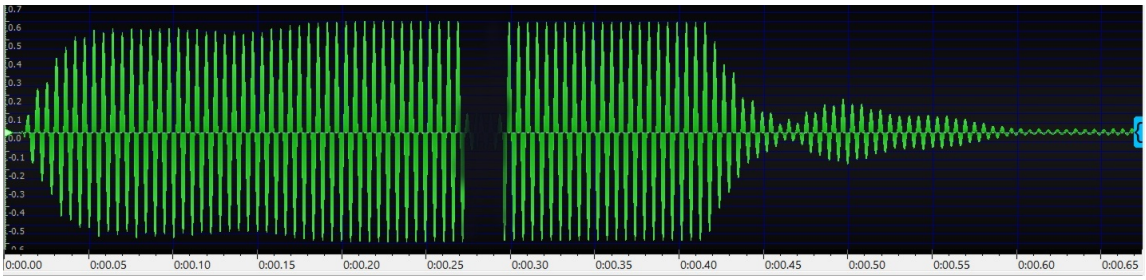

Figure 32: Start and end of tone burst at 181 Hz applied to centre back of 'cello.

9. The 'cello resonance near 94 Hz is the Helmholtz air cavity resonance. It occurs close to F♯ on the C string. I confirmed this in a supporting measurement made with a small electret microphone placed inside the body of the instrument.

10. Using the spectrum analyser software I estimated the 5 dB width of several peaks of the viola – 5 dB rather than 6 because the screen of WaveSpectra is graduated in 5 dB divisions. The few results are reported in §9.3.3.

11. The strength of some resonances varied significantly with the position of the exciter on the back plate. The response at 302 Hz was a case in point; it is much stronger with the exciter to the right of the back, under the C string. Such variation is to be expected, depending on the spatial patterns of each mode.

9.3 Experimental results

After this preliminary exploration I settled to the following experimental technique:

1. Scan slowly through each peak, about ±20 Hz either side. Display the waveform, select a small portion at the peak amplitude, convert to text file and use the Basic program to determine the peak frequency, nominally μ_m, from counting zero crossings.

2. Return to the 'cello, set the driving frequency to this nominal μ_m and record two to three tone bursts with the exciter at close but different positions on the back of the instrument, with the top plate facing the microphone.

3. In some cases also vary the carrier frequency of the tone burst in 1 Hz steps.

4. Display the tone burst in GoldWave and from it select three portions, namely a) a central steady portion, b) the rising edge, c) the falling tail. Convert each to a text file. Use the central portion to check the driving frequency. Display the leading and trailing transients in Excel, fitting exponential curves, mainly by least squares.

5. Return to the swept scan in 1, take it into Excel and attempt to fit a curve with the form of Eq A2.7, A2.9.

Below are some notable points about the resonant peaks of the 'cello, all obtained with the exciter on the back plate behind the bridge.

9.3.1 Cello Helmholtz resonance, 94 Hz

I will give a fairly detailed account of this resonance to illustrate the extent to which the various potential methods for measuring τ compare. This resonance peaked at $\mu_m = 94 \cdot 2$ Hz. When given a short tone burst at or near this frequency, the fall of the emitted sound was monotonic and looked exponential. Several such decay curves were examined, and the one already presented in Figure 31, left, is the one measured at the end of a slow sweep frequency scan from 80 to 100 Hz, so at this point the driving frequency was 100Hz. The time constant here is 655/11025 seconds, or $59 \cdot 4$ msec, as determined by curve fitting in Excel. The tone burst created by hand, by dabbing the exciter onto the cello, seems to have somewhat slower decay. For instance, in the tail of one hand-held pulse driven at $94 \cdot 5$ Hz, τ was $67 \cdot 8$ msec, and in another with 93 Hz driving was $77 \cdot 3$. I suspect that my imperfect reaction time will be adding at least 10 msec to this. This would be consistent with human reaction time in response to a touch stimulus.

The rising pulse too looks exponential when the driving frequency is at $\mu_m = 94$ Hz, but we have already seen in Figure 27 that beating modulates the rise when the driving frequency is a few percent away from this. By eye I judge that the signal has settled after about 320 msec. If this is 4τ, then τ is 80 msec. Again at least 10 msec of this would be my human reaction time.

Probably the most reliable result was obtained using the exciter driven from the NCH generator in a tone burst at $94 \cdot 2$ Hz, exactly at μ_m. There is clear exponential shape to the rising and falling transients. The envelope of the rise is shown in Figure 33, and τ found to be $67 \cdot 8$ Hz. Similar

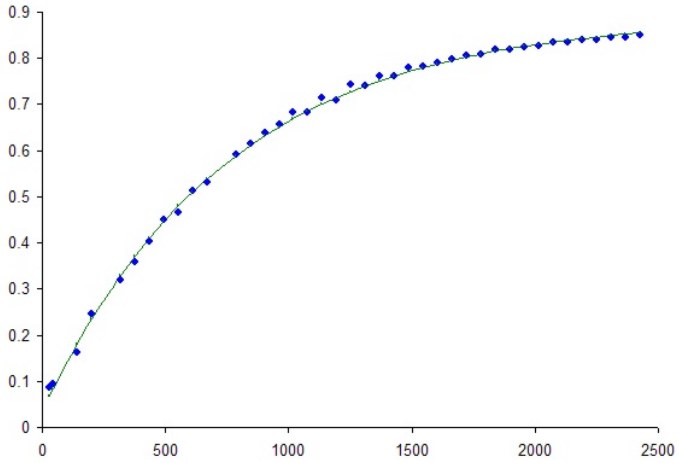

Figure 33: Envelope of rising transient of a tone burst, produced electronically, on the 'cello at drive frequency $94 \cdot 2$ Hz. Horizontal scale is samples at 11,025 per second.

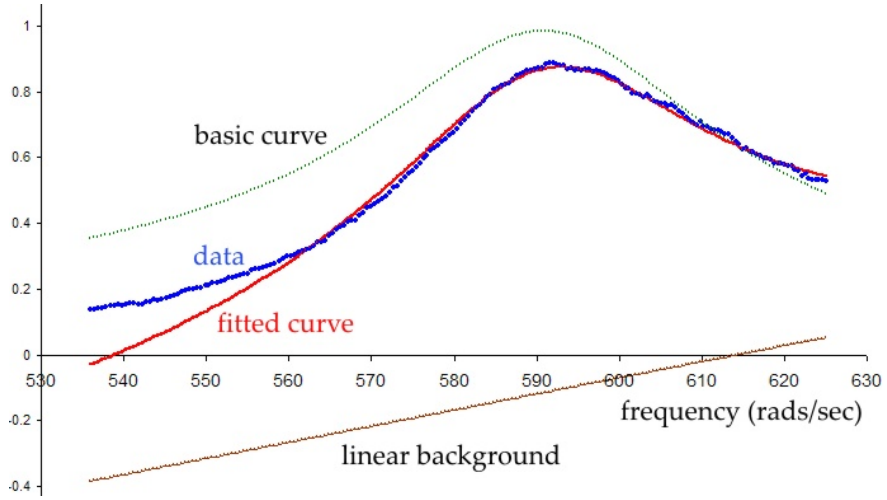

Figure 34: Curve with form of Eq A2.7 fitted to frequency response through Helmholtz resonance, with μ swept 80 to 100 Hz. The added linear background is also shown.

analysis of the trailing transient gave $\tau = 68 \cdot 4$ Hz, encouragingly close. The frequency during this end transient, measured from zero crossing counts, was $\omega_d = 95 \cdot 3 \pm 0 \cdot 3$, slightly greater than μ_m. When converted to radians/sec the difference $\mu_m^2 - \omega_d^2 = 1/\tau^2$, giving τ to be only 11 msec. Clearly this is not a secure way to measure τ.

I also tried fitting curves of the form of Figures 24 and 25 to the Helmholtz resonance peak as the frequency is swept. I found it necessary to add a linearly sloping background to the basis curve to compensate for the rise towards the strong resonance at 172 Hz. There is no one best fit, but several parameter sets give a good fit and one example is shown in Figure 34. The values here are $\omega_0 = 94 \cdot 16$ Hz, $\tau = 495$ msec. This time constant is not wholly inconsistent with other other estimates, but I think it is difficult to estimate τ from the width of the frequency response through the resonance because of the overlap with adjacent peaks.

I judge that the most likely value of τ for this Helmholtz resonance is 68 msec. Included in this is any immediate reverberation from the room.

9.3.2 Other cello resonances

I have measured τ for most of the other prominent resonances of the 'cello up to 1400 Hz. The results are listed in Table 2 and plotted in Figure 35. I have separated the points into two groups, based on my judgement of the quality and reliability. I have more confidence in the blue points than the orange, though there are significant discrepancies amongst some blue points at the same frequency. In all cases the electromagnetic exciter was held by hand on the back of the instrument with the top plate towards the microphone and about 15 cm away. In most cases the exciter was on the centre line of the back in line with the bridge, but for some resonances, such as the one at 302 Hz, a much stronger sound was emitted with the exciter to the right on the C string side. All measurements were made by observing the rising or trailing transient when the exciter delivered a 2 or 3 second tone burst. Where a clear exponential curve was apparent, I used Excel to fit an exponential curve and took τ from this. These are the most precise values. Where the rise or fall was heavily modulated, it was still possible to make a by-eye estimate of 4τ by judging the time for the signal almost to settle to its steady value. GoldWave measures a selected time interval to 1 msec. In some cases I used a tone

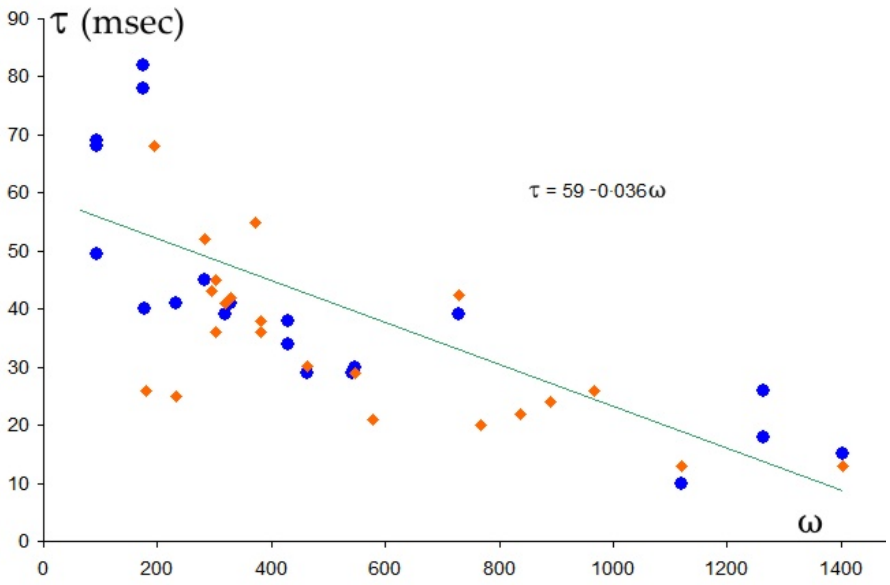

Figure 35: Damping time constant τ in milliseconds for resonances of a 'cello plotted against resonant frequency ω. Orange points: lower accuracy / lower confidence.

burst with exponential growth and tail, time constant τ_0, and subtracted this value from the best fit to the data. Where methods could be compared, I obtained acceptable agreement, particularly when the rising and falling transients of several tone bursts were averaged. The meanings of words in the 'Method' column are as follows:

- rising: τ obtained using curve fitting in Excel on rising transient,
- tail decay: τ obtained using curve fitting in Excel on trailing transient,
- rising; time to 4τ: by-eye estimate of time interval in rising transient,
- falling, time to 4τ: by-eye estimate of time interval in trailing transient.
- smoothed rise, smoothed tail: driven with burst with exponential rise and decay, with τ_0 subtracted.

The points in Figure 35 clearly have considerable scatter. Indeed, I know no reason why they should be monotonic. Nevertheless, there is a trend towards shortening τ as the resonant frequency rises. In the main text this data is replotted on a logarithmic scale and shows a roughly linear variation with pitch, musical pitch being proportional to the logarithm of frequency. Specifically, τ decreases by about 13 milliseconds for each octave rise in pitch. This fits with common experience of sounds, that lower pitches generally resonate for longer.

9.3.3 Viola

We should not presume that all violin-family instruments have this decrease in τ with pitch, or even all 'cellos. I made some perfunctory observations on a viola and found a large scatter in decay times, but no sign of a trend with pitch. More careful investigations may change this view. Most of the transients from 245 Hz to 1120 Hz were not simple exponentials, but were heavily modulated making only the most crude estimate of τ possible without considerably more effort than I was prepared to

Peak & driving frequency μ_m	Method	Freq in tail	τ msec	Comment
$94 \cdot 2$	tail decay	$95 \cdot 3$	68	clear exponential
$94 \cdot 2$	rising		68	clear exponential
$94 \cdot 2$	fit to spectrum		50	Figure 34
$175 \cdot 7$	tail decay	$175 \cdot 7$	82	minimal modulation
$175 \cdot 7$	tail decay	$175 \cdot 9$	78	slight modulation
177	fit to spectrum		40	
1802	smoothed tail		26	10 msec smoothing
194	rising; time to 4τ		68	
232	smoothed rise		41	10 msec smoothing
232	smoothed tail		25	10 msec smoothing
282	tail decay	280	52	moderate scatter
282	rising		45	slight modulation
302	rising; time to 4τ		36	modest modulation
302	tail decay	296	45	modest modulation
296	falling, time to 4τ		43	modest modulation
320	rising		39	slight modulation
320	tail decay		41	modest modulation
$328 \cdot 5$	rising; time to 4τ		41	slight modulation
$328 \cdot 5$	tail decay	$325 \cdot 5$	42	significant modulation
372	falling, time to 4τ		55	significant modulation
372	rising, time to 4τ		55	significant modulation
$382 \cdot 5$	rising, time to 4τ		36	significant modulation
$382 \cdot 5$	falling, time to 4τ		38	significant modulation
$429 \cdot 5$	rising		38	clear exponential
$429 \cdot 5$	tail decay		34	clear exponential
$463 \cdot 5$	rising		29	slight modulation
$463 \cdot 5$	tail decay	$462 \cdot 8$	30	modest modulation
546	rising		29	moderate scatter
543	tail decay	$546 \cdot 7$	29	slight scatter
546	tail decay	547	30	slight scatter
579	rising		21	slight modulation
730	rising		43	slight scatter
730	tail decay	731	39	clear exponential
767	falling, time to 4τ		20	significant modulation
838	falling, time to 4τ		22	significant modulation
891	rising, time to 4τ		24	significant modulation
967	rising, time to 4τ		26	significant modulation
967	falling, time to 4τ		26	significant modulation
1120	smoothed rise	1110	13	10 msec smoothing
1120	smoothed tail		10	10 msec smoothing
1265	smoothed rise		26	8 msec smoothing
1265	smoothed tail		18	8 msec smoothing
$1402 \cdot 5$	tail decay	1400	15	clear exponential
$1402 \cdot 5$	rising, time to 4τ		13	modest modulation

Table 2: Damping time constant τ in milliseconds for resonances of a 'cello.

commit. I found in several resonances that the falling, end transient of a tone burst was shorter than the starting one. This was seen also in the 'cello and may be because other resonances (perhaps close to a harmonic of the driving frequency) are also slightly excited and their effect is more apparent in the tail when there is no large forced motion present. Table 3 gives τ for a few resonances. The values were obtained, as for the 'cello, by curve fitting in Excel where the transients were relatively free of modulation.

Other estimates of τ were found from measuring the width of the peak in the frequency spectrum. As an example of how this was done, I used Eqs A2.7 and A2.8 to express the theoretical amplitude as a fraction of the peak. Using WaveSpectra I found the 5 dB down ($0 \cdot 562$) frequency on the low and high frequency sides of the spectral peak. Substituting these into the expression in a symbolic maths package, I solved numerically for τ. Thus there is a resonance peaking at about 246 Hz, $\omega = 246 \times 2\pi$. The 5 dB down frequencies were at $231 \cdot 5$ Hz and $263 \cdot 8$ Hz. The corresponding τ values are 12 and 17 milliseconds, with average 15 msec. The viola's time constant are considerably shorter than those of the 'cello at the same pitch. Thus, even though the viola is a good quality resonant instrument with a good sound, it rings less than a 'cello playing the same notes. Whether a listener would hear this is doubtful, since so much depends on the bowing.

Frequency Hz	Method	τ msec
245	5 dB width	15
245	rising	$17 \cdot 8$
245	tail decay	$22 \cdot 6$
412	5 dB width	21
412	rising	$11 \cdot 8$
412	tail decay	$13 \cdot 4$
821	5 dB width	28
911	5 dB width	24

Table 3: Time constant τ in milliseconds for resonances of a viola.

John Coffey, Cheshire, England, January 2016